July 2020

Nano- and micro-structured temperature-sensitive hydrogels for rapidly responsive devices

Qi Lu
University of Massachusetts Amherst

Nano- and micro-structured temperature-sensitive hydrogels for rapidly responsive devices

A Dissertation Presented

by

Qi Lu

Submitted to the Graduate School of the
University of Massachusetts in partial fulfillment
of the requirement for the degree of

DOCTOR OF PHILOSOPHY

May 2020

Polymer Science and Engineering

Nano- and micro-structured temperature-sensitive hydrogels for rapidly responsive devices

A Dissertation Presented

by

Qi Lu

Approved as to style and content by:

_____
Ryan C. Hayward, Chair

_____
Alfred J. Crosby, Member

_____
Shelly R. Peyton, Member

_____
David A. Hoagland, Department Head
Polymer Science & Engineering

DEDICATION

To my parents, for your unconditional love

ACKNOWLEDGMENTS

First and foremost, I would like to express my sincere gratitude to my Ph.D. advisor, Professor Ryan Hayward. Ryan's guidance enabled me to conduct research of my interest and shaped me into a better scientist than I aspired to be. Ryan has a great mind: always curious about science, straightforward and systematic in explaining and reasoning, cultivating my critical thinking, and acute of the essence of a problem. Ryan also has a kind heart: he is very patient and understanding during my struggling times, generous to help my professional development, and always accessible, friendly and encouraging. I clearly remember that Ryan encouraged me to try more options, step out my comfort zone, and be fearless, and I have kept that as my motto ever since. I am very fortunate to have such a knowledgeable and supportive advisor.

I also would like to thank my thesis committee members, Professor Alfred Crosby and Professor Shelly Peyton. Their enthusiasm and scientific insights shaped my thesis work into a better form. Al always asks the hard questions and encourages me to think deeper, improve my answers and convince him. Shelly offers detailed feedback from a biological angle, helps solidifying my knowledge background, and the collaboration with her is very pleasant. I would like to thank my other collaborators: Dr. Maria Gencoglu, Dr. Weiguo Huang and Aritra Kundu. This interdisciplinary collaboration taught me a lot, Maria and Aritra are responsible and easy to communicate with; Weiguo for setting up the foundation of the work.

I am grateful to the previous and present group members, Dr. Maria Chiappelli, Dr. Jinhye Bae, Dr. Kyle Bryson, Dr. Anesia Auguste, Dr. Rachel Letteri, Dr. Nakul Bende, Dr. Daniel Acevedo, Dr. Adam Hauser, Dr. Ying Zhou, Dr. Di Zeng, Dr. Tetsu Ouchi, Hyunki Kim, Alexa Kuenstler, Carolyn Zhao, David Limberg, Minjung Lee, Jaechul Ju, Hantao Zhou, Demi Moed, Dr. Junhee Na, Dr. Seog-Jin Jeon, Dr. Weiguo Huang, Dr. Soonyong So, Dr. Ji-Hwan Kang, Dr. Hyeong-Jun Kim, Dr. Wenwen Xu, Dr. Matt McBride and Dr. Elayne Thomas. I am fortunate to conduct research and develop friendship with these amazing people. Especially, I would like to thank Ying for firstly introducing the group to me, mentoring me from the start, holding in-depth discussions, and her warm kindness; Hyunki for being a wonderful classmate, lab mate and office mate, selflessly offering help and advice, and sharing happy, confused and struggling times; Tetsu for asking the hard questions and holding me to higher standards; Minjung for the happy times and leisure chats; David and Alexa for offering advice on my presentations and written documents.

I acknowledge the funding agencies that financially supported my research: National Institutes of Health Exploratory/Developmental Research Grant (1 R21 EB022748-01), and Defense Threat Reduction Agency (HDTRA1-15-1-0030 and HDTRA1-10-1-0099).

I want to thank all the PSE faculty members. The coursework in first year laid a strong foundation of my professional development as a polymer scientist, and the discussion helped me a lot. I would like to thank technical staff members for helping me with the experiments, especially John Nicolson for offering advice, managing facilities and discussing procedures regarding the micro-fabrication process in the cleanroom; Jim Chambers for helping me with confocal microscopy and customizing the facility for my experimental requirements. Also, I thank all PSE staff members for helping me with

administration and allowing me to concentrate on research, especially Lisa Groth, Linda Chatfield and Madelyne Skrocki.

I would like to thank my friends that supported me all along. Class of 2014 is consisted of people of different backgrounds, and we supported each other and travelled this journey together. The Chinese community in PSE feels like family away from home, I will cherish the great times we shared together. Wenhao Li is my closest friend in Amherst, and I cannot imagine going through this without his help and accompany. Minchao Zhang and Ying Zhou are like older sisters, always considerate and caring, and they support me through the difficult times. Xin Li is always there with me, sharing excitement and shouldering frustrations. Yan Cong's believing in me gave me strength. Yiliang Zhou, Di Zeng and Yifeng Du always make me happy. Outside Amherst, I cherish the friendship with Jian Li and Xiaoquan Zhou, it is so warm and comforting to chat with old friends. I gained much energy and inspiration from the music and character of Hins Cheung and Denise Ho. I thank Wei Wen, Qianqian Cheng, Weiying, Yue Zeng, and other pals that deeply resonated with me, accompanied me and supported me from afar.

I would like to thank my boyfriend, Bolun Zhao. Long-distance relationship is hard, but he managed to stay close to me all the time, ups and downs, in laughter and in tears.

Finally, I cannot thank my family enough. It gives me so much courage to march on knowing that they will always have my back. Nothing would be possible without their unconditional support.

ABSTRACT

NANO- AND MICRO-STRUCTURED TEMPERATURE-SENSITIVE HYDROGELS FOR RAPIDLY RESPONSIVE DEVICES

MAY 2020

QI LU, B.ENG., BEIHANG UNIVERSITY

M.S., UNIVERSITY OF MASSACHUSETTS AMHERST

PH.D., UNIVERSITY OF MASSACHUSETTS AMHERST

Directed by: Professor Ryan C. Hayward

This thesis aims to extend the understanding and explore the application of temperature-responsive hydrogel systems by integrating microelectromechanical systems (MEMS). Stimuli-responsive hydrogel systems are immensely investigated and applied in numerous fields, and interfacing with micro- and nano-fabrication techniques will open up more possibilities.

In Chapter 2, the first biologically relevant, *in vitro* cell stretching device based on hydrogel surface instability was developed. This dynamic platform is constructed by embedding micro-heater devices under temperature-responsive surface-attached hydrogels. The fast and regional temperature change actuates the stretching and relaxation of the seeded human artery smooth muscle cell (HASMC) via controllable surface creasing instability. This

device is engineered to mimic the *in vivo* environment of HASMCs, with independent control over substrate stiffness, mechanical cues and peptide attachment chemistry, and the response of HASMCs is inspected by the differentiation marker expression change.

In Chapter 3, the swelling and deswelling kinetics of hydrogel sheets with high polymer content is inspected, with micro-heaters providing abrupt local temperature change. Poly(N-isopropylacrylamide) (PNIPAM) molecules can form hydrogen bonds with both water molecules and polymer chains, while poly(N,N-diethylacrylamide) (PDEAM) molecules can only form hydrogen bonds with water. The kinetics of the two hydrogel systems are systematically compared, revealing that while PDEAM shows one-step mass transport-limited kinetics, PNIPAM shows two-step kinetics behavior, presumably reflecting the strong influence of inter-molecular hydrogen bonding.

The following two chapters document the attempts to further investigate into the hydrogel/MEMS interface. In Chapter 4, photo-patterning technique assists the study of regional modulus contrast influencing the formation of creases on the soft hydrogel surface, and it is demonstrated that the dimensions of the stiff patterns are relevant in directing the creasing direction. In Chapter 5, a photo-patternable sacrificial layer is designed based on crosslinking chemistry and gelation physics to potentially enable the construction of more complex MEMS devices.

TABLE OF CONTENTS

LIST OF TABLES

Page

LIST OF FIGURES

Page

CHAPTER 1

INTRODUCTION

1.1 Responsive hydrogels

Hydrogels are three-dimensional hydrophilic polymer networks that adopt a specific volume when exposed to water, and can contain the water within their structure. The hydrophilicity of the polymer network is usually provided by high polarity moieties, so the most frequently used materials include synthetic polymers like poly(2-hydroxyethyl methacrylate) (PHEMA), poly(vinyl alcohol) (PVA) and poly(ethylene glycol) (PEG), as well as natural derivatives like cellulose, alginate, and hyaluronic acid[1]. The crosslinking in the network prevents the polymer chains from dissolving into the aqueous solution, and the crosslinking can be categorized into chemical crosslinking of covalent bonds and physical crosslinking of non-covalent interactions, such as hydrogen bonding, ionic interactions, metal-ligand coordination, and guest-host complexation. The solvent contained in the network helps to prevent the network from collapsing, so the small molecules can transport into and out of the hydrogel through its porous structure, providing resemblance to biological tissues and allowing for biocompatibility.

As is described in Flory-Rehner theory, osmotic pressure drives the water to flow into the hydrophilic hydrogel network, but the network elasticity prohibits the network from infinite expansion, and the swelling equilibrium is achieved when the elasticity of the network is counterbalanced by the expansion due to the solvent absorption[2]. This equilibrium swollen state depends on the hydrogel properties, such as

hydrophobicity/hydrophilicity balance, crosslinking density and degree of ionization, which can be altered by the environmental stimuli, such as temperature, pH, ionic strength, chemical reagents, light, and electric field[3,4]. When the hydrogel property is changed by the formation or destruction of secondary chemical interactions, reactions of functional moieties, or corresponding osmotic pressure differentials, the swelling equilibrium will be interrupted and the hydrogels will undergo volumetric expansion or shrinkage, known as swelling and deswelling[5,6]. This stimuli-responsiveness of hydrogel systems makes them useful in many areas, including drug delivery, sensing devices and soft actuators, tissue engineering, smart optical systems and smart surfaces[7–11].

1.1.1 Thermal responsive hydrogel

Among various stimuli responsive hydrogel systems, temperature triggered hydrogels are the most widely studied because they can respond to an easily regulated environmental cue and they can be developed to *in vivo* devices or controlled drug delivery carriers. The temperature responsive hydrogels can be constructed using physical crosslinks whose properties depend on ambient temperature, such as hydrogen bonding and hydrophobic interactions. More commonly, temperature-responsive hydrogels are constructed from monomers with both hydrophobic groups such as methyl, ethyl and propyl groups and a hydrophilic moiety such as an amide, and the switching between hydrophobicity and hydrophilicity is dependent on the ambient temperature. This temperature responsiveness is reflected as solubility change for linear polymers, and volumetric change for crosslinked networks. The temperature where the transition occurs is called the volume phase transition temperature, where a phase change occurs between the polymer and the solvent. Some polymer solutions undergo phase separation below the critical temperature, thus showing

a upper critical solution temperature (UCST) behavior, such as polysulfobetain in aqueous solution[12], and the interpenetrating network composed of polyacrylamide and poly(acrylic acid)[13]. But the more commonly observed and investigated hydrogels have lower critical solution temperature (LCST) properties, where the polymer becomes more soluble in the solvent upon cooling. The LCST of a polymer system can be tuned by the changing ratio of hydrophilic and hydrophobic groups, the co-solvent, crosslinking density and other molecular architectures[14–19]. There are many polymers that have LCSTs in water, such as poly(N-isopropylacrylamide), poly(N,N-diethylacrylamide), poly(N,N-dimethylamino ethylmethacrylate), poly(vinylisobutyroamide) and hydroxypropyl cellulose[20–24].

Among all polymers with a LCST, poly(N-isopropylacrylamide) (PNIPAM) is the most intensively studied, because its LCST in water is 32 ℃, close enough to the physiological relevant temperature for biomedical applications. At temperatures below LCST, the enthalpy decrease from the hydrogen bonding between the amide and the ambient water molecules is dominant over the entropy decrease from the interaction between hydrophobic parts and the surrounding water molecules, resulting in a negative free energy for mixing, so hydration is favored. When the temperature is elevated above the transition temperature, the hydrogen bonds are disrupted, resulting in a positive mixing free energy dominated by the positive entropy change, so dehydration is favored and the polymer chain collapses[20,25,26]. One important property of PNIPAM is the sharp volume phase transition at critical temperature, and the only other known non-ionic polymer that shares this feature is poly(N,N-diethylacrylamide) (PDEAM), because of their rather hydrophobic alkyl side-groups[21,27–29]. DEAM monomer has a chemical structure that is very similar to NIPAM, and an LSCT of 30 ℃, close to 32 ℃ of PNIPAM. However, by PNIPAM having a

isopropyl group and PDEAM two ethyl groups as the substituting alkyl groups, PNIPAM has a hydrogen bond donor group of –NH, so it can form inter-molecular hydrogen bonds, while PDEAM cannot. This difference makes PDEAM an ideal molecule to investigate the effect of inter-hydrogen bonding in hydrogel systems, such as the hysteresis between the association and disassociation process of PNIPAM chains in water[30], and the difference in single-chain elongation mechanics between PNIPAM and PDEAM[31].

1.1.2 Surface instabilities and constrained swelling

When soft elastic materials are under compression, constrained swelling or differential growth, and the loading exceeds some critical point, the surface can form instability features to minimize the total energy of the system. The surface instabilities include wrinkling, creasing, buckling, folding, ridging and so forth, and they are observed in our daily lives at various length scales[32–34]. Surface instabilities used to be considered as failures in fabrication, but are currently under extensive study as a method to generate surface patterns and construct responsive surfaces. Researchers have exploited the instability of soft materials to dynamically control wettability[35], and optical properties[36], as well as to fabricate stretchable circuits for flexible electronics[37], active components in microfluidic devices[38] and serve as probes for material properties[39].

Among the surface instabilities, wrinkling and creasing are most extensively studied. Wrinkling occurs when a thin layer supported on a thicker soft substrate is compressed, and the total energy is minimized through balancing the bending energy of the stiff film and the stretching energy of the soft substrate. A well-ordered sinusoidal curve shape is

adopted, and the critical strain $\varepsilon_{wrinkle} = 0.25\left(\frac{3\overline{E_s}}{\overline{E_f}}\right)^{\frac{2}{3}}$, wrinkling wavelength $\lambda_{wrinkle} = 2\pi h_f\left(\frac{\overline{E_f}}{3\overline{E_s}}\right)^{\frac{1}{3}}$, and amplitude $A = h_f\left(\frac{\varepsilon}{\varepsilon_{wrinkle}} - 1\right)^{\frac{1}{2}}$, where $\overline{E_f}$ is the plane strain modulus of the film, $\overline{E_s}$is the plane strain modulus of the substrate, h_f is the film thickness and ε is the strain.

It is predicted by Biot using a semi-infinite neo-Hookean scenario that the free surface of an elastomer would form sinusoidal waves when the plane strain exceeds 0.46, but this was never observed experimentally, because creasing instability occurs before this critical strain[40]. Creasing is the instability where a soft material surface releases the compressive stress by folding against itself, forming self-contacting regions with a discontinuity at the tip[41–44]. The onset strain for creases to form is 0.438 for uniaxial compression, and 0.35 for plane strain condition[44]. The wavelength of creasing $\lambda = 3.5H(1 - \varepsilon)$, where H is the thickness and ε is the compressive strain[45].

Creases can occur when a thin, soft hydrogel film attached on a non-swelling rigid substrate swells above a critical value. The gel takes up water, but the lateral expansion is restricted by the underlying substrate, so it only swells in the thickness direction. This constrained swelling process generate an equibiaxial in-plane compression in comparison to the free-standing hydrogel that can equilibrate to a stress free state, and when this compression strain ε ($\varepsilon = 1 - \frac{l_0}{l}$, where l_0 is the initial dimension of the hydrogel sheet and l is the dimension of the free-standing gel at equilibrium) is over the critical value, the creases will form on the hydrogel surface to relieve the compression, as is shown in Figure 1-1[46]. When

the surface-attached hydrogel is stimuli-responsive, the formation, shape or the disappearance of the creases can also be controlled accordingly upon environmental change.

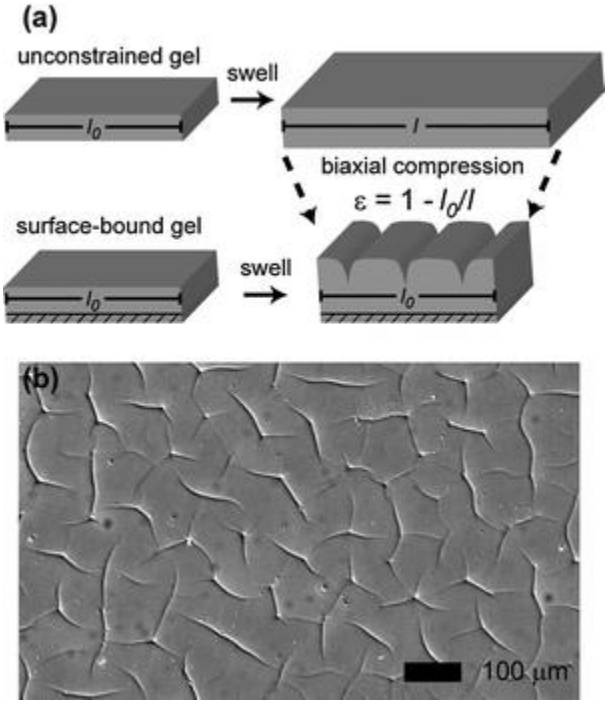

Figure 1- 1 Creasing on a surface-attached hydrogel. (a) Unidirectional swelling of a surface-attached gel results in a biaxial compressive stress, which can be partially relieved by localized creasing of the gel surface. (b) An optical micrograph of the crease structures formed upon swelling of a surface-attached gel. (Reproduced from Ref. 46 with permission from The Royal Society of Chemistry.)

When the swelling ratio of the surface-attached hydrogel can respond to environmental stimuli, the formation, shape or the disappearance of the creases can be controlled accordingly. Researchers have used this tunable creasing instability to study the buckling modes of hydrogel beams[47], control the dynamic display of surface patterns[48,49], trigger surface instabilities by electrical field[50], develop dynamic cell stretching devices[51], direct the formation of ordered structure of liquid crystals in hydrogels[52,53], and fabricate smart surfaces with adjustable adhesive properties[54].

1.1.3 Kinetics of hydrogel swelling

The swelling of a hydrogel is a kinetic process where mass transport and mechanical deformation are coupled[55]. For relatively small deformation, linear kinetic theories can describe the swelling kinetics of polymer gels. Tanaka, Hocker and Benedek developed a linear diffusion theory where the hydrogel is treated as a mixture of solid and liquid, and the swelling is treated as a polymer network diffusing into a solvent negligible fluid displacements[56,57]. However, hydrogels usually undergo large deformation when swelling, so linear poroelasticity theory was adopted because it treats the hydrogel as a continuum with pore pressure as a state variable, and it describes the process of solvent migrating into the network, making it a good tool to describe the coupled process of matrix deformation and mass transport[58–62]. Also, non-linear approaches were developed to describe occasions with even larger deformations[63–66]. The diffusion theory in a poroelastic matrix predicts that in a diffusion-limited swelling transition of a hydrogel, the characteristic time is directly proportional to the square of the size of the gel and inversely proportional to the diffusion coefficient of the network ($\tau = \frac{a^2}{D}$, where a is the gel size and D is the diffusion coefficient).

For the materials system that will be used in this thesis, i.e. temperature-responsive hydrogel thin films initially prepared at low polymer concentration (e.g., ~10% by weight), it is reported that Biot's theory of linear poroelasticity is capable of describing the kinetics process of both free 3D swelling and constrained 1D swelling[67]. The thickness of the hydrogel is much smaller than the lateral dimensions, and it is the distance that solvents have to migrate for equilibrium. This greatly reduces the swelling time constant, and also

makes the hydrogel swell uniformly across the lateral area by ignoring the lateral diffusion (except for very close to edges). Based on Fick's law, if the swelling process is limited by the 1D solvent diffusion in a poroelastic network, then for a hydrogel thin film attached to a stiff substrate, the characteristic time for swelling is given by $\tau = \frac{4H^2}{\pi^2 D}$, where H is the hydrogel thickness as made.

1.2 Microfabrication technologies

Microfabrication is a collection of techniques that are used to fabricate devices in the micrometer to sub-micron range. It has not only been applied to the semicondustor industry that it originated from, but is also leveraged in the development of various other fields, including microelectromechanical systems (MEMS), micro-fluid devices, solar cells, flat-panel displays and optoelectronics[68]. The development of microfabrication technologies is rapid and now there is an extensive collection of tools that are tailored to various purposes, so this section intended to give an introduction of the techniques that are used in this thesis, both established procedures carried out in cleanroom facilities and lab based systems that offer better flexibility.

1.2.1 Photolithography and benzophenone crosslinking

Among the many operations in microfabrication, the microlithography process is the limiting factor for feature dimensions, and photolithography is the most widely used method. It is a technique to transfer the pattern from a master mask to the samples on a substrate by selectively removing parts of the photoresist and exposing the other parts of the substrate. Photoresists are photosensitive materials, whose solubility can be changed

by photochemical reactions upon the illumination of UV light through the photomask. Some photoresists dissolves faster when exposed to UV light, making the exposed areas soluble in developers, so the pattern on the substrate will have the same binary feature as on the photomask, so they are called positive tone photoresists; other photoresists becomes insoluble in developers after exposure, so the pattern on the substrate is the negative counterpart to that of the photomask, and they are called negative tone photoresists. These photoresists act as a recording medium for the features as well as a barrier material to protect the underlying substrate from the later etching processes.

Photolithography techniques were used in the fabrication of many devices in the thesis, however, many of the photo-patterning, photo-grafting and photo-crosslinking processes are carried out using benzophenone chemistry. Crosslinking occurs upon illumination, rendering the network insoluble; this process can be compared to the negative tone photoresists, only it does not require soft bake and post exposure bake procedures. Benzophenone chemistry is widely studied and used because it is chemically stable, inactive under ambient illumination, and its working wavelength does not damage the majority of biomolecules[69,70]. As is shown in Figure 1-2, when benzophenone is activated by UV light, ground state benzophenone is excited to a singlet state, which rapidly and efficiently transforms to the n-π^* triplet state[71]. This triplet being a diradical, can abstract an aliphatic hydrogen, especially the one α to electron rich heteroatoms (most commonly nitrogen, sulfur and oxygen) or the one on a weak carbon-hydrogen bond, yielding a ketyl radical and an aliphatic carbon-centered radical. These radicals can initiate a polymerization of vinyl monomers, and also can form C-C bonds upon coupling[72,73]. To prevent phase separation and the migration of benzophenone, instead of doping into the

system, benzophenone is often covalently linked to the polymer backbone as a pendent group[74]. These copolymers are employed for photo-crosslinking and photo-grafting purposes, and these reactions do not require oxygen-free environment and can proceed in ambient conditions[75–77].

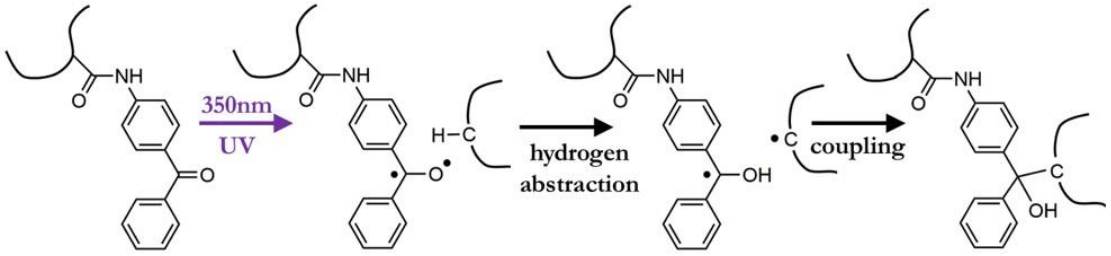

Figure 1- 2 Photo-crosslinking process of polymers by benzophenone pendant groups.

1.2.2 Thin film deposition

Thin films are the building blocks of microstructures, and they serve various functions such as conductors, insulators, semiconductors, reflectors and so on. The common methods to deposit a thin film onto substrate or constructed surfaces are physical vapor deposition (PVD) and chemical vapor deposition (CVD). The difference between the two is whether chemical reactions take place in the deposition process[78].

Physical vapor deposition is an atomistic deposition process where thin film forms by condensation of atoms or molecules on the surface of the substrate due to evaporation, ion bombardment, or sputtering[79,80]. In this thesis work, thin films of metal are deposited onto the substrate by E-beam evaporation, where the metal source crucible is heated and melted under a high energy electron beam, then the vaporized metal is grown onto the substrate with a slow rate and highly directional fashion.

Compared to physical vapor deposition, chemical vapor deposition has a higher deposition rate, lower operation temperature, better uniformity, and can be used to for more categories of materials[81]. The thin film is grown onto the surface by one or a series of chemical reactions in the vapor phase. In this thesis work, thin films of silicon dioxide is fabricated using plasma enhanced chemical vapor deposition (PECVD). It is a technique where the chemical reaction takes place after a plasma is generated in the reactor chamber[82,83].

1.3 Thesis organization

With regards to the aforementioned background and current challenges, this thesis focuses on understanding nano- and micro-structured temperature-sensitive hydrogel systems, and using them for rapidly responsive devices.

In Chapter 2, a hydrogel-based cell stretching device is developed to serve as *in vitro* models of atherosclerotic vessel walls. This stretching device is actuated by controlling hydrogel surface instabilities via regional rapid temperature change, and it achieved robust cyclic stretching of human artery smooth muscle cells (HASMCs) at physiologically relevant conditions.

Chapter 3 focuses on the swelling/deswelling kinetics of high polymer concentration temperature-responsive hydrogel films. With rapid temperature change provided by micro-heater devices, the kinetics of two polymer networks with LCST behavior (PNIPAM and PDEAM) are investigated in order to study the effect of inter-molecular hydrogen bonding.

In Chapter 4, the influence of stiff patterns on the formation of creases on hydrogel surface will be examined. The formation and development of creases on spatially patterned hydrogel surface under biaxial compression is systematically studied.

In Chapter 5, a copolymer system with two orthogonal crosslinking modalities are used to fabricate a photo-patternable sacrificial layer.

1.4 References

(1) Buwalda, S. J.; Boere, K. W. M.; Dijkstra, P. J.; Feijen, J.; Vermonden, T.; Hennink, W. E. Hydrogels in a Historical Perspective: From Simple Networks to Smart Materials. *Journal of Controlled Release*. 2014. https://doi.org/10.1016/j.jconrel.2014.03.052.

(2) Tokarev, I.; Minko, S. Stimuli-Responsive Hydrogel Thin Films. *Soft Matter*. 2009. https://doi.org/10.1039/b813827c.

(3) Ganji, F.; Vasheghani-Farahani, S.; Vasheghani-Farahani, E. Theoretical Description of Hydrogel Swelling: A Review. *Iran. Polym. J. (English Ed.* **2010**.

(4) Roy, D.; Cambre, J. N.; Sumerlin, B. S. Future Perspectives and Recent Advances in Stimuli-Responsive Materials. *Progress in Polymer Science (Oxford)*. 2010. https://doi.org/10.1016/j.progpolymsci.2009.10.008.

(5) Gerlach, G.; Arndt, K.-F. Hydrogel Sensors and Actuators. *Springer Ser. Chem. Sensors Biosens.* **2009**, *6*, 1–15. https://doi.org/10.1007/b100321.

(6) Jeon, S. J.; Hauser, A. W.; Hayward, R. C. Shape-Morphing Materials from Stimuli-Responsive Hydrogel Hybrids. *Acc. Chem. Res.* **2017**, *50* (2), 161–169. https://doi.org/10.1021/acs.accounts.6b00570.

(7) Stuart, M. A. C.; Huck, W. T. S.; Genzer, J.; Müller, M.; Ober, C.; Stamm, M.; Sukhorukov, G. B.; Szleifer, I.; Tsukruk, V. V.; Urban, M.; et al. Emerging Applications of Stimuli-Responsive Polymer Materials. *Nature Materials*. 2010. https://doi.org/10.1038/nmat2614.

(8) Hoffman, A. S. Hydrogels for Biomedical Applications. *Advanced Drug Delivery Reviews*. 2012. https://doi.org/10.1016/j.addr.2012.09.010.

(9) Hoare, T. R.; Kohane, D. S. Hydrogels in Drug Delivery: Progress and Challenges. *Polymer*. 2008. https://doi.org/10.1016/j.polymer.2008.01.027.

(10) Schmidt, S.; Zeiser, M.; Hellweg, T.; Duschl, C.; Fery, A.; Möhwald, H. Adhesion and Mechanical Properties of PNIPAM Microgel Films and Their Potential Use as Switchable Cell Culture Substrates. *Adv. Funct. Mater.* **2010**. https://doi.org/10.1002/adfm.201000730.

(11) Holtz, J. H.; Asher, S. A. Polymerized Colloidal Crystal Hydrogel Films as Intelligent Chemical Sensing Materials. *Nature* **1997**. https://doi.org/10.1038/39834.

(12) Xue, W.; Huglin, M. B.; Khoshdel, E. Behaviour of Crosslinked and Linear Poly[1-(3-sulphopropyl)-2-vinyl-pyridinium-betaine] in Aqueous Salt Solutions. *Polym. Int.* **1999**. https://doi.org/10.1002/(sici)1097-0126(199901)48:1<8::aid-pi105>3.3.co;2-e.

(13) Katono, H.; Maruyama, A.; Sanui, K.; Ogata, N.; Okano, T.; Sakurai, Y. Thermo-Responsive Swelling and Drug Release Switching of Interpenetrating Polymer Networks Composed of Poly(Acrylamide-Co-Butyl Methacrylate) and Poly (Acrylic Acid). *J. Control. Release* **1991**. https://doi.org/10.1016/0168-3659(91)90045-F.

(14) Feil, H.; Bae, Y. H.; Feijen, J.; Kim, S. W. Effect of Comonomer Hydrophilicity and Ionization on the Lower Critical Solution Temperature of N-Isopropylacrylamide Copolymers. *Macromolecules* **1993**. https://doi.org/10.1021/ma00062a016.

(15) Liu, H. Y.; Zhu, X. X. Lower Critical Solution Temperatures of N-Substituted Acrylamide Copolymers in Aqueous Solutions. *Polymer (Guildf).* **1999**. https://doi.org/10.1016/S0032-3861(98)00858-1.

(16) Furyk, S.; Zhang, Y.; Ortiz-Acosta, D.; Cremer, P. S.; Bergbreiter, D. E. Effects of End Group Polarity and Molecular Weight on the Lower Critical Solution Temperature of Poly(N-Isopropylacrylamide). *J. Polym. Sci. Part A Polym. Chem.* **2006**. https://doi.org/10.1002/pola.21256.

(17) Dalkas, G.; Pagonis, K.; Bokias, G. Control of the Lower Critical Solution Temperature - Type Cononsolvency Properties of Poly(N-Isopropylacrylamide) in Water - Dioxane Mixtures through Copolymerisation with Acrylamide. *Polymer (Guildf).* **2006**. https://doi.org/10.1016/j.polymer.2005.10.115.

(18) Costa, R. O. R.; Freitas, R. F. S. Phase Behavior of Poly (N-Isopropylacrylamide) in Binary Aqueous Solutions. *Polymer (Guildf).* **2002**. https://doi.org/10.1016/S0032-3861(02)00507-4.

(19) Senff, H.; Richtering, W. Influence of Cross-Link Density on Rheological Properties of Temperature-Sensitive Microgel Suspensions. *Colloid Polym. Sci.* **2000**. https://doi.org/10.1007/s003960000329.

(20) Schild, H. G. Poly(N-Isopropylacrylamide): Experiment, Theory and Application. *Progress in Polymer Science*. 1992. https://doi.org/10.1016/0079-6700(92)90023-R.

(21) Idziak, I.; Avoce, D.; Lessard, D.; Gravel, D.; Zhu, X. X. Thermosensitivity of Aqueous Solutions of Poly(N,N-Diethylacrylamide). *Macromolecules* **1999**. https://doi.org/10.1021/ma981171f.

(22) Cho, S. H.; Jhon, M. S.; Yuk, S. H. Temperature-Sensitive Swelling Behavior of Polymer Gel Composed of Poly (N,N-Dimethylaminoethyl Methacrylate) and Its Copolymers. *Eur. Polym. J.* **1999**. https://doi.org/10.1016/S0014-3057(98)00277-8.

(23) Akashi, M.; Nakano, S.; Kishida, A. Synthesis of Poly(N-Vinylisobutyramide) from Poly(N-Vinylacetamide) and Its Thermosensitive Property. *J. Polym. Sci. Part A Polym. Chem.* **1996**. https://doi.org/10.1002/(SICI)1099-0518(19960130)34:23.0.CO;2-U.

(24) Winnik, F. M. Effect of Temperature on Aqueous Solutions of Pyrene-Labeled (Hydroxypropyl)Cellulose. *Macromolecules* **1987**. https://doi.org/10.1021/ma00177a019.

(25) Cho, E. C.; Lee, J.; Cho, K. Role of Bound Water and Hydrophobic Interaction in Phase Transition of Poly(N-Isopropylacrylamide) Aqueous Solution. *Macromolecules* **2003**. https://doi.org/10.1021/ma034851d.

(26) Ashraf, S.; Park, H. K.; Park, H.; Lee, S. H. Snapshot of Phase Transition in Thermoresponsive Hydrogel PNIPAM: Role in Drug Delivery and Tissue Engineering. *Macromolecular Research*. 2016. https://doi.org/10.1007/s13233-016-4052-2.

(27) Hirokawa, Y.; Tanaka, T. Volume Phase Transition in a Nonionic Gel. *J. Chem. Phys.* **1984**. https://doi.org/10.1063/1.447548.

(28) Bae, Y. H.; Okano, T.; Kim, S. W. Temperature Dependence of Swelling of Crosslinked Poly(N,N′-alkyl Substituted Acrylamides) in Water. *J. Polym. Sci. Part B Polym. Phys.* **1990**. https://doi.org/10.1002/polb.1990.090280609.

(29) Koetting, M. C.; Peters, J. T.; Steichen, S. D.; Peppas, N. A. Stimulus-Responsive Hydrogels: Theory, Modern Advances, and Applications. *Materials Science and Engineering R: Reports*. 2015. https://doi.org/10.1016/j.mser.2015.04.001.

(30) Lu, Y.; Zhou, K.; Ding, Y.; Zhang, G.; Wu, C. Origin of Hysteresis Observed in Association and Dissociation of Polymer Chains in Water. *Phys. Chem. Chem. Phys.* **2010**. https://doi.org/10.1039/b918969f.

(31) Pang, X.; Cui, S. Single-Chain Mechanics of Poly(N, N -Diethylacrylamide) and Poly(N -Isopropylacrylamide): Comparative Study Reveals the Effect of Hydrogen Bond Donors. *Langmuir* **2013**, *29* (39), 12176–12182. https://doi.org/10.1021/la403132e.

(32) Genzer, J.; Groenewold, J. Soft Matter with Hard Skin: From Skin Wrinkles to Templating and Material Characterization. *Soft Matter* **2006**, *2* (4), 310. https://doi.org/10.1039/b516741h.

(33) Wang, Q.; Zhao, X. A Three-Dimensional Phase Diagram of Growth-Induced Surface Instabilities. *Sci. Rep.* **2015**, *5* (iv), 8887. https://doi.org/10.1038/srep08887.

(34) Wang, Q.; Zhao, X. Beyond Wrinkles: Multimodal Surface Instabilities for Multifunctional Patterning. *MRS Bull.* **2016**, *41* (02), 115–122. https://doi.org/10.1557/mrs.2015.338.

(35) Chen, D.; McKinley, G. H.; Cohen, R. E. Spontaneous Wettability Patterning via Creasing Instability. *Proc. Natl. Acad. Sci.* **2016**, *113* (29), 8087–8092. https://doi.org/10.1073/pnas.1522700113.

(36) Görrn, P.; Lehnhardt, M.; Kowalsky, W.; Riedl, T.; Wagner, S. Elastically Tunable Self-Organized Organic Lasers. *Adv. Mater.* **2011**. https://doi.org/10.1002/adma.201003108.

(37) Khang, D. Y.; Jiang, H.; Huang, Y.; Rogers, J. A. A Stretchable Form of Single-Crystal Silicon for High-Performance Electronics on Rubber Subtrates. *Science (80-.).* **2006**. https://doi.org/10.1126/science.1121401.

(38) Gau, H.; Herminghaus, S.; Lenz, P.; Lipowsky, R. Liquid Morphologies on Structured Surfaces: From Microchannels to Microchips. *Science (80-.).* **1999**. https://doi.org/10.1126/science.283.5398.46.

(39) Stafford, C. M.; Harrison, C.; Beers, K. L.; Karim, A.; Amis, E. J.; Vanlandingham, M. R.; Kim, H. C.; Volksen, W.; Miller, R. D.; Simonyi, E. E. A Buckling-Based Metrology for Measuring the Elastic Moduli of Polymeric Thin Films. *Nat. Mater.* **2004**. https://doi.org/10.1038/nmat1175.

(40) Biot, M. A. Surface Instability of Rubber in Compression. *Appl. Sci. Res. Sect. A* **1963**. https://doi.org/10.1007/BF03184638.

(41) Chen, D.; Cai, S.; Suo, Z.; Hayward, R. C. Surface Energy as a Barrier to Creasing of Elastomer Films: An Elastic Analogy to Classical Nucleation. *Phys. Rev. Lett.* **2012**. https://doi.org/10.1103/PhysRevLett.109.038001.

(42) Mora, S.; Abkarian, M.; Tabuteau, H.; Pomeau, Y. Surface Instability of Soft Solids under Strain. *Soft Matter* **2011**. https://doi.org/10.1039/c1sm06051a.

(43) Hohlfeld, E.; Mahadevan, L. Scale and Nature of Sulcification Patterns. *Phys. Rev. Lett.* **2012**. https://doi.org/10.1103/PhysRevLett.109.025701.

(44) Cai, S.; Chen, D.; Suo, Z.; Hayward, R. C. Creasing Instability of Elastomer Films. *Soft Matter* **2012**. https://doi.org/10.1039/c2sm06844c.

(45) Weiss, F.; Cai, S.; Hu, Y.; Kyoo Kang, M.; Huang, R.; Suo, Z. Creases and Wrinkles on the Surface of a Swollen Gel. *J. Appl. Phys.* **2013**, *114* (7). https://doi.org/10.1063/1.4818943.

(46) Trujillo, V.; Kim, J.; Hayward, R. C. Creasing Instability of Surface-Attached Hydrogels. *Soft Matter* **2008**, *4* (3), 564. https://doi.org/10.1039/b713263h.

(47) DuPont Jr., S. J.; Cates, R. S.; Stroot, P. G.; Toomey, R. Swelling-Induced Instabilities in Microscale, Surface-Confined Poly(N-Isopropylacryamide) Hydrogels. *Soft Matter* **2010**, *6* (16), 3876. https://doi.org/10.1039/c0sm00021c.

(48) Kim, J.; Yoon, J.; Hayward, R. C. Dynamic Display of Biomolecular Patterns through an Elastic Creasing Instability of Stimuli-Responsive Hydrogels. *Nat. Mater.* **2010**, *9* (2), 159–164. https://doi.org/10.1038/nmat2606.

(49) Yoon, J.; Bian, P.; Kim, J.; McCarthy, T. J.; Hayward, R. C. Local Switching of Chemical Patterns through Light-Triggered Unfolding of Creased Hydrogel Surfaces. *Angew. Chemie - Int. Ed.* **2012**, *51* (29), 7146–7149. https://doi.org/10.1002/anie.201202692.

(50) Xu, B.; Hayward, R. C. Low-Voltage Switching of Crease Patterns on Hydrogel Surfaces. *Adv. Mater.* **2013**. https://doi.org/10.1002/adma.201300968.

(51) Chen, D.; Hyldahl, R. D.; Hayward, R. C. Creased Hydrogels as Active Platforms for Mechanical Deformation of Cultured Cells. *Lab Chip* **2015**, *15* (4), 1160–1167. https://doi.org/10.1039/c4lc01296h.

(52) Arifuzzaman, M.; Wu, Z. L.; Kurokawa, T.; Kakugo, A.; Gong, J. P. Swelling-Induced Long-Range Ordered Structure Formation in Polyelectrolyte Hydrogel. *Soft Matter* **2012**. https://doi.org/10.1039/c2sm25814e.

(53) Arifuzzaman, M.; Wu, Z. L.; Takahashi, R.; Kurokawa, T.; Nakajima, T.; Gong, J. P. Geometric and Edge Effects on Swelling-Induced Ordered Structure Formation in Polyelectrolyte Hydrogels. *Macromolecules* **2013**. https://doi.org/10.1021/ma401773w.

(54) Chan, E. P.; Karp, J. M.; Langer, R. S. A "Self-Pinning" Adhesive Based on Responsive Surface Wrinkles. *J. Polym. Sci. Part B Polym. Phys.* **2011**, *49* (1), 40–44. https://doi.org/10.1002/polb.22165.

(55) Bouklas, N.; Huang, R. Swelling Kinetics of Polymer Gels: Comparison of Linear and Nonlinear Theories. *Soft Matter* **2012**. https://doi.org/10.1039/c2sm25467k.

(56) Tanaka, T.; Hocker, L. O.; Benedek, G. B. Spectrum of Light Scattered from a Viscoelastic Gel. *J. Chem. Phys.* **1973**. https://doi.org/10.1063/1.1680734.

(57) Tanaka, T.; Fillmore, D. J. Kinetics of Swelling of Gels. *J. Chem. Phys.* **1979**, *70* (3), 1214–1218. https://doi.org/10.1063/1.437602.

(58) Biot, M. A. General Theory of Three-Dimensional Consolidation. *J. Appl. Phys.* **1941**. https://doi.org/10.1063/1.1712886.

(59) Scherer, G. W. Drying Gels. VIII. Revision and Review. *J. Non. Cryst. Solids* **1989**. https://doi.org/10.1016/0022-3093(89)90029-X.

(60) Doi, M. Gel Dynamics. *J. Phys. Soc. Japan* **2009**, *78* (5), 1–19. https://doi.org/10.1143/JPSJ.78.052001.

(61) Galli, M.; Comley, K. S. C.; Shean, T. A. V.; Oyen, M. L. Viscoelastic and Poroelastic Mechanical Characterization of Hydrated Gels. *J. Mater. Res.* **2009**. https://doi.org/10.1557/jmr.2009.0129.

(62) Hu, Y.; Zhao, X.; Vlassak, J. J.; Suo, Z. Using Indentation to Characterize the

Poroelasticity of Gels. *Appl. Phys. Lett.* **2010**. https://doi.org/10.1063/1.3370354.

(63) Durning, C. J.; Morman, K. N. Nonlinear Swelling of Polymer Gels. *J. Chem. Phys.* **1993**, *98* (5), 4275–4293. https://doi.org/10.1063/1.465034.

(64) Rajagopal, K. R. Diffusion through Polymeric Solids Undergoing Large Deformations. *Materials Science and Technology*. 2003. https://doi.org/10.1179/026708303225004729.

(65) Hong, W.; Zhao, X.; Zhou, J.; Suo, Z. A Theory of Coupled Diffusion and Large Deformation in Polymeric Gels. *J. Mech. Phys. Solids* **2008**. https://doi.org/10.1016/j.jmps.2007.11.010.

(66) Baek, S.; Srinivasa, A. R. Diffusion of a Fluid through an Elastic Solid Undergoing Large Deformation. *Int. J. Non. Linear. Mech.* **2004**. https://doi.org/10.1016/S0020-7462(02)00153-1.

(67) Yoon, J.; Cai, S.; Suo, Z.; Hayward, R. C. Poroelastic Swelling Kinetics of Thin Hydrogel Layers: Comparison of Theory and Experiment. *Soft Matter* **2010**, *6* (23), 6004–6012. https://doi.org/10.1039/c0sm00434k.

(68) Franssila, S. *Introduction to Microfabrication*; 2010. https://doi.org/10.1002/9781119990413.

(69) Dormán, G.; Prestwich, G. D. Benzophenone Photophores in Biochemistry. *Biochemistry* **1994**. https://doi.org/10.1021/bi00185a001.

(70) Prucker, O.; Naumann, C. A.; Rühe, J.; Knoll, W.; Frank, C. W. Photochemical Attachment of Polymer Films to Solid Surfaces via Monolayers of Benzophenone Derivatives. *J. Am. Chem. Soc.* **1999**. https://doi.org/10.1021/ja990962+.

(71) Scott, G. Mechanisms of Photophysical Processes and Photochemical Reactions in Polymers: Theory and Applications J. F. Rabek, John Wiley and Sons, Chichester, 1987. Pp. Xix + 756, Price £99.00. ISBN 0-47 1-9 11 80-1. *Br. Polym. J.* **1988**. https://doi.org/10.1002/pi.4980200510.

(72) Li, G.; He, G.; Zheng, Y.; Wang, X.; Wang, H. Surface Photografting Initiated by Benzophenone in Water and Mixed Solvents Containing Water and Ethanol. *J. Appl. Polym. Sci.* **2012**. https://doi.org/10.1002/app.34683.

(73) Higuchi, H.; Yamashita, T.; Horie, K.; Mita, I. Photo-Cross-Linking Reaction of Benzophenone-Containing Polyimide and Its Model Compounds. *Chem. Mater.* **1991**. https://doi.org/10.1021/cm00013a038.

(74) Christensen, S. K.; Chiappelli, M. C.; Hayward, R. C. Gelation of Copolymers with Pendent Benzophenone Photo-Cross-Linkers. *Macromolecules* **2012**, *45* (12), 5237–5246. https://doi.org/10.1021/ma300784d.

(75) Lin, A. A.; Sastri, V. R.; Tesoro, G.; Reiser, A.; Eachus, R. On the Crosslinking Mechanism of Benzophenone-Containing Polyimides. *Macromolecules* **1988**. https://doi.org/10.1021/ma00182a052.

(76) Kim, J.; Hanna, J. A.; Byun, M.; Santangelo, C. D.; Hayward, R. C. Designing Responsive Buckled Surfaces by Halftone Gel Lithography. *Science (80-.).* **2012**. https://doi.org/10.1126/science.1215309.

(77) Kim, J.; Hanna, J. A.; Hayward, R. C.; Santangelo, C. D. Thermally Responsive Rolling of Thin Gel Strips with Discrete Variations in Swelling. *Soft Matter* **2012**. https://doi.org/10.1039/c2sm06681e.

(78) Chopra, K. L.; Paulson, P. D.; Dutta, V. Thin-Film Solar Cells: An Overview. *Prog. Photovoltaics Res. Appl.* **2004**. https://doi.org/10.1002/pip.541.

(79) Mahan, J. E. Physical Vapor Deposition of Thin Films. *Physical Vapor Deposition of Thin Films, by John E. Mahan, pp. 336. ISBN 0-471-33001-9. Wiley-VCH , January 2000.* 2000.

(80) Martin, P. M. *Introduction to Surface Engineering and Functionally Engineered Materials*; 2011. https://doi.org/10.1002/9781118171899.

(81) Holmberg, K.; Mathews, A. Coatings Tribology: A Concept, Critical Aspects and Future Directions. *Thin Solid Films* **1994**. https://doi.org/10.1016/0040-6090(94)90315-8.

(82) Li, Y.; Mann, D.; Rolandi, M.; Kim, W.; Ural, A.; Hung, S.; Javey, A.; Cao, J.; Wang, D.; Yenilmez, E.; et al. Preferential Growth of Semiconducting Single-Walled Carbon Nanotubes by a Plasma Enhanced CVD Method. *Nano Lett.* **2004**. https://doi.org/10.1021/nl035097c.

(83) Hozumi, A.; Takai, O. Preparation of Ultra Water-Repellent Films by Microwave Plasma-Enhanced CVD. *Thin Solid Films* **1997**. https://doi.org/10.1016/S0040-6090(97)00076-X.

CHAPTER 2

DEVELOPMENT OF HYDROGEL-BASED CELL SCTRETCHING DEVICES AS *IN VITRO* MODELS OF ATHEROSCLETOTIC WALLS

2.1 Introduction

Atherosclerosis is the hardening and narrowing of arteries caused by the accumulation of plaque[1]. It is a slowly progressing disease that limits blood flow, thus restricting the amount of oxygen and other nutrients transported to the body. Furthermore, the built-up plaque is a threat to cause blood clots that can block the artery and is the leading cause of heart attacks and strokes. Despite the prevalence of atherosclerosis in the general population, much about the underlying biology of the disease is unknown and is the subject of ongoing research[2,3].

It is known that atherosclerosis develops by the dedifferentiation of smooth muscle cells (SMCs)[4,5]. Unlike many muscle cell types, mature vascular SMCs are not terminally differentiated, and can alter their phenotype in response to environmental cues and extracellular signals[6]. SMCs in healthy blood vessels adopt a contractile phenotype and act to regulate both blood pressure and blood flow, whereas the SMCs involved in pathogenesis of atherosclerosis are synthetic phenotype[7,8]. If an SMC dedifferentiates from a contractile phenotype to a synthetic phenotype, it will experience elasticity decrease and shape change from spindle to rhomboid. More importantly, it will have higher migration

activity and invade into the intima, where it can proliferate faster and produce more ECM proteins, which further stiffens the affected artery wall[9,10].

It is known that cell function is regulated by the combined effect of inter-cellular interactions, ECM components, chemical conditions and mechanical cues[11,12]. The complexity of native biological environments makes it difficult to isolate the effect of a specific factor on SMC differentiation *in vivo*. To overcome this limitation, there is significant interest in developing *in vitro* platforms where several variables can be independently controlled to systematically probe the effect of biological cues and environment on the behavior of SMCs[11,13–16].

Depending on the material of the substrate, there are two main categories of biologically-relevant *in vitro* platforms. For research that focuses on monitoring the mechanotransduction of SMCs when subject to active, especially cyclic, stretching, silicone-based flexible substrate or matrix are widely used, among which Flexcell® Tension System and STREX Cell Stretching System are the most commonly used systems[17–20]. These pneumatically controlled devices can provide macroscopic strain with fast speed and high accuracy, but they have limited selections of substrate moduli, and the silicone-based material system limits the possibilities of surface modifications to increase physiological-relevancy. Also, these systems operate by macroscopic deformation, so the cells are constantly moving in relative to the observing microscope, which makes it difficult to monitor the stretching deformation of a single cell. Furthermore, the cells on one substrate are under the same strain condition, surface chemistry and substrate stiffness, not allowing for high-throughput analysis of cells under different conditions. Due to these limitations of silicone-based flexible substrate, there are increasing research efforts contributed to

designing and constructing hydrogel-based cell culture substrates. Hydrogel materials are biocompatible, and they offer great tunability in substrate properties, making them excellent candidates to mimic the ECM for *in vitro* experiments. Hydrogels can be made from biologically derived networks, such as alginate[21] and Type I collagen[22], as well as synthetic polymers, such as polyacrylamide (PAA)[23] and poly(ethylene glycol) (PEG)[24]. Biological hydrogels usually inherently contain integrin-binding domains, so they are closer to the living conditions of cells *in vivo* and easier to adapt, but the substrate modulus and integrin-binding content cannot be tuned independently[25]. On the other hand, synthetic hydrogels can be engineered to change one factor while maintaining other conditions the same, rendering these system suitable for systematic *in vitro* study[26–29]. However, currently these systems are used to analyze the effect of static factors (substrate modulus, integrin-binding and the differentiation/growth media) on the phenotype change of SMCs[30], but not capable of offering active stretching cycles, making these systems less physiologically relevant the actual living conditions of SMCs. So it is highly desired to develop an *in vitro* platform that can offer both materials property tunability and active mechanical straining.

It has been reported that a hydrogel-based active platform has been developed for the study of mechanical deformation on cultured cells[31]. This active platform used patterned surface creases on a constrained hydrogel to exert tensile strain on cells seeded onto the gel, as shown in Figure 2-1. Upon swelling, the confined gel experienced equibiaxial compression and buckled into creases above the critical strain. The designed topographical features on the substrate directed the shape and position of creases[32], thus the cell seeded in between two neighboring parallel creases were stretched under plane strain. Furthermore, because the swelling of the hydrogel is responsive to the environmental temperature change, the

depth of the creases, and thus the strain imposed on the attached cells, can be controlled by the ambient temperature of the water bath. While this concept of profiling single cell response to stretching has already been proved to be feasible, there are shortcomings of this platform. Firstly, the environmental temperature change was slow because it was achieved by adjustment of media bath temperature. The operating frequency (~30 min/cycle) of the device was not representative of physiological condition[33]. Also, this device was not suitable for high-throughput design because it was restricted to one hydrogel with one surface peptide functionality, and offered the same actuation condition across every crease on the same chip.

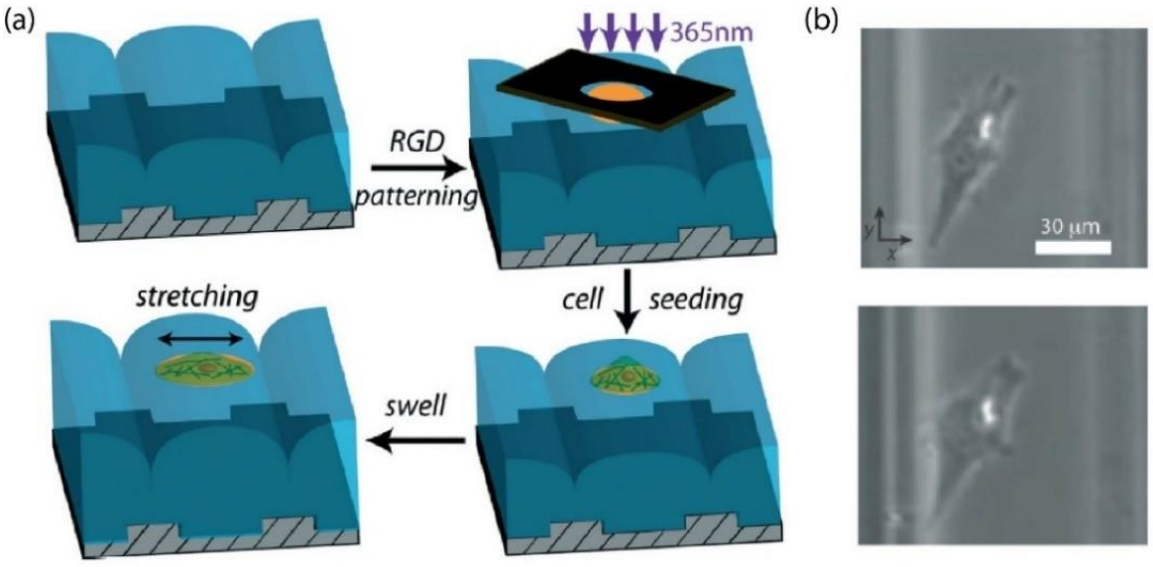

Figure 2- 1 (a) A schematic illustration of the prototypic cell stretching device with creased hydrogels. (b) Optical microscope pictures of C2C12 myoblast cells subjected to strains in the x-direction of (upper) 0 at 37 ℃ and (lower) 20% at 26 ℃. (Figure Reproduced from Ref. 30 with permission from The Royal Society of Chemistry.)

Building upon the prototype cell stretching platform described above, a physiologically relevant cell stretching platform to study the response of SMCs to different factors is developed. This micro-heater driven hydrogel-based cell stretching device can operate at a frequency that is similar to resting pulse rates (≈1 Hz), and the temperature is near body temperature (≈37 ℃). This active cell stretching device includes several improvements and overcomes the major shortcomings of the previous device design. The device structure is shown in Figure 2-2. First and foremost, faster kinetics are achieved by regional temperature control and actuation. Micro-heaters are embedded under the temperature-responsive hydrogels, providing fast temperature change by Joule heating instead of slow heating of the entire bath, and at the same time, reducing the distance over which water molecules must be transported in and out of the poroelastic hydrogel network when driven by osmotic pressure. Another merit of the micro-heaters is the controllability of frequency, amplitude and actuation area by altering the electric signal input and the dimension of the micro-heaters. Secondly, the important features that control cell response *in vivo*, such as substrate stiffness, cell stretch ratio, and cell matric interactions can be individually altered by adjusting the hydrogel composition, tuning the electrical input, and changing the chemical modification on the hydrogel surface, respectively. This allows for a systematic method to characterize the single cell response to stretching and how each physiological factor influences cell behaviour. Finally, the platform has the potential to be scaled up to high-throughput arrays, where different stretch regimes are applied to individual cells on different integrin-binding patches on a single chip.

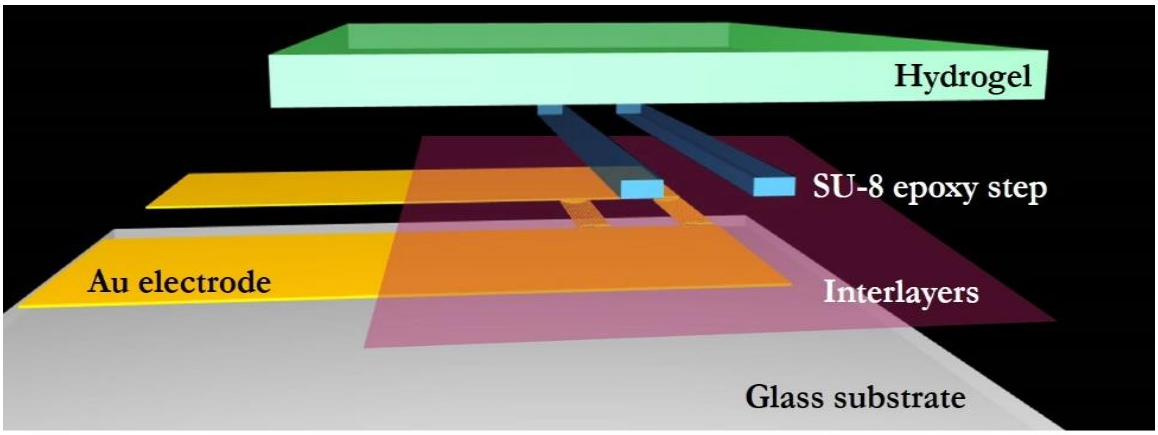

Figure 2-2 Schematic of the micro-heater driven hydrogel-based cell stretching platform.

2.2 Materials and methods

This work is in collaboration with the Peyton Group in Chemical Engineering at UMass Amherst. We focus on device design, fabrication and evaluation, while the Peyton group carries out peptide synthesis, cell culture and phenotype characterization.

2.2.1 Microfabrication

The micro-heaters were fabricated by a photolithography – metal deposition – lift-off process. Coverslip substrates were cleaned by sequential sonication in water, ethanol and acetone for 10 min each. After cleaning, negative tone photoresist NR9-1000PY was used to pattern the substrates via photolithography performed on a Suss MicroTech Mask Aligner. Then a 200 nm thick gold layer was deposited onto the template following the deposition of a 10 nm chromium adhesion layer by CHA Electron Beam Evaporator with Cryopump, followed by another 10 nm chromium adhesion layer. The micro-heater circuits were harvested after a lift-off process in acetone.

To prevent current leakage from the heating circuit, an 350 nm insulation layer of silicon dioxide was deposited onto part of the substrate by plasma enhanced chemical vapor deposition using an STS Vision 310 PECVD System, while leaving part of the circuit not covered for connection to the function generator signal source.

The topographical features on the substrate were fabricated by photolithography of SU-8 (MicroChem), an epoxy-based negative photoresist. A 500 nm thick film of SU-8 2000.5 was firstly overlaid on the insulating SiO_2 by photolithography to promote adhesion, then SU-8 2050 photoresist was spin-coated onto the substrate to achieve 40 μm thickness, followed by exposure under UV light (356 nm) and development in propylene glycol methyl ether acetate (PGMEA). The SU-8 surface was then treated by a monolayer of benzophenone to covalently bond the upcoming hydrogel network to the epoxy substrate[34].

2.2.2 Preparation of surface attached hydrogels

The temperature responsive hydrogel was prepared from a degassed aqueous pre-gel solution containing 811.7 mM N-isopropylacrylamide (NIPAM), 81.2 mM sodium acrylate (NaAc), and 6.3 mM N,N'-methylenebisacrylamide (BisAA). Methacrylate functionalized Rhodamine B was added to the pre-gel solution to prepare fluorescent hydrogels used for confocal microscopy. For every 200 μL of pre-gel solution, 1.5 μL of N,N,N',N'-tetramethylethylenediamine was added as catalyst and then 1.5 μL of a 10 wt% aqueous ammonium persulfate solution was added as initiator. Immediately after initiation, the mixture was loaded between a methacryloxypropyltrichlorosilane treated substrate and a (tridecafluoro-1,1,2,2-tetrahydrooctyl)dimethylchlorosilane treated release coverslip separated by 300 HN Kapton spacers, defining the hydrogel thickness to be 75 μm. The

gelation process was allowed to proceed for over 30 min in a vessel constantly purged with nitrogen. The gelation process is under 365 nm UV light to activate the benzophenone into radicals, covalently anchoring the formed hydrogel network to the substrate.

It should be noted that the hydrogel composition can be engineered to different stiffness, as shown in Table 2-1. The storage modulus (G') and loss modulus (G'') of each hydrogel composition were characterized by rheometer, and the Young's modulus was estimated from the equation $E = 2G(1 + \nu)$, where ν is Poisson's ratio, taken as 0.5 for hydrogels.

Table 2- 1 Hydrogel compositions and moduli

	NIPAM		BisAA		NaAc		G' (Pa)	G" (Pa)	E (est) (kPa)
No.	(mM)	(Wt%)	(mM)	(Wt%)	(mM)	(Wt%)			
1	322	3.5	2.5	0.037	32.1	0.29	550	80	1.6
2	644	6.7	5	0.07	64.3	0.56	3800	20	12
3	644	6.6	15	0.2	193	1.6	4900	200	15
4	861	8.6	15	0.2	258	2.14	5500	200	17
5	1072	10.4	15	0.2	322	2.6	7000	200	21
6	1288	12.2	15	0.2	385	3.0	7800	200	24
7	1610	14.9	11	0.14	322	2.5	15500	400	46
8	1610	14.5	22.5	0.28	635	4.8	24500	500	73

2.2.3 Photo-patterning of peptide cocktail on hydrogel surfaces

Following gelation, the hydrogel surface was patterned with patches of peptides, as markers to control the cell seeding positions, so that SMCs can be stretched as designed/ facilitate the selective seeding of SMCs. As shown in Table 2-1, there were two sets of peptide cocktail compositions mimicking the integrin-binding sites of an artery with atherosclerosis and a healthy artery, respectively[35–39]. All peptides were synthesized using a Liberty Blue Microwave peptide synthesizer and were modified with benzophenone end

groups to allow for UV crosslinking. After applying 10 μL of 0.1 mg/mL peptide in PBS solution onto the hydrogel surface, mask-free photolithography was performed with a pattern of UV light (365 nm, pE-100, CoolLED) generated using a digital micromirror device (DLP Discovery 4100, 0.7 XGA, Texas Instruments) attached to an inverted optical microscope (Nikon ECLIPSE Ti). Finally, the hydrogel was washed with fresh PBS to remove the unattached peptide.

Table 2- 2 Peptide cocktail compositions

Peptide cocktail	Sequence	% Weight	% Molar
Healthy cocktail	**Collagen III** BP-CGPGPPGPPGPPGPPGPPGAOGERGPPGPP GPPGPPGPP	70%	41%
	Collagen I BP-CGPGPPGPPGPPGPPGPPGFOGERGPPGPP GPPGPPGPP	15%	25%
	Elastin BP-GCGVGVAPG	15%	34%
Unhealthy cocktail (Athero cocktail)	**Collagen I** BP-CGPGPPGPPGPPGPPGPPGFOGERGPPGPP GPPGPPGPP	40%	21.5%
	Fibronectin BP-CG-PHSRN-GGGGGG-RGD-S	40%	46%
	Osteopontin BP-CGG-SVVYGLR	20%	32.5%

Primary human aortic smooth muscle cells (HASMCs) were purchased from a commercial source and routinely cultured in Dulbecco's Modified Eagle Medium (DMEM, Fisher Scientific) supplemented with HEPES (Fisher Scientific) as the buffer, 10% fetal bovine serum (FBS, Fisher Scientific) and 1% penicillin/streptomycin (P/S, Fisher Scientific) at 37°C. Cells between passages 4–12 were used for all experiments. Cells were seeded on

the peptide patterned hydrogels and incubated for 96 hours in CO_2 free incubator before device actuation.

2.2.4 Characterization methods

To characterize the temperature of the gel surface above a microheater, a 24-gauge flexible microprobe (5.5 Hz, IT-24P from Physitemp) was connected to a MAX 6675 signal amplifier and then to an Arduino Uno board, which finally transmit the acquired temperature data to a laptop.

A Nikon A1R Multiphoton laser scanning confocal fluorescence microscope was used to characterize the 3D shape of the hydrogel devices at different temperatures. The 3D-stacked confocal images were generated by Nikon's Confocal NIS-Elements software.

A Keithley 3390 function generator was used to drive the micro-heaters. Ga-In liquid alloy was used to promote connection between needle from micro-positioner (Quarter) and the micro-heater.

The actuation was observed under a Zeiss optical microscope and recorded by ZEN software. The images were analyzed by Image-J, and the tracking was accomplished by Tracker software.

2.3 Results and discussion

2.3.1 Microheater and temperature change

The designed shape and dimension of the micro-heaters are shown in Figure 2-3(a). In order to locally change the temperature to actuate two parallel creases, the micro-heaters

were designed in pairs. They were separated by 100 μm, which was comparable to the length of a single HASMC. The micro-heaters were designed to be double-spiral for a more uniform temperature spatial profile[40]. The microheater devices was made of gold of 200 nm thickness, thus the resistance can be calculated to be $R = \frac{\rho L}{S} = 78\,\Omega$.

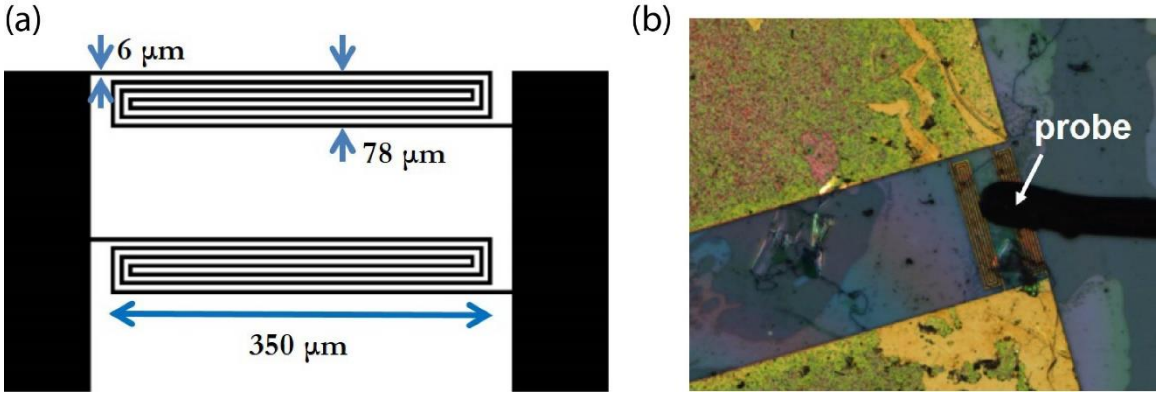

Figure 2- 3 (a) Micro-heater design and dimensions; (b) Micro-probe detecting temperature change.

The local temperature will change upon the cyclic heating of the micro-heaters, and this change is highly dependent on the spatial position. The relevant position of interest is where the cell would occupy, i.e. on the gel surface in the middle of two neighboring micro-heaters. So a micro-probe is placed in the desired position using a micro-manipulator, as shown in Figure 2-3(b).

Figure 2-4(a) shows the temperature read-out of a system operating under 1.5 V at 1 Hz (0.5 s on, 0.5 s off). The y-axis is the temperature change in comparison to the ambient temperature, $T-T_0$. The first few cycles showed a trend of temperature elevation until the system reached thermal steady state after ~10 s, where the highest temperature in the 'on' state, and the lowest temperature in the 'off' state were constant for each cycle. The

temperature increase above ambient temperature for 'on' and 'off' state were 7.9 ± 0.7 ℃ and 4.4 ± 0.6 ℃, respectively.

When the micro-heaters are driven at a different voltage, the heating power is different, so the highest temperature when the heater is on and the lowest temperature when the heater is off will change accordingly. The high and low temperature for different operating voltages is shown in Figure 2-4(b). The greater the temperature difference between the high point and the low point of the heating cycle, the larger the swelling ratio change, and thus the higher the strain exerted on the cell in the center.

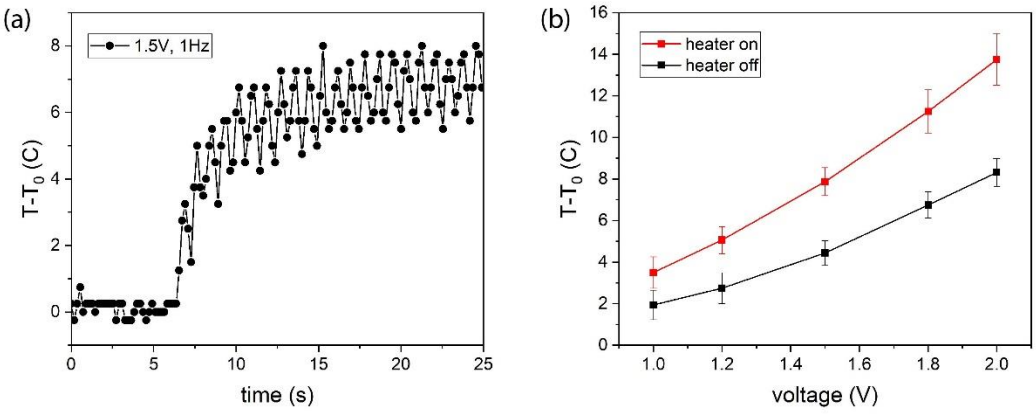

Figure 2- 4 Performance of micro-heaters under the hydrogel. (a) Temperature change when the micro-heaters are driven at 1Hz, 1.5V. (b) Gel surface temperature when micro-heaters are on and off at different input voltage.

It is important to choose a suitable operating voltage, because the temperature change being either too large or too small will render the system less physiologically relevant. If the operating voltage is too low and the temperature difference between the high point and the low point is too small, the mechanical stretch exerted on the cell will be too small comparing to the *in vivo* conditions. On the other hand, if the operating voltage is too high, not only the mechanical strain will be too high due to the large swelling ratio change, but

also the living cells on the gel surface will experience drastic cyclic temperature change. Thus, 1.5 V was chosen as the operating voltage as it gave a physiological temperature variation range as well as sufficient dynamic swelling to produce creases that strain the cells at physiologically-relevant strains[41–43]. To mimic physiological temperature, the ambient temperature was changed in the incubation box so that the high and low temperature during actuation was approximately 39 ℃ and 35 ℃.

2.3.2 Responsive swelling/deswelling and crease depth

With the micro-heater system fabricated and characterized, it was important to understand the swelling behavior of the hydrogel at different temperatures. The 3-D shape of a device was inspected using laser scanning confocal microscopy and reconstructed by z-stacking the captures slices at different thickness position.

From a starting temperature of 26 ℃, 1.1 V and 0.8 V direct current was used to elevate the temperature to 39 ℃ and 35 ℃, respectively, matching the peak and valley temperatures during a heating cycle. As shown in Figure 2-5, the hydrogel had a higher swelling ratio at lower temperature, so the creases were deeper and thus the stretch ratio applied to the hydrogel surface was higher. On the contrary, when local temperature was raised, the hydrogel swelled less, leading to a decrease in the crease depth and thus the stretch applied to the hydrogel surface was lower. If we used the contour length change along the gel surface between two crease tips as a measure of stretching deformation, then this length was increased from 240 μm to 261 μm by the change of temperature from 39 ℃ to 35 ℃. This suggested that the tensile strain at this cross-section was 8.8%, and it was due to the deepening and relaxing of creases from cyclic temperature change. Also, as the

single HASMC were to be seeded at the apex of arc, it was noted that the z-position of the plane of interest was elevated by 15 μm from 39 ℃ to 35 ℃. Accordingly, adjustments would be made during cell imaging.

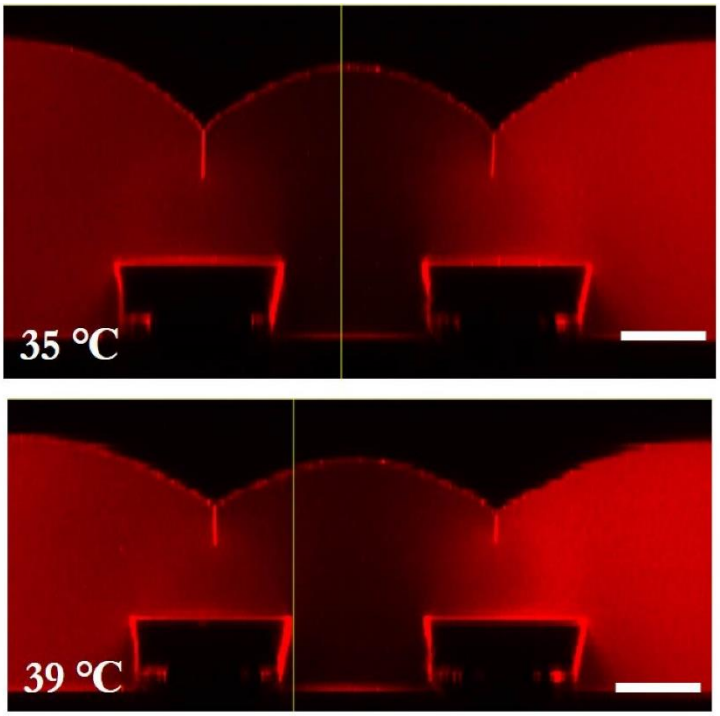

Figure 2- 5 Confocal micrograph of hydrogel cross-section at 35 ℃ (top) and 39 ℃ (bottom) (Scale bar = 50 μm);

2.3.3 Peptide patterning and cell seeding

To seed cells onto soft material surface with a spatially resolved pattern, photo-patterning of light-responsive cell-binding peptides can be used to define cell attachment sites. The peptide was attached to the hydrogel surface via benzophenone chemistry activated under UV light. Figure 2-6 (a) shows the pattern on the maskless photolithography. When the attached peptide was RGD peptide, the lysine on the peptide can be labeled by fluorescein isothiocyanate (FITC) and the fluorescent microscope picture of Figure 2-6 (b) showed the

patterning was successful. The green background corresponds to the non-specific adsorption of FITC molecules into the hydrogel network.

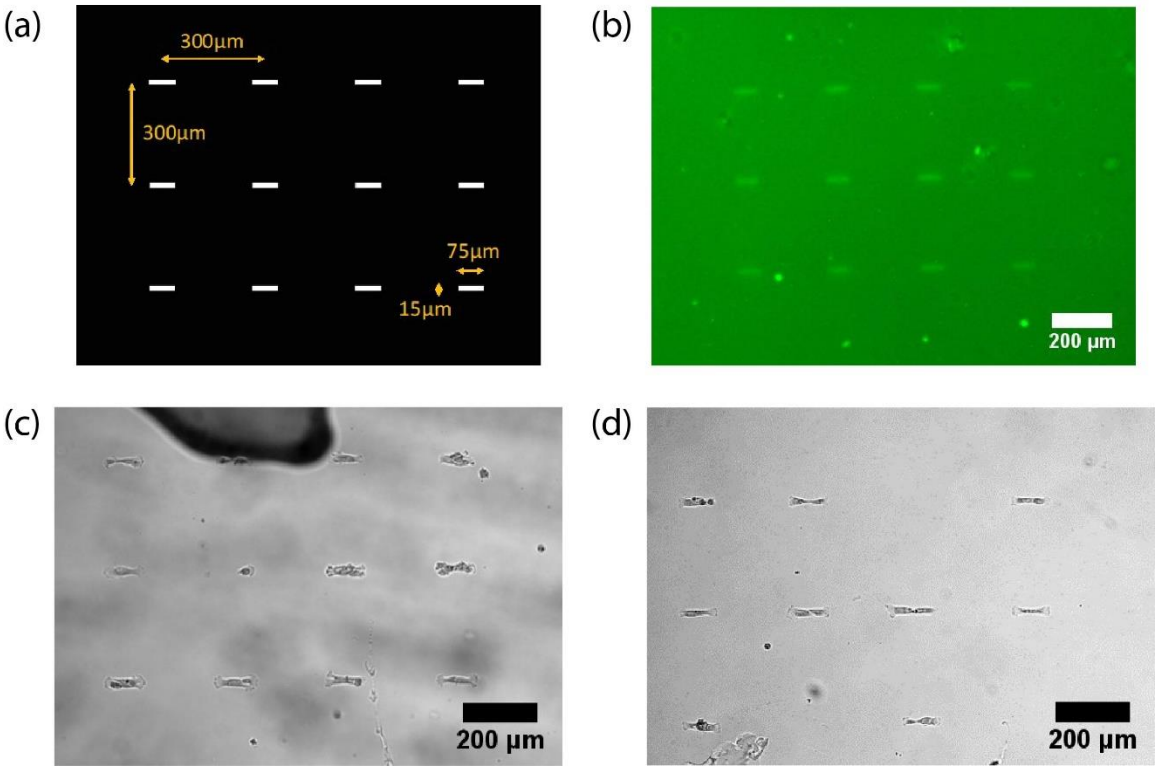

Figure 2- 6 UV-patterning of binding peptide and cell seeding. (a) the mask pattern uploaded to Digital Micro-mirror Devices; (b) Fluorescent microscope picture of the patterned hydrogel surface after FITC labeling; (c) HASMCs cultured on 5 kPa hydrogels patterned with atherosclerosis peptide cocktail. (d) HASMCs cultured on 25 kPa hydrogels patterned with healthy peptide cocktail.

To spatially control the location of HASMCs, we changed the peptide composition to the cocktail shown in Table 2-2, and seeded HASMCs on the patterned gel surface. The cell seeding experiments showed that the peptide patterning was successful and the HASMCs selectively resided on sites patterned with peptides. It should be noted that the pattern shape and dimensions were designed to accommodate one HASMC per site, and the concentration of the peptide cocktail were selected so that enough anchoring was provided

in the patterned surface, while the background absorption is not sufficient for seeding. As shown in Figure 2-6 (c), seeded HASMCs showed the same pattern as the mask when the peptide cocktail mimicking atherosclerosis affected arteries were patterned onto a hydrogel of shear modulus 5 kPa. Figure 2-5 (d) shows the cell positions after the healthy peptide cocktail solution was photo-patterned onto a hydrogel of modulus 25 kPa. These results indicated that this method was a feasible approach to selectively seed cell onto desired location at single cell level.

It was desired to pattern one HASMC per location to cut off the communication between cells. Using the same method, a single HASMC was seeded on the hydrogel surface in the center of two neighboring micro-heaters, as shown in Figure 2-7. The dark lines are part of the micro-heaters and the two grey rectangular pads are the SU-8 steps.

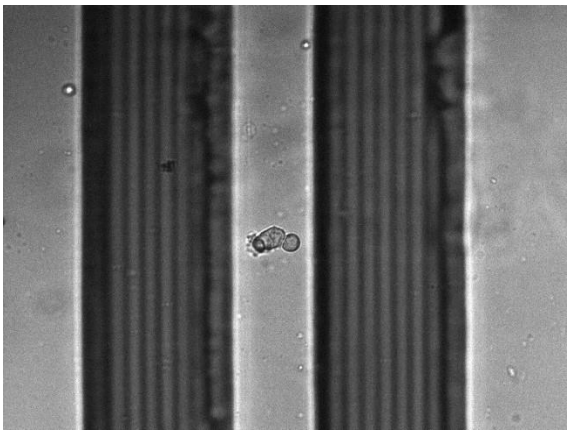

Figure 2-7 One HASMC is patterned in between two micro-heaters.

2.3.4 Cell stretching

When the micro-heaters were cyclically driven to actuate the hydrogel to swell/deswell, the cells were repeatedly stretched and relaxed, as shown in Figure 2-8. Figures 2-8 (a)

shows the optical micrographs of a single HASMC in the relaxed state (up) and under tensile stretch (down). The position of the two ends of the cell were tracked using Tracker software and the distance was plotted against time, as shown in Figure 2-8 (b). The frequency of this cyclic stretching process was calculated by the reciprocal of the time interval between neighboring peaks, and it is calculated that this cell was stretched at a frequency of 0.99 Hz, matching the frequency of the driving voltage. It should be noted this calculation has an uncertainty 0.04 Hz, and it is comes from the limitation of imaging speed, 14 frames per second. The stretch ratio of this SMC, defined as the cell length at elongated state divided by the cell length at relaxed state, was measured to be 6.4 ± 1.0 %. More specifically, the stretch ratio was obtained by dividing the maximum length of each cycle by the minimum length of the same cycle, and the uncertainty came from the variation among the cycles. Besides the cyclic stretching of this SMC, six more stretching experiments were analyzed, as is shown in Figure 2-8 (c). The stretching frequencies were calculated to be 1.01 ± 0.11 Hz, 1.00 ± 0.10 Hz, 1.00 ± 0.17 Hz, 1.02 ± 0.22 Hz, 1.00 ± 0.08 Hz and 0.98 ± 0.03 Hz, respectively, yielding the average stretching frequency to be 1.00 ± 0.10 Hz. The strain ratios were calculated to be 5.9 ± 0.3 %, 5.5 ± 0.2 %, 5.2 ± 0.4 %, 6.9 ± 0.6 %, 6.0 ± 0.4 % and 6.0 ± 0.4 %, respectively, giving the average stretch ratio of 6.0 ± 0.5 %. This result is reasonably close to the rough estimate based on contour length change as discussed above, and is comparable to the physiological stretch that HASMCs experience *in vivo*[44]. Currently, this cell stretching device can operate for as long as 40 minutes and exert steady cyclic strain onto the cell at a constant rate.

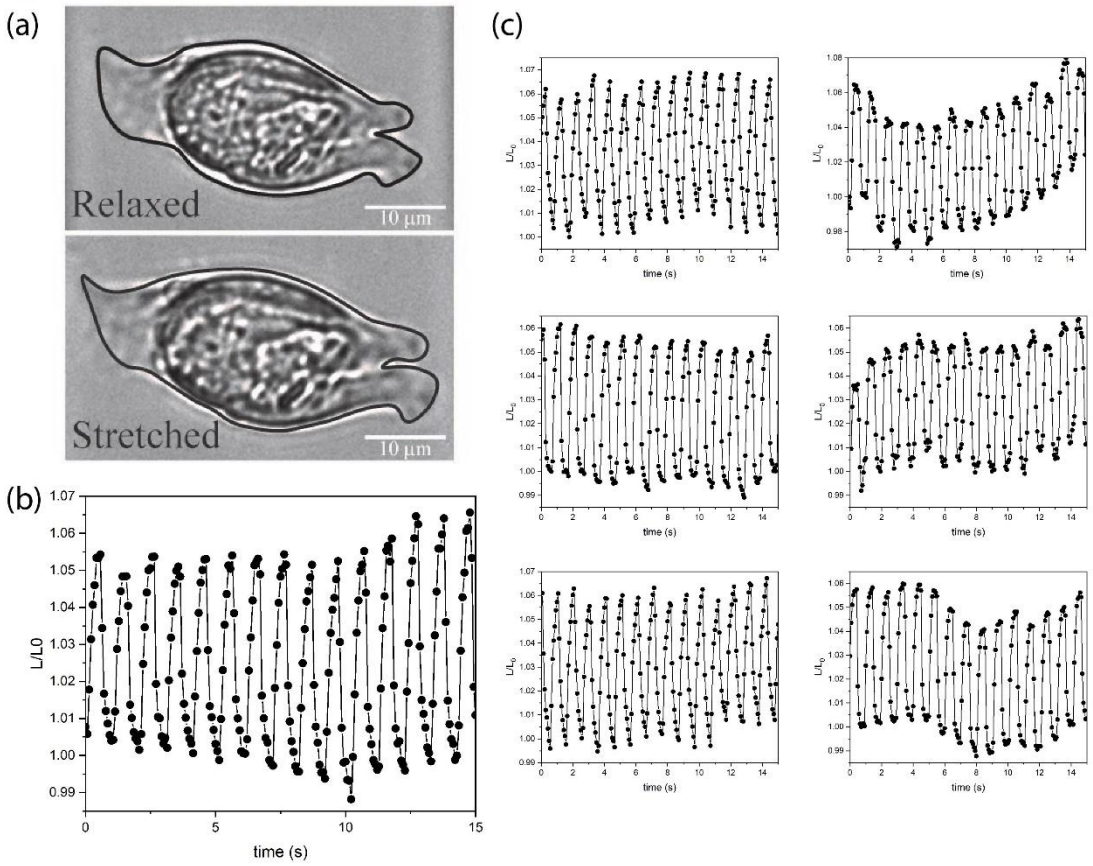

Figure 2- 8 Deformation of a single HASMC under cyclic actuation. (a) Micrograph of an HASMC in the relaxed state (top) and stretched state (bottom); (b) The length of the HASMC change with time during cyclic actuation. (c) the length change of 6 other HASMCs tested

2.3.5 Effect of stretching on cell phenotype

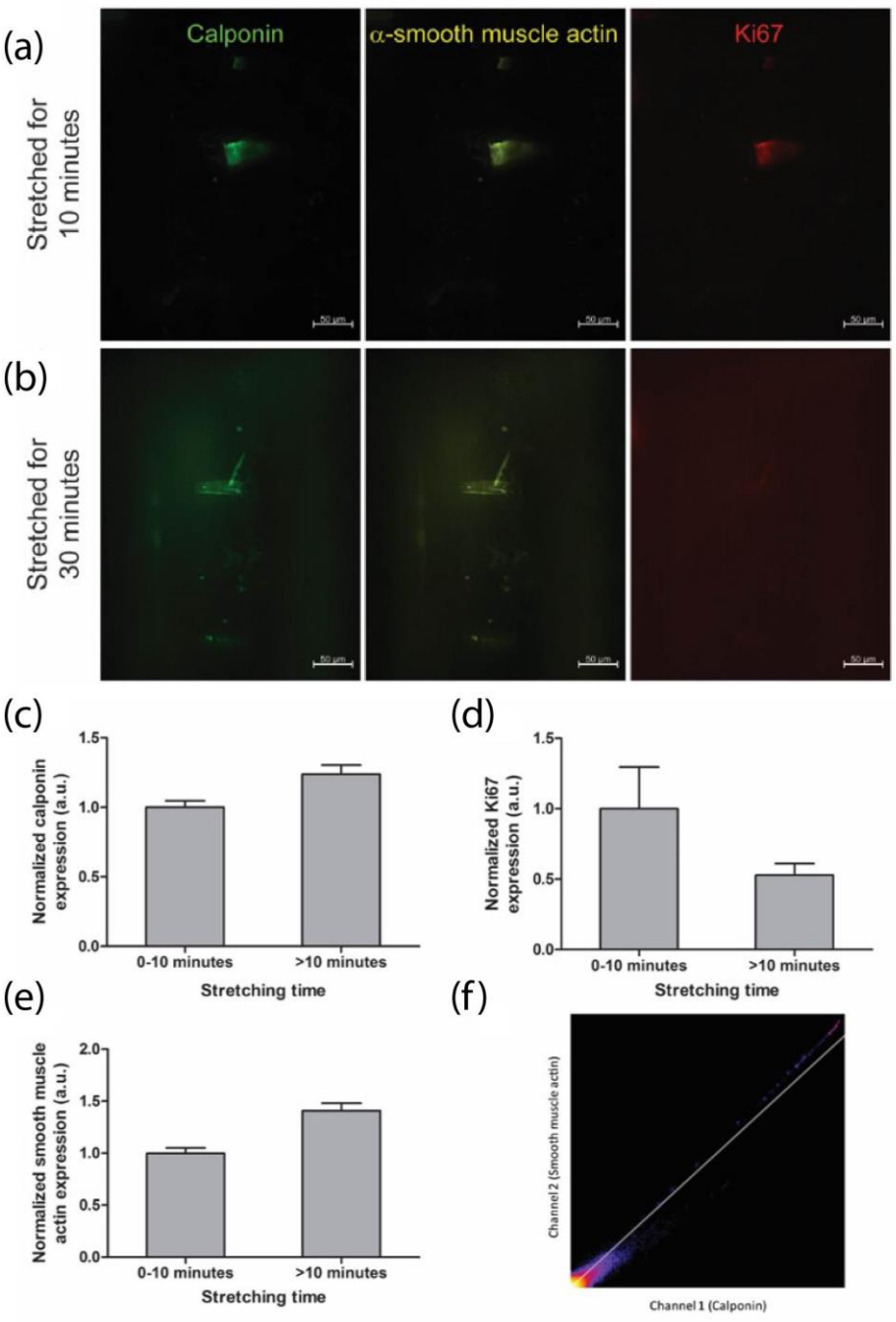

Figure 2- 9 Expression of differentiation markers by smooth muscle cells on SMC stretching device. (a) Calponin, smooth muscle actin and Ki67 expression by SMC stretched for 10 minutes. (b) Calponin, smooth muscle actin and Ki67 expression by SMC stretched for 30 minutes. (c-e) Quantification of expression of (c) calponin, (d) smooth muscle actin and (e) Ki67 in stretched and unstretched cells. (f) Colocalization analysis on calponin and smooth muscle actin expressed by the single SMCs.

It is known that atherosclerosis develops by the dedifferentiation of SMCs. SMCs alter their phenotypes in response to environmental cues and extracellular signals. During atherosclerosis, SMCs dedifferentiate from a contractile phenotype to a synthetic phenotype. More importantly, they have higher migration activity and invade into the tunica intima, where they can proliferate faster and produce more ECM proteins, which further stiffens the affected artery wall.

To obtain the phenotype of the SMCs after stretching, immunofluorescence staining for differentiation markers such as α-smooth muscle actin (α-SMA) and calponin was done as shown in Figure 2-9 (a) and 2-9 (b). The stretched cells were also stained for proliferation marker Ki67. Preliminary staining experiments showed that SMCs assumed differentiated morphology after the stretching as seen *in vivo*. The SMCs stretched for more than 10 minutes (stretched) expressed more α-SMA and calponin than the cells stretched for less than 10 minutes (control), which are quantified in Figure 2-9 (c) and 2-9 (d). α-SMA and calponin were also observed to be colocalized in the stretched cells, with a Pearson's R value of 0.96, as is shown in Figure 2-9 (f). Preliminary result also showed reduced Ki67 expression in the stretched SMCs compared to the control ones as shown in Figure 2-9 (e). Hence, the creased hydrogel-based device provided an *in vitro* cell stretching platform with ECM mimicking peptides to capture ECM-cell interactions.

2.4 Conclusion and future work

We created a well-controlled, biologically-relevant, hydrogel-based *in vitro* cell stretching device. This platform mimicked the active environment that human artery smooth muscle cells (HASMC) live in, providing a platform to study the response of a HASMC to different substrate modulus, mechanical stretch, and insoluble chemical signals. Ultimately, this platform is anticipated to provide insight into how these factors conspire in HASMC dedifferentiation and development of atherosclerosis.

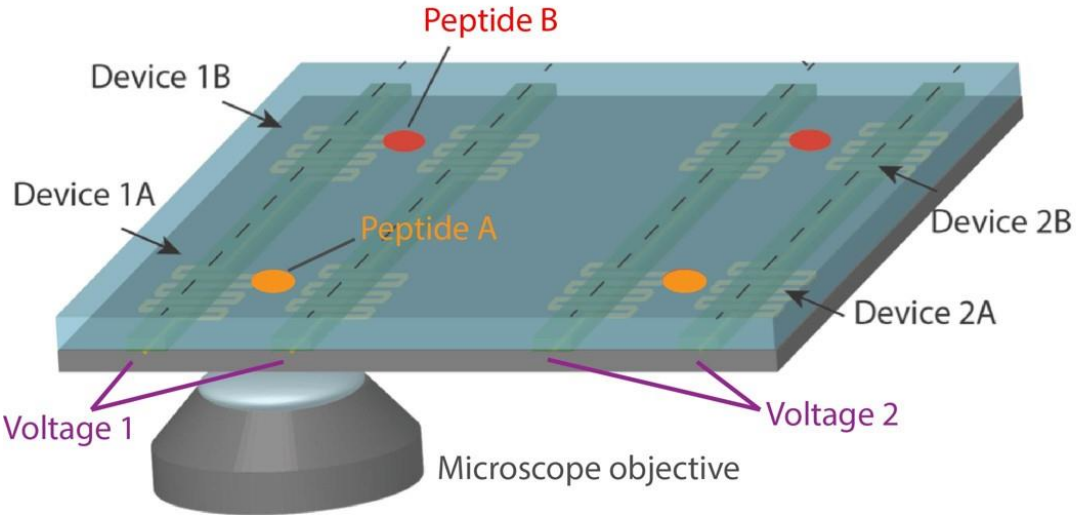

Figure 2- 10 Device design for high-throughput actuation and analysis, where multiple conditions are integrated onto one chip.

This platform has the potential for actuating and analyzing cells in a high throughput fashion. The device can be engineered in chemical integrin-binding motifs, hydrogel modulus and stretch ratio. Different peptide cocktails can be patterned on different regions of the hydrogel surface. With a more complex circuit design, different parts of this device can be actuated at different voltages, thus different stretching strains. It is expected that

future systems will enable the independent control of multiple regions on one device, as is shown in Figure 2-10.

2.5 References

(1) Libby, P.; Ridker, P. M.; Hansson, G. K. Progress and Challenges in Translating the Biology of Atherosclerosis. *Nature*. 2011. https://doi.org/10.1038/nature10146.

(2) Libby, P. Vascular Biology of Atherosclerosis: Overview and State of the Art. In *American Journal of Cardiology*; 2003. https://doi.org/10.1016/S0002-9149(02)03143-0.

(3) Glass, C. K.; Witztum, J. L. Atherosclerosis: The Road Ahead. *Cell*. 2001. https://doi.org/10.1016/S0092-8674(01)00238-0.

(4) Ip, J. H.; Fuster, V.; Badimon, L.; Badimon, J.; Taubman, M. B.; Chesebro, J. H. Syndromes of Accelerated Atherosclerosis: Role of Vascular Injury and Smooth Muscle Cell Proliferation. *Journal of the American College of Cardiology*. 1990. https://doi.org/10.1016/0735-1097(90)92845-S.

(5) Li, Z.; Cheng, H.; Lederer, W. J.; Froehlich, J.; Lakatta, E. G. Enhanced Proliferation and Migration and Altered Cytoskeletal Proteins in Early Passage Smooth Muscle Cells from Young and Old Rat Aortic Explants. *Exp. Mol. Pathol.* **1997**, *64* (1), 1–11. https://doi.org/10.1006/exmp.1997.2204.

(6) Stegemann, J. P. Mechanical, Biochemical, and Extracellular Matrix Effects on Vascular Smooth Muscle Cell Phenotype. *J. Appl. Physiol.* **2005**, *98* (6), 2321–2327. https://doi.org/10.1152/japplphysiol.01114.2004.

(7) Gomez, D.; Owens, G. K. Smooth Muscle Cell Phenotypic Switching in Atherosclerosis. *Cardiovasc Res* **2012**, *95* (2), 156–164. https://doi.org/10.1093/cvr/cvs115.

(8) Rensen, S. S. M.; Doevendans, P. A. F. M.; Van Eys, G. J. J. M. Regulation and Characteristics of Vascular Smooth Muscle Cell Phenotypic Diversity. *Netherlands Heart Journal*. 2007. https://doi.org/10.1007/BF03085963.

(9) Milewicz, D. M.; Kwartler, C. S.; Papke, C. L.; Regalado, E. S.; Cao, J.; Reid, A. J. Genetic Variants Promoting Smooth Muscle Cell Proliferation Can Result in Diffuse and Diverse Vascular Diseases: Evidence for a Hyperplastic Vasculomyopathy. *Genetics in Medicine*. 2010. https://doi.org/10.1097/GIM.0b013e3181cdd687.

(10) Blindt, R.; Vogt, F.; Lamby, D.; Zeiffer, U.; Krott, N.; Hilger-Eversheim, K.; Hanrath, P.; Vom Dahl, J.; Bosserhoff, A. K. Characterization of Differential Gene Expression in Quiescent and Invasive Human Arterial Smooth Muscle Cells. *J. Vasc. Res.* **2002**. https://doi.org/10.1159/000065546.

(11) Trappmann, B.; Chen, C. S. How Cells Sense Extracellular Matrix Stiffness: A Material's Perspective. *Curr. Opin. Biotechnol.* **2013**, *24* (5), 948–953. https://doi.org/10.1016/j.copbio.2013.03.020.

(12) Mann, B. K.; Gobin, A. S.; Tsai, A. T.; Schmedlen, R. H.; West, J. L. Smooth Muscle Cell Growth in Photopolymerized Hydrogels with Cell Adhesive and Proteolytically Degradable Domains: Synthetic ECM Analogs for Tissue Engineering. *Biomaterials* **2001**, *22* (22), 3045–3051. https://doi.org/10.1016/S0142-9612(01)00051-5.

(13) Leung, D. Y. M.; Glagov, S.; Mathews, M. B.; Url, S.; Brient, L. V. O. Cyclic Stretching Stimulates Synthesis of Matrix Components by Arterial Smooth Muscle Cells in Vitro Cyclic Stretching Stimulates Synthesis of Matrix Components by Arterial Smooth Muscle Cells in Vitro Abstract . Rabbit Aortic Medial Cells Were Grown on P. **2014**, *191* (4226), 475–477.

(14) Peyton, S. R.; Raub, C. B.; Keschrumrus, V. P.; Putnam, A. J. The Use of Poly(Ethylene Glycol) Hydrogels to Investigate the Impact of ECM Chemistry and Mechanics on Smooth Muscle Cells. *Biomaterials* **2006**, *27* (28), 4881–4893. https://doi.org/10.1016/j.biomaterials.2006.05.012.

(15) Matheson, L. A.; Fairbank, N. J.; Maksym, G. N.; Santerre, J. P.; Labow, R. S. Characterization of the Flexcell™ Uniflex™ Cyclic Strain Culture System with U937 Macrophage-like Cells. *Biomaterials* **2006**. https://doi.org/10.1016/j.biomaterials.2005.05.070.

(16) Chandorkar, Y.; Castro Nava, A.; Schweizerhof, S.; Van Dongen, M.; Haraszti, T.; Köhler, J.; Zhang, H.; Windoffer, R.; Mourran, A.; Möller, M.; et al. Cellular Responses to Beating Hydrogels to Investigate Mechanotransduction. *Nat. Commun.* **2019**, *10* (1), 1–13. https://doi.org/10.1038/s41467-019-11475-4.

(17) Mantella, L. E.; Quan, A.; Verma, S. Variability in Vascular Smooth Muscle Cell Stretch-Induced Responses in 2D Culture. *Vasc. Cell* **2015**, *7* (1), 1–9. https://doi.org/10.1186/s13221-015-0032-0.

(18) Kona, S.; Chellamuthu, P.; Xu, H.; Hills, S. R.; Nguyen, K. T. Effects of Cyclic Strain and Growth Factors on Vascular Smooth Muscle Cell Responses. *Open Biomed. Eng. J.* **2009**, *3* (1), 28–38. https://doi.org/10.2174/1874120700903010028.

(19) Putnam, A. J.; Cunningham, J. J.; Dennis, R. G.; Linderman, J. J.; Mooney, D. J. Microtubule Assembly Is Regulated by Externally Applied Strain in Cultured Smooth Muscle Cells. *J Cell Sci* **1998**, *111 (Pt 2*, 3379–3387. https://doi.org/http://dx.doi.org/10.1016/B978-0-12-374739-6.00011-7.

(20) Liu, G.; Hitomi, H.; Hosomi, N.; Lei, B.; Nakano, D.; Deguchi, K.; Mori, H.; Masaki, T.; Ma, H.; Griendling, K. K.; et al. Mechanical Stretch Augments Insulin-Induced Vascular Smooth Muscle Cell Proliferation by Insulin-like Growth Factor-1 Receptor. *Exp. Cell Res.* **2011**. https://doi.org/10.1016/j.yexcr.2011.07.016.

(21) Rowley, J. A.; Madlambayan, G.; Mooney, D. J. Alginate Hydrogels as Synthetic Extracellular Matrix Materials. *Biomaterials* **1999**. https://doi.org/10.1016/S0142-9612(98)00107-0.

(22) Wozniak, M. A.; Desai, R.; Solski, P. A.; Der, C. J.; Keely, P. J. ROCK-Generated Contractility Regulates Breast Epithelial Cell Differentiation in Response to the Physical Properties of a Three-Dimensional Collagen Matrix. *J. Cell Biol.* **2003**. https://doi.org/10.1083/jcb.200305010.

(23) Pelham, R. J.; Wang, Y. L. Cell Locomotion and Focal Adhesions Are Regulated by Substrate Flexibility. *Proc. Natl. Acad. Sci. U. S. A.* **1997**. https://doi.org/10.1073/pnas.94.25.13661.

(24) Fairbanks, B. D.; Schwartz, M. P.; Halevi, A. E.; Nuttelman, C. R.; Bowman, C. N.; Anseth, K. S. A Versatile Synthetic Extracellular Matrix Mimic via Thiol-Norbornene Photopolymerization. *Adv. Mater.* **2009**. https://doi.org/10.1002/adma.200901808.

(25) Zaman, M. H.; Trapani, L. M.; Siemeski, A.; MacKellar, D.; Gong, H.; Kamm, R. D.; Wells, A.; Lauffenburger, D. A.; Matsudaira, P. Migration of Tumor Cells in 3D Matrices Is Governed by Matrix Stiffness along with Cell-Matrix Adhesion and Proteolysis. *Proc. Natl. Acad. Sci. U. S. A.* **2006**. https://doi.org/10.1073/pnas.0604460103.

(26) Hern, D. L.; Hubbell, J. A. Incorporation of Adhesion Peptides into Nonadhesive Hydrogels Useful for Tissue Resurfacing. *J. Biomed. Mater. Res.* **1998**. https://doi.org/10.1002/(SICI)1097-4636(199802)39:2<266::AID-JBM14>3.0.CO;2-B.

(27) Bryant, S. J.; Anseth, K. S. Controlling the Spatial Distribution of ECM Components in Degradable PEG Hydrogels for Tissue Engineering Cartilage. *J. Biomed. Mater. Res. - Part A* **2003**. https://doi.org/10.1002/jbm.a.10319.

(28) Peyton, S. R.; Putnam, A. J. Extracellular Matrix Rigidity Governs Smooth Muscle Cell Motility in a Biphasic Fashion. *J. Cell. Physiol.* **2005**, *204* (1), 198–209. https://doi.org/10.1002/jcp.20274.

(29) Engler, A.; Bacakova, L.; Newman, C.; Hategan, A.; Griffin, M.; Discher, D. Substrate Compliance versus Ligand Density in Cell on Gel Responses. *Biophys. J.* **2004**. https://doi.org/10.1016/S0006-3495(04)74140-5.

(30) Herrick, W. G.; Rattan, S.; Nguyen, T. V.; Grunwald, M. S.; Barney, C. W.; Crosby, A. J.; Peyton, S. R. Smooth Muscle Stiffness Sensitivity Is Driven by Soluble and Insoluble ECM Chemistry. *Cell. Mol. Bioeng.* **2015**, *8* (3), 333–348. https://doi.org/10.1007/s12195-015-0397-4.

(31) Chen, D.; Hyldahl, R. D.; Hayward, R. C. Creased Hydrogels as Active Platforms for Mechanical Deformation of Cultured Cells. *Lab Chip* **2015**, *15* (4), 1160–1167. https://doi.org/10.1039/c4lc01296h.

(32) Kim, J.; Yoon, J.; Hayward, R. C. Dynamic Display of Biomolecular Patterns through an Elastic Creasing Instability of Stimuli-Responsive Hydrogels. *Nat.*

Mater. **2010**, *9* (2), 159–164. https://doi.org/10.1038/nmat2606.

(33) Kim, B. S.; Nikolovski, J.; Bonadio, J.; Mooney, D. J. Cyclic Mechanical Strain Regulates the Development of Engineered Smooth Muscle Tissue. *Nat. Biotechnol.* **1999**. https://doi.org/10.1038/13671.

(34) Yuk, H.; Zhang, T.; Parada, G. A.; Liu, X.; Zhao, X. Skin-Inspired Hydrogel-Elastomer Hybrids with Robust Interfaces and Functional Microstructures. *Nat. Commun.* **2016**. https://doi.org/10.1038/ncomms12028.

(35) Herrick, W. G.; Nguyen, T. V.; Sleiman, M.; McRae, S.; Emrick, T. S.; Peyton, S. R. PEG-Phosphorylcholine Hydrogels as Tunable and Versatile Platforms for Mechanobiology. *Biomacromolecules* **2013**. https://doi.org/10.1021/bm400418g.

(36) Jufri, N. F.; Mohamedali, A.; Avolio, A.; Baker, M. S. Mechanical Stretch: Physiological and Pathological Implications for Human Vascular Endothelial Cells. *Vascular Cell*. 2015. https://doi.org/10.1186/s13221-015-0033-z.

(37) Weintraub, A. S.; Schnapp, L. M.; Lin, X.; Taubman, M. B. Osteopontin Deficiency in Rat Vascular Smooth Muscle Cells Is Associated with an Inability to Adhere to Collagen and Increased Apoptosis. *Lab. Investig.* **2000**. https://doi.org/10.1038/labinvest.3780171.

(38) Clark, J. M.; Glagov, S. Transmural Organization of the Arterial Media. The Lamellar Unit Revisited. *Arterioscler. Thromb. Vasc. Biol.* **1985**. https://doi.org/10.1161/01.ATV.5.1.19.

(39) Voss, B.; Rauterberg, J. Localization of Collagen Types I, III, IV and V, Fibronectin and Laminin in Human Arteries by the Indirect Immunofluorescence Method. *Pathol. Res. Pract.* **1986**. https://doi.org/10.1016/S0344-0338(86)80151-0.

(40) Guruviah, V. Design of Microheaters with Better Thermal Management for Sensor Applications. *Int. J. Mech. Eng. Technol.* **2017**.

(41) Felder, E.; Siebenbrunner, M.; Busch, T.; Fois, G.; Miklavc, P.; Walther, P.; Dietl, P. Mechanical Strain of Alveolar Type II Cells in Culture: Changes in the Transcellular Cytokeratin Network and Adaptations. *Am. J. Physiol. - Lung Cell. Mol. Physiol.* **2008**. https://doi.org/10.1152/ajplung.00503.2007.

(42) Haga, J. H.; Li, Y. S. J.; Chien, S. Molecular Basis of the Effects of Mechanical Stretch on Vascular Smooth Muscle Cells. *Journal of Biomechanics*. 2007. https://doi.org/10.1016/j.jbiomech.2006.04.011.

(43) Lacolley, P.; Regnault, V.; Nicoletti, A.; Li, Z.; Michel, J. B. The Vascular Smooth Muscle Cell in Arterial Pathology: A Cell That Can Take on Multiple Roles. *Cardiovascular Research*. 2012. https://doi.org/10.1093/cvr/cvs135.

(44) Rezvani-Sharif, A.; Tafazzoli-Shadpour, M.; Avolio, A. Progressive Changes of

Elastic Moduli of Arterial Wall and Atherosclerotic Plaque Components during Plaque Development in Human Coronary Arteries. *Medical and Biological Engineering and Computing*. 2018. https://doi.org/10.1007/s11517-018-1910-4.

CHAPTER 3

SWELLNG KINETICS OF HIGH POLYMER CONCENTRATION TEMPERATURE-RESPONSIVE HYDROGEL FILMS BY FAST TEMPERATURE CHANGES

3.1 Introduction

Hydrogels containing poly(N-isopropylacrylamide) (PNIPAM) and other temperature-sensitive copolymers have broad applications, such as drug delivery vehicles, sensors, actuators and tissue engineering matrices. Upon environmental stimuli change, the volume of the hydrogel may change accordingly to reach the new equilibrium between network elastic energy and osmotic pressure, and this volume expansion or shrinkage is called swelling and deswelling, respectively. The kinetics of these swelling and deswelling processes is important in the performance of these hydrogel systems. For instance, slower kinetics would be favored for the controlled, sustained drug release purposes, while faster kinetics would benefit a actuator or sensing system. Thus, a thorough understanding of the swelling/deswelling kinetics is crucial in these applications and device designing. Although there have been substantial efforts to understand the kinetics of hydrogel swelling and deswelling over the decades[1,2], unanswered question remain.

The swelling kinetics of PNIPAM hydrogels have been found to vary substantially cased on fabrication method and thus monomer density. A PNIPAM hydrogel can be fabricated

from the copolymerization of pre-gel solutions containing monomers, initiator and acrylamide crosslinkers, and this hydrogel will have high water content and relatively low monomer fraction of around 10%. This composition is used in the hydrogel kinetics study by Yoon et al[1], and the light responsive composite hydrogel system by Hauser et al[3], where both studies report that the swelling and deswelling kinetics were limited by the mass transport in a poroelastic system, where the time constant is proportional to the square of dimension of interest, and inversely proportional to the diffusivity. More specifically, in Hauser's free-standing thin hydrogel sheets, gel sheets undergo deswelling when the illumination is turned on, and reswell when the light is turned off. When the normalized dimension of the gel sheet ($\frac{d}{d_0}$) is plotted against time (t), the curve is fitted well by a single exponential curve, as is shown in Figure 3-1 (a) and (b), where the characteristic time τ is determined by the equation following the equation $\tau = \frac{4H^2}{\pi^2 D}$, where H is the thickness of film and D is the diffusivity of water molecules in the network[1]. Figure 3-1 (c) shows the scaling relation between characteristic time and sample thickness is consistent with the poroelastic mass-transport limited process.

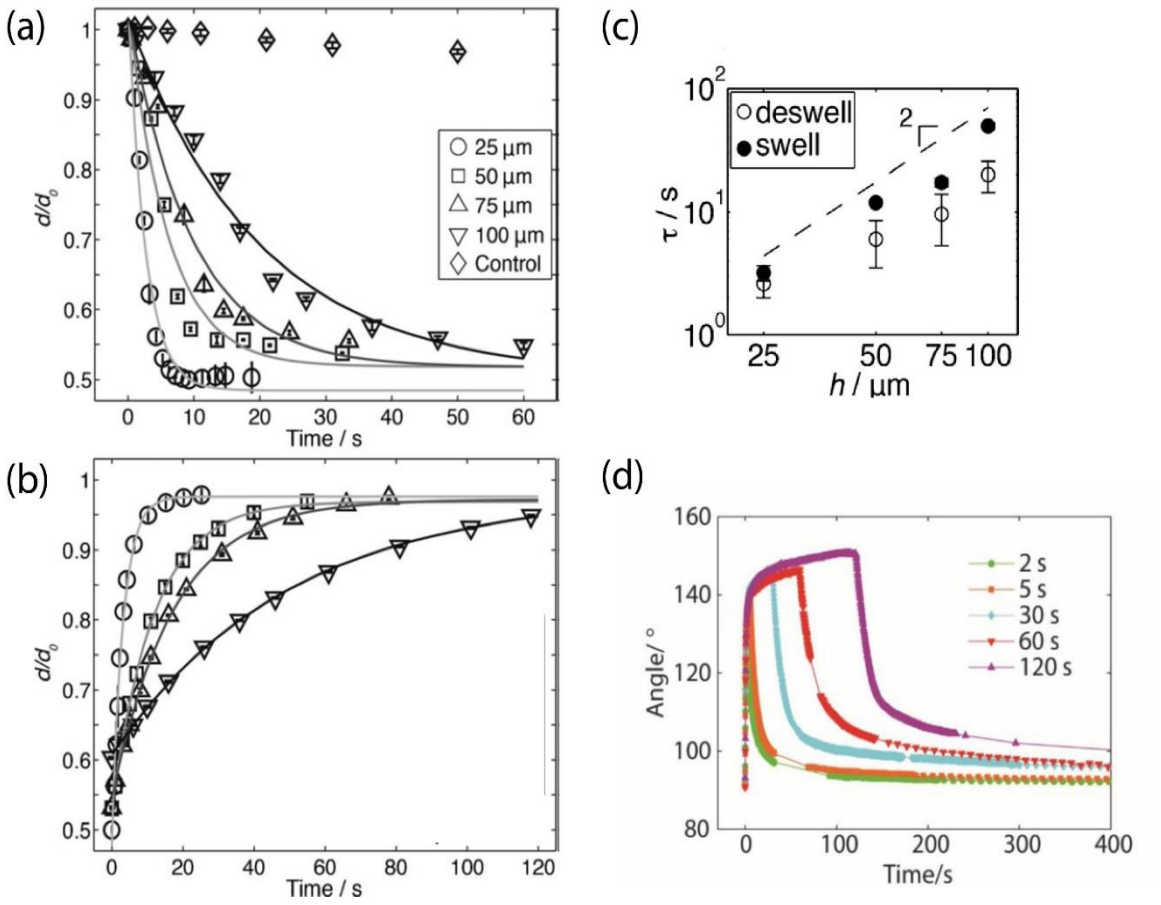

Figure 3- 1 The kinetics curves of the (a) deswelling and (b) swelling process of PNIPAM composite gel sheets of different thickness; (c) The log-log plot of time constants vs. film thickness; (d) The kinetics curves of dense PNIPAM waveguiding actuators changing bending angle when exposed to light and when the light is off. Different curves correspond to different exposure time. Figures are reproduced with permission from Ref 3: Hauser, A.W., Evans, A.A., Na, J. - H. and Hayward, R.C. (2015), Photothermally Reprogrammable Buckling of Nanocomposite Gel Sheets. Angew. Chem. Int. Ed., 54: 5434-5437 (Copyright John Wiley and Sons) and Ref. 4: Zhou, Y., Hauser, A.W., Bende, N.P., Kuzyk, M.G. and Hayward, R.C. (2016), Waveguiding Microactuators Based on a Photothermally Responsive Nanocomposite Hydrogel. Adv. Funct. Mater., 26: 5447-5452. (Copyright John Wiley and Sons)

On the other hand, PNIPAM hydrogels can also be fabricated by hydrating a crosslinked, nearly dry polymer film in the glassy or melt state, where the water content is lower and the monomer content is relatively high, depending on the crosslinking density but typically over 25 %. In the systems discussed here, the crosslinking is carried out by the UV activated

benzophenone radicals extracting a hydrogen from another polymer chain and forming covalent C-C bonds. In the waveguiding micro-actuator work by Zhou and coworkers, these dense PNIPAM gels are made into a thin strip, whose volumetric change controls the bending angle of the bilayer system[4]. In Chiappelli et al's thermochromic photonic multilayer device, these pre-made PNIPAM networks are casted into thin films, whose thickness change alters the peak reflective wavelength of the Bragg mirror multilayer system[5]. Both works report that the kinetics of the system responding to the environmental stimuli change show a two-step pattern. More specifically, as is shown in Figure 3-1(d), the bending angle of Zhou's waveguiding micro-actuator is plotted against time, and the curve is well described by a bi-exponential fit with two characteristic times. The reported shorter characteristic time is not far from the time scale of a mass transport limited poroelastic system , taking a typical diffusion constant of ~ 10^{-11} m^2 s^{-1} for PNIPAM gels in poroelastic transport[6]. And the longer characteristic time suggests that there are slower, more complex internal relaxation processes that controls the later stages of swelling/deswelling kinetics. As for the possible source of this slower relaxation process, it is interesting to learn that Schmaljohann and coworkers also observed that surface attached, crosslinked PNIPAM gels show two time ranges of swelling. In their system, the time scale is much slower, and the slow kinetics is attributed to the existence of poly(ethylene glycol) (PEG) side chains[7]. This raises the possibility that the second step of the dense PNIPAM gel swelling/deswelling kinetics is associated with hydrogen bonding effects, as PEG side chains may interact with neighboring moieties.

Hydrogen bonding effect is important in the swelling and deswelling behavior of PNIPAM gels. It is known that the hysteresis between PNIPAM swelling and deswelling is due to

the inter-molecular hydrogel bonds[8–10]. To better understand the role of hydrogen bonding in the hysteresis, poly(N,N-diethylacrylamide) (PDEAM) is often used as a control molecule, for it has a similar chemical structure to PNIPAM, a LCST (~30 ℃) close to PNIPAM (32 ℃), but unable to form hydrogen bonds due to the lack of –NH group[9,11].

Here, to investigate whether the two-step kinetic pattern of dense PNIPAM hydrogels is associated with the inter-molecular hydrogen bonding effect, we use PDEAM and PNIPAM copolymers of the same composition to compare against each other, while all other factors, such as sample dimension, hydrogel composition, environmental stimuli change, should remain the same.

In a smart system, the environmental cues will trigger the actuating part of this system, thus in a kinetics study, it is important that the environmental stimuli change is abrupt, so that the response of the system reflects its own properties, instead of being limited by the gradual environment change rate. This requirement is particularly challenging in this study of characterizing the swelling/deswelling kinetics of temperature responsive PNIPAM gels, because firstly, the high specific heat capacity of water makes it difficult to rapidly alter temperature of a relatively large volume; and secondly, the motion of fluids under temperature gradient and the heat transfer in the process is difficult to control. So the micro-heater systems developed in Chapter 2 can be used in here to achieve fast, regional control of the temperature.

3.2 Materials and methods

The copolymers used in this research are a random copolymer of N-isopropylacrylamide and 4-acryloyloxybenzophenone [P(NIPAM-BP)] and a random copolymer of N,N-

diethylacrylamide and 4-acryloyloxybenzophenone [P(DEAM-BP)]. Both copolymers can form hydrogen bonds with adjacent water molecules, so they exhibit an LCST behavior in aqueous solution, making the hydrogel swell/deswell upon temperature change. Both copolymers are crosslinkable under UV illumination, so the polymer films can be photopatterned. The difference between the two polymers is that the –NH group on P(NIPAM-BP) can act as hydrogen bond donors to form inter-chain hydrogen bonding, while the lack of it makes P(DEAM-BP) not able to form any inter-molecular hydrogen bonds.

3.2.1 Synthesis of P(NIPAM-BP) and P(DEAM-BP)

Polymers were synthesized by conventional free radical polymerization using azobisisobutyronitrile (AIBN) re-crystallized from methanol as the initiator. The monomer of 4-acryloyloxybenzophenone (BP) was used as received.

2.218 g of N-isopropylacrylamide (NIPAM) monomer and 0.1 g of 4-acryloyloxybenzophenone (BP) were copolymerized in 20 mL of 1,4-dioxane at 70 ℃ for 16 h under nitrogen following three freeze-pump-thaw cycles, resulting in a copolymer containing 1.4% of BP. The polymer was purified by precipitation into hexane, washed under vacuum filtration and dried overnight in a vacuum oven prior to use. ^{1}H NMR was performed using a Bruker 400 MHz spectrometer with chloroform-d as the solvent to characterize the composition of PNIPAM copolymer.

2.493 g of N,N-diethylacrylamide (DEAM) monomer and 0.1 g of 4-acryloyloxybenzophenone (BP) were copolymerized in 20 mL of 1,4-dioxane at 70 ℃ for 16 h under nitrogen following three freeze-pump-thaw cycles, resulting in a copolymer

containing 1.8% of BP. The polymer was purified by precipitation into hexane, washed under vacuum filtration and dried overnight in a vacuum oven prior to use. ^{1}H NMR is performed using a Bruker 400 MHz spectrometer with chloroform-d as the solvent to characterize the composition of PDEAM copolymer.

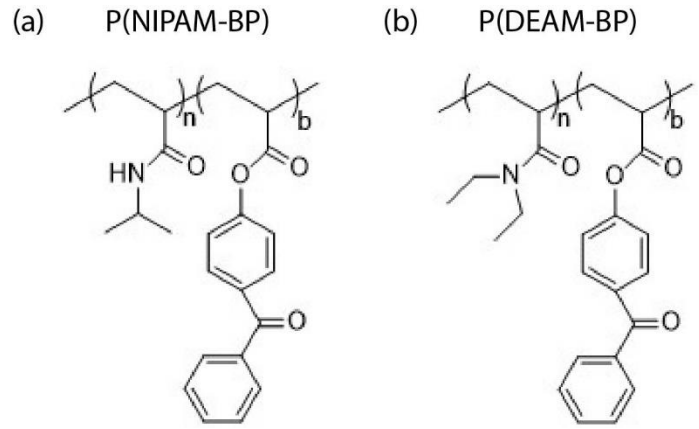

Figure 3- 2 Chemical structures of (a) poly(N-isopropylacrylamide)-r-(benzophenone acrylate) and (b) poly(N,N-diethylacrylamide)-r-(benzophenone acrylate).

3.2.2 Preparation of free-standing hydrogel disks

Drop-casting was used to prepare PNIPAM and PDEAM films with a uniform thickness. To facilitate the later release of hydrogel films from the substrate, a layer of poly(acrylic acid) (PAA) was first spin-casted (3 wt% in water, 2000 rpm) onto the silicon substrate and then crosslinked with calcium ion in saturated $CaCl_2$ solution as the sacrificial layer[12]. The PNIPAM and PDEAM copolymers were dissolved in anhydrous 1-propanol, and then the solution was drop casted onto the silicon wafers coated with PAA sacrificial layer. The solvent was slowly evaporated at 45 °C in a closed glass jar (0.13 oz, Freund Container), resulting in polymer films of different thickness by changing the solution concentration and amount. The thickness of the dry polymer films were measured with a mechanical profilometer (Bruker Dektak XT® stylus profiler).

The polymer film was then patterned using maskless photolithography based on a digital micromirror array device (DMD, DLP Discovery 4100, 0.7XGA, Texas Instruments). Each mirror of the DMD can be controlled through a computer between on and off state, generating light patterns with a resolution of 1024x768 pixels by reflecting collimated UV light (365 nm, pE-100, CoolLED). Then the UV light patterns are projected to the sample through an inverted microscope (Nikon ECLIPSE Ti) to photo-crosslink desired regions on the polymer film. Then the film is developed in a marginal solvent to dissolve the uncrosslinked regions without swelling the crosslinked parts too much, followed by nitrogen blow drying. The marginal developing solution was a mixture of ethanol and water (5:3, v/v) for PNIPAM copolymer films, and a mixture of toluene and hexane (5:7, v/v) for PDEAM copolymer films.

Finally, the PAA sacrificial layer was dissolved in 1x phosphate buffered saline (PBS), exchanging the Ca^{2+} crosslinkers out and allowing the patterned samples to release from the substrate into the desired position.

3.2.3 Micro-heater fabrication and experimental set-up

It has been reported that micro-heaters of double spiral design provide a more uniform temperature profile compared to other shapes such as meander, honeycomb, S-shape and fan-shape[13]. The temperature uniformity can be improved when the center region has relatively lower heating power compared with outer regions, which will be compensated by the heat distribution behavior. In this Joule heating case, the heating power depends on the resistance of the metal lines, so by changing the width and gap of the features, regional resistance can be tuned. Thermo-graphic analysis shows that optimum temperature

uniformity can be obtained when every stripe is reduced by a factor of 0.85 moving outwards from the center[14]. Based on this analysis, the micro-heaters are designed and fabricated accordingly. The size of the micro-heaters are designed to be larger than the hydrogel disks, so that the temperature variation across the hydrogel lateral dimensions is minimized. Figure 3-3 (a) displays a micro-heater device with side length of 620 μm, thickness of 100 nm, and width of 20 μm at the outer line. The resistance of this micro-heater is calculated to be 90.7 Ω, as confirmed using a multi-meter (Fluke 87V). It should be noted that the resistance of metals increases with higher temperature, following the equation $R = R_0[1 + \alpha(T - T_0)]$, where R_0 is resistance at reference temperature T_0, R is resistance at T and α is the temperature coefficient of resistance, which has the value of 0.0034 /℃ for gold.

As described in Chapter 2, the fabrication of microheaters followed a photolithography – metal deposition – lift-off process. A 100 nm layer of gold was deposited onto the patterned photoresist, and the double spiral circuit was made after acetone washing off the remaining photoresist. The fabricated micro-heater device was shown in Figure 3-3 (a). Then a 350 nm layer of SiO_2 was deposited onto the heaters for insulation purposes, while leaving the far ends of the micro-heater foots uncovered for future connection to the power source.

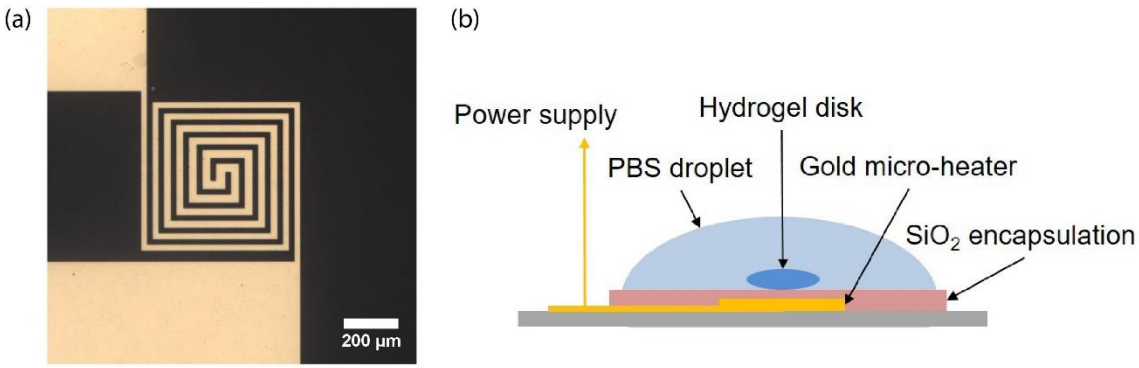

Figure 3- 3 (a) Micrograph of the microheaters; (b) illustration of the kinetics testing set-up (not to scale).

The kinetics testing set-up is shown in Figure 3-3 (b). A droplet of PBS was placed on the substrate, and the free-standing hydrogel disks were placed on the top of the micro-heaters by micro manipulator (Burleigh, PCS-4100).

It is known that the initial swelling process of crosslinked PNIPAM is slow in kinetics due to the complex chain correlations in the collapsed state[4], so this kinetic study would focus on the deswelling and the re-swelling. The dry film is released in PBS and kept in solution for a period of time long enough to allow full swelling in room temperature.

The swelling/deswelling process upon temperature change is monitored and recorded using an upright optical microscope (Zeiss, Axiotech Vario). The heating and cooling process was run several cycles to check the reproducibility. The graph processing and analysis is done using Image J software.

3.3 Results and discussion

3.3.1 Micro-heater performance

For a system where the kinetics of swelling and deswelling is limited by mass transport in a poroelastic system, the characteristic time τ is estimated by $\tau = \frac{4H^2}{\pi^2 D}$. The typical diffusivity for PNIPAM hydrogel in poroelastic transport is approximately 1.5×10^{-11} m^2s^{-1}[1], so the time scale for the swelling/deswelling of a 10 μm thick hydrogel should be around 10 s. This is an important time scale to compare with the ambient temperature change rate. Zhou, et al attempted to investigate the kinetic behavior of hydrogel sheets but were limited by the slow temperature change provided by a temperature stage used to heat the entire solution bath in which the hydrogel sheet was immersed[15].

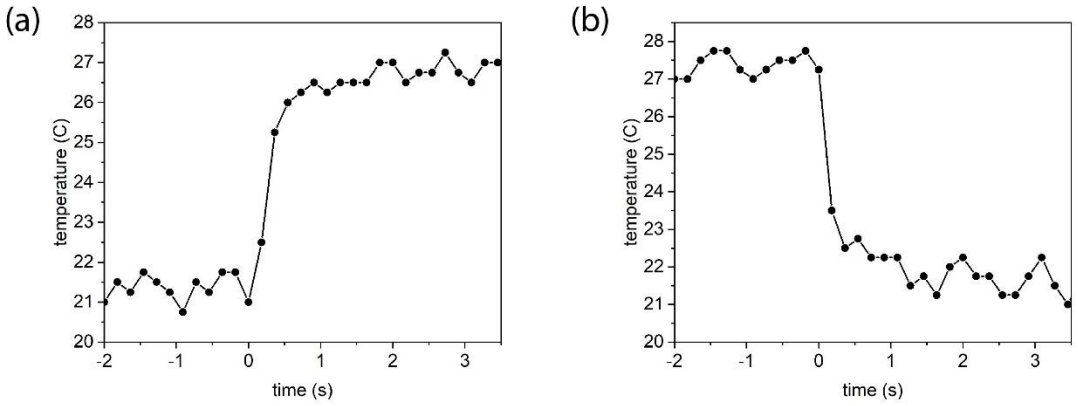

Figure 3- 4 Temperature change in PBS solution above the micro-heater device when (a) micro-heater is turned on at 0 s and (b) microheater is turned off at 0 s.

The local temperature change when the micro-heater was turned on was recorded by a microprobe placed above the micro-heaters in the PBS solution. When the heater was turned on at t=0 s, the temperature change is shown in Figure 3-4 (a), and this trend was fitted by an exponential to give a characteristic time of 0.31 ± 0.05 s. Similarly, when the

heater was turned off at t=0 s, the local temperature decrease was shown in Figure 3-4(b), and the characteristic time was fitted to be 0.17 ± 0.03 s. Both time scales are significantly shorter than the estimated 10 s time scale based on diffusion limitation.

3.3.2 Weighting fits to exponential decay curves

When the ambient temperature was changed, the dimension of the hydrogel sheet changed in response. This change was recorded by capturing pictures of the hydrogel sample at a certain frame rate. So the dimensions were monitored at a linear relation to the time, but the exponential decay nature of this change determines that the importance of the data points on describing the fit are not the same. To be more specific, the dimensions recorded at the earlier stage should weigh more in the exponential decay fitting compared to the dimensions acquired at the later stages. If the plot was not adjusted or weighted accordingly, the data points at the later stage of the transition would have a disproportionately important impact on the fitting results, while the earlier stages are relatively overlooked. So it is important to find a weighting method that can take into account the importance of data changing with the location of the data on the timeline, so that the dimension change is better described by the fitted exponential curve.

The most straightforward method of weighting the data is to put a pre-factor on each dimension measurement, and this pre-factor is determined by when this measurement was taken on an exponential decay function of $C_t = C_0 e^{-\frac{t}{\tau}}$, where C_t is the weighting pre-factor at time t, C_0 is the initial weighting factor at time t=0, and τ is the characteristic time of this exponential decay. It is expected that this characteristic time would match the characteristic time of the dimension change transition.

One shortcoming of this weighting method is that a pre-factor has to be calculated for each measurement. Also, at the later stages of the dimension change, this pre-factor would be very small, making each dimension measurement have little impact on the fitting, but still all measurements have to be taken. To simplify this weighting method, binning method combined with an averaged representation value can be used in here. Firstly, dimension measurements taken at different times are categorized into different time periods, time Category 1 being from 0 to T, Category 2 being from T to 2T, Category 3 being from 2T to 4T, and so on. Then the weight of data in each category is set, and would be the same within the category, W_1 for Category 1, W_2 for category 2, W_3 for Category 3, and so on. Finally, instead of having W_n as the pre-factor for Category n, measurements in Category n would be taken 1 out of $\frac{1}{W_n}$ with a pre-factor of 1, so that the required measurement is reduced while the weight of this category is not changed.

The binning method here is designed as this: for measurements taken in Category 1 (0-T), W_1=1, i.e. all measurements are counted as effective. For measurements in Category 2 (T-2T), $W_2=\frac{1}{2}$, meaning one out of 2 measurements is counted as effective. For Category 3 (2T-4T), $W_3=\frac{1}{4}$, one out 4 measurements is counted, moving on with this method, one out of 8 for Category 4 (4T to 8T), one out of 16 for Category 5 (8T to 16T), one out of 32 for Category 6 (16T to 32T) and so forth.

Whether this binning method is a representative way of describing the exponential decay nature can be tested by plotting the weight in each category against normalized time. To be specific, for Category n, the weight, W_n, is the probability of one measurement being counted as effective, and the associated time is the median time of the category: 0.5T for Category 1, 1.5T for Category 2, 3T for Category 3 and so forth. The plot is shown in Figure 3-5, and the red curve indicates the exponential decay curve of $W = W_0 + Ae^{-\frac{t/T}{t_0}}$, where A=1.3±0.1 and t_0=1.6±0.1, with a R^2 of 0.99, showing it is a good description of the exponential decay. With the characteristic time of this binning method t_0 being 1.6, the binning time unit T should be $\frac{\tau}{1.6}$, where τ is the characteristic time of the dimension change, so that the characteristic time of this binning method matches the characteristic time of the actual dimension change.

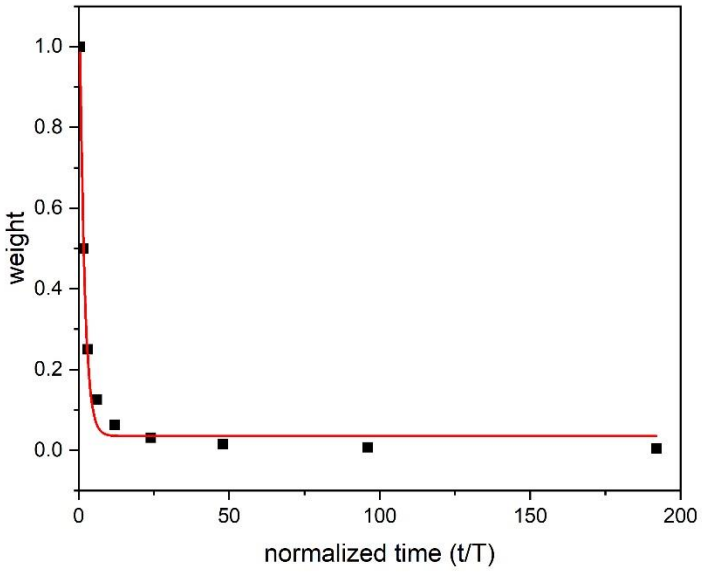

Figure 3- 5 The category weight in binning method and the exponential decay fit.

This binning method can be extended to bi-exponential decay fittings. For a biexponential decay with two characteristic times τ_1 and τ_2, the categories could be decided as followings, where $T_1=\frac{\tau_1}{1.6}$ and $T_2=\frac{\tau_2}{1.6}$: 0-T_1 is Category 1, T_1-$2T_1$ is Category 2, $2T_1$-$4T_1$ is Category 3, and so on, until the upper limit of Category N is greater than T_2, then this category is decided as $2^{(N-2)}T_1$-T_2, and then T_2 is used as the binning unit to categorize later stages: T_2-$2T_2$ is Category (N+1), $2T_2$-$4T_2$ is Category (N+2), and so forth. This data weighting and averaging method was applied to data analysis for all kinetic measurements.

3.3.3 Deswelling kinetics of P(DEAM-BP) and P(NIPAM-BP) hydrogel sheets

Firstly, the relationship between the two-step exponential trend and the existence of inter-molecular hydrogen bonding was investigated. As the hydrogen bonding free control system, PDEAM hydrogel sheets of different thickness (15.0 μm, 26.5 μm and 39.6 μm at dry state) were used to test the deswelling behavior under increased temperature induced by the micro-heater. As the materials system with inter-chain hydrogen bonding, PNIPAM hydrogel sheets of different thicknesses (5.2 μm, 11.7 μm and 35.9 μm) were tested under the same condition. The hydrogel disks were allowed to fully swell in PBS solution at room temperature, and then the deswelling process was initiated by switching the micro-heater on. The dimension change was monitored and recorded, and the radii at different times were normalized against the initial radius of the hydrogel disk.

The dimension change of the 39.6 μm thick PDEAM hydrogel disk was plotted against time in Figure 3-6 (a). To investigate whether single exponential decay ($y = y_0 + Ae^{-\frac{t}{\tau}}$) or double exponential decay ($y = y_0 + A_1e^{-\frac{t}{\tau_1}} + A_2e^{-\frac{t}{\tau_2}}$) should be used to describe this

trend, both fitting are shown in Figure 3-6 (a), blue curve being single exponential and red curve being double exponential. It can be observed that a single exponential decay is sufficient in describing the trend, while the double exponential curve almost overlaps with the single exponential curve. Moreover, because the single exponential decay equation $y = y_0 + Ae^{-\frac{t}{\tau}}$ can be replotted into $(y - y_0) = lnA - \frac{t}{\tau}$, so dimension change against time can be plotted in semi-log scale to investigate whether the trend can be described by a single exponential fitting. As is shown in the inset of Figure 3-6 (a), the normalized radius was semi-log replotted against time, and a linear fit is shown as the blue line. The characteristic time τ extracted from the slope (τ=13.3 ± 0.5 s) agreed with the characteristic time from the direct single exponential decay fitting (τ=12.9 ± 0.7 s). In summary, the deswelling of a PDEAM hydrogel disk is a one-step exponential decay process.

Similarly, the dimension change of the 5.2 μm thick PNIPAM hydrogel disk was plotted against time in Figure 3-6 (b), and both single and double exponential decay fittings were attempted, shown as the blue curve and the red curve, respectively. It can be observed that the blue single exponential decay curve did not describe the deswelling trend well, while the red double exponential curve fits the data well. Moreover, when the dimension change data is replotted in the semi-log scale as in the inset, it is clear that the trend is not linear, but suggests two steps. These features indicated that the deswelling of a PNIPAM hydrogel disk is a two-step process, and it needs a double exponential fit to describe.

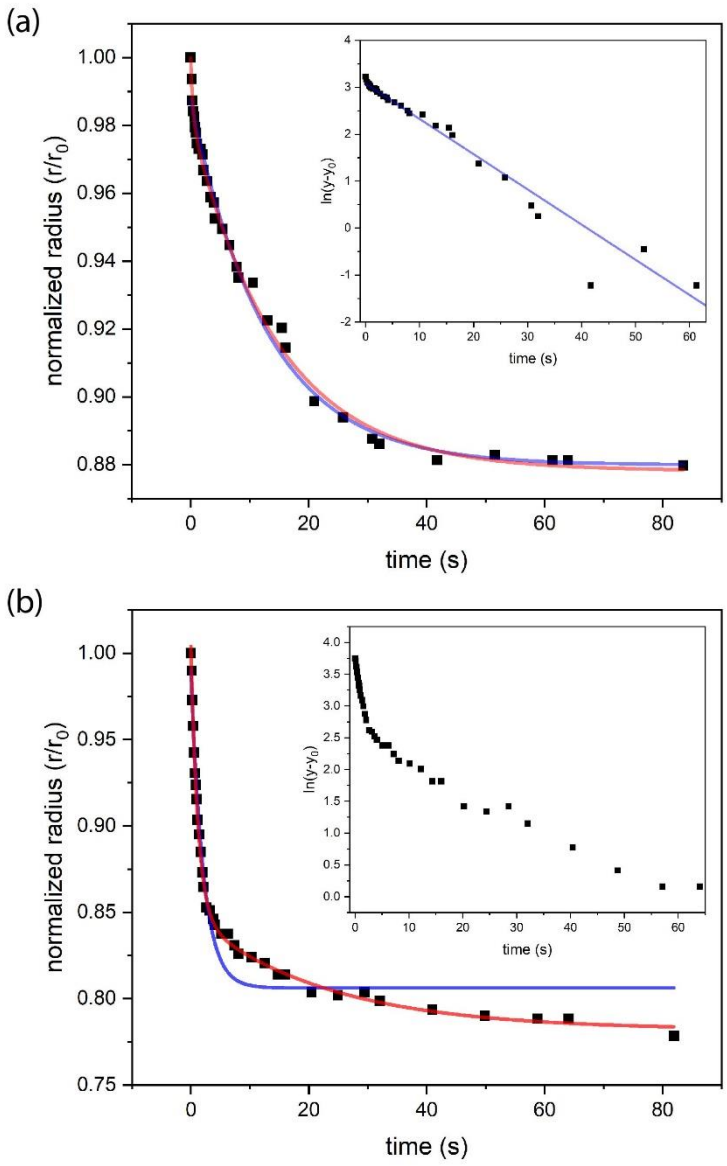

Figure 3- 6 The dimension change of (a) a 36.9 μm thick PDEAM hydrogel disk and (b) a 5.2 μm thick PNIPAM hydrogel disk in the deswelling process. The blue curve is the single exponential decay fit, and the red curve is the double exponential decay fit. Inset: semi-log replotting of the dimension change with the blue line showing the linear fit.

The investigation of deswelling of hydrogel disks not only yields the qualitative correlation of hydrogen-bond containing systems and the two-step kinetics behavior, but can also be used for quantitative study. As is shown in Figure 3-7 (a), the deswelling process of

PDEAM hydrogel disks of different thickness were all fitted well by the single exponential decay curve of $y = y_0 + Ae^{-\frac{t}{\tau}}$, where the characteristic times for hydrogels disks of 15.0 μm, 26.5 μm and 39.6 μm were 2.3 ± 0.1 s, 7.6 ± 0.3 s and 12.9 ± 0.7 s, respectively. As is shown in Figure 3-7 (b), the time constants were plotted with respects to hydrogel thickness, and the relation was fitted by a $\tau = kH^x$ line, where H is the sheet thickness, and k is a constant determined by diffusivity. The exponent x was fitted to be 1.82 ± 0.22, and was close to the poroelastic mass-transport limited situation of $\tau = \frac{4H^2}{\pi^2 D}$, and the diffusivity can be calculated to be approximately 2.3×10^{-11} m^2/s, which is not far away from the reported value of a hydrogel system with similar modulus and polymer fraction[6].

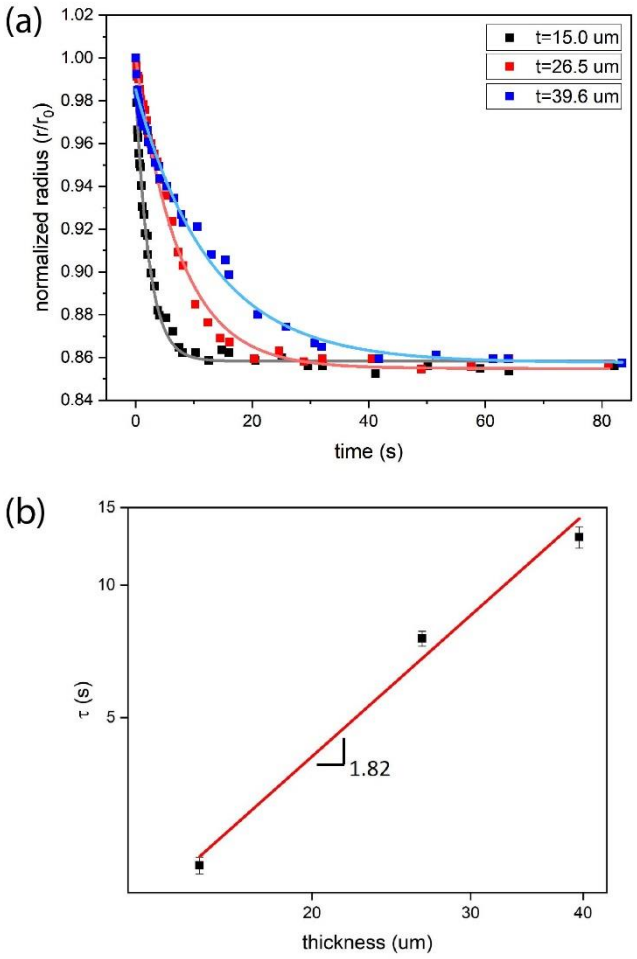

Figure 3- 7 (a) Deswelling kinetics of PDEAM hydrogel sheets of different thickness, fitted with single exponential decay curves; (b) log-log plot of characteristic time against thickness, fitted with $\tau \sim H^x$ relation.

The deswelling kinetics of PNIPAM hydrogel sheets was also further studied. The dimension change of PNIPAM hydrogel sheets was also recorded, normalized, and plotted against time. All the curves showed a two-step process, and were fitted by the double exponential equation of $y = y_0 + A_1 e^{-\frac{t}{\tau_1}} + A_2 e^{-\frac{t}{\tau_2}}$. The parameters to describe the deswelling process of PNIPAM hydrogel sheets of different thickness were listed in Table 3-1. While the two characteristic times of the bi-exponential fit, τ_1 and τ_2, do not exhibit a clear trend, it should be noted that the ratio between the pre-factors, A_1 and A_2, does not vary much across different samples and thicknesses. This observation shows that the contribution ratio of the two steps in the deswelling kinetics is related to the material property.

Table 3- 1 The kinetic parameters of the deswelling process of PNIPAM hydrogel sheets

Thickness(μm)	**Sample**	**A_1%**	**A_2%**	**τ_1 (s)**	**τ_2 (s)**
5.2	1	69.5	30.5	1.1 ± 0.04	21.0 ± 2.3
	2	70.1	29.9	1.2 ± 0.04	22.4 ± 2.8
11.7	1	77.9	22.1	0.9 ± 0.3	9.0 ± 0.8
	2	60.2	39.8	0.7 ± 0.1	26.7 ± 5.2
35.9	1	82.0	18.0	1.8 ± 0.7	8.2 ± 0.7
	2	76.8	23.2	0.8 ± 0.04	11.3 ± 2.1

3.3.4 Swelling kinetics of P(DEAM-BP) and P(NIPAM-BP) hydrogel sheets

As the counter-process of the deswelling kinetics experiment discussed before, the hydrogel disks were kept at elevated temperature to equilibrate in the shrunken state, and then triggered to re-swell by abruptly switching off the micro-heater and decreasing the ambient temperature. The dimension change of PDEAM hydrogel disks (15.0 μm, 26.5 μm and 39.6 μm thick) and PNIPAM hydrogel disks (5.2 μm, 11.6 μm and 35.9 μm thick) were monitored and recorded.

Similar to the deswelling process, the swelling process of PDEAM hydrogel sheets are well described by single exponential equation of $y = y_0 + Ae^{-\frac{t}{\tau}}$, and the characteristic times for hydrogel disks with thickness of 15.0 μm, 26.5 μm and 39.6 μm were 1.7 ± 0.1 s, 8.6 ± 0.4 s and 12.9 ± 1.3 s, respectively. The time constants were plotted against gel thickness, and the relation was fitted by $= kH^x$, where H is the sheet thickness, and k is a diffusivity-related constant, as is shown in Figure 3-8. The exponent x was fitted to be 2.2 ± 0.5, close to the poroelastic mass-transport limited situation, and the diffusivity is estimated to be 1.0 × 10^{-10} m^2/s.

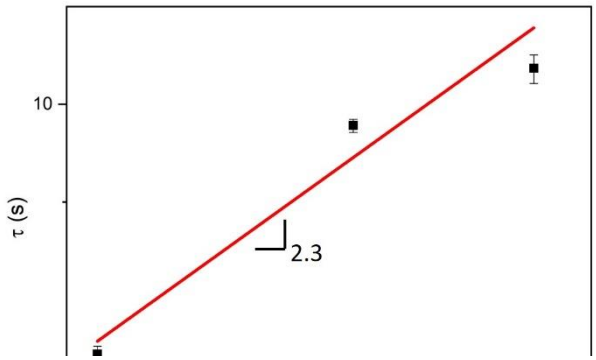

Figure 3- 8 Reswelling process characteristic times against PDEAM hydrogel disk thickness, in log-log plot and fitted by $\tau \sim H^x$ relation.

The swelling kinetics of PNIPAM hydrogel sheets were more complex. The normalized dimension change of PNIPAM disks were plotted against time, as is shown in Figure 3-9 for different thickness. Firstly, it is observed that the radius of the hydrogel disk do not increase immediately after switching off the micro-heater. This delay is not due to the slow temperature change, as is characterized by the temperature probe. Also, this delay was not observed in the PDEAM system, suggesting that it is related to the inter-molecular hydrogen bonding that only exists in PNIPAM hydrogels. This delay possibly displays the disassociation of inter-molecular hydrogen bonding, before which the network cannot expand freely. Also, it is observed that the length of this delay increases with the increase of hydrogel disk thickness. It takes 3-5 s before the 5.2 μm thick disk starts to rapidly expand, 7-9 s for the 11.6 μm sample, and more than 1 min for the 35.9 μm sample. Secondly, after the initial plateau, the dimension change of the hydrogel disk follows an exponential decay trend. This trend is more easily observed in the two thinner samples, while the 5-minute recording did not capture the full swelling process of the thick sample. It shows that with the increase of disk thickness, the time required to reach the equilibrium dimension increases accordingly. A more quantitative investigation was attempted. The onset t=0 s was shifted to the onset of rapid dimension increase, and then the dimension change was fitted by the single exponential decay equation. All three samples are well described by the curve, yielding characteristic times of 5.9 ± 0.2 s for 5.2 μm thickness, 13.9 ± 0.5 s for 11.6 μm thickness, and 170 ± 27 s for 35.9 μm thickness. It should be noted that these fittings are not accurate due to the difficulty in the determination of the onset of expansion. In summary, the inter-molecular hydrogen bonding in the PNIPAM system

yields a very different swelling kinetics behavior in contrast to the mass transport limited process in the hydrogen-bond free PDEAM system.

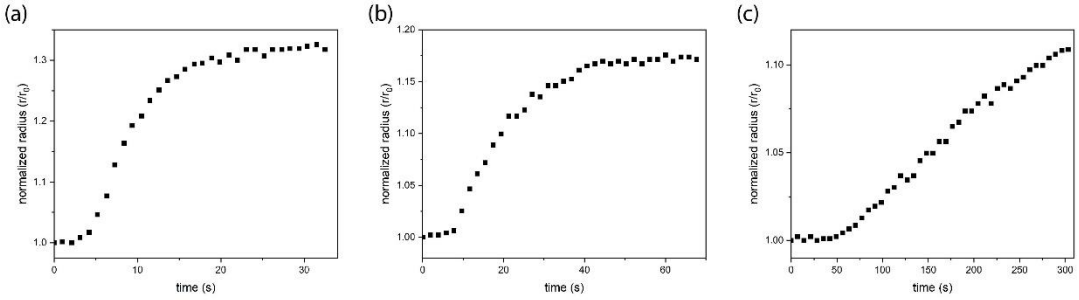

Figure 3- 9 Swelling kinetics of PNIPAM hydrogel sheets of thickness (a) 5.2 μm, (b) 11.6 μm and (c) 35.9 μm.

3.4 Conclusion and future work

The observed two-step behavior of a high monomer concentration PNIPAM hydrogel during swelling and deswelling was investigated using the fast temperature change provided by the micro-heater platform. PNIPAM and PDEAM dense hydrogels were fabricated and compared against each other to investigate the effect of hydrogen bonding on the two-step swelling/deswelling kinetics pattern. With the deswelling kinetics of PDEAM gels well described by single exponential relation, and that of PNIPAM gels requiring bi-exponential fitting, it is concluded that the two-step deswelling behavior of PNIPAM gels is associated with the inter-molecular hydrogen bonding in the system. The effect of inter-molecular hydrogen bonding on the kinetics is also present in the swelling process. In contrast to PDEAM hydrogel disk swelling being limited by mass transport, the swelling process of PNIPAM hydrogel disk shows a delay at the initial stages, followed by a single exponential decay expansion. Both the delay time and the later expansion characteristic time increase with the higher thickness.

The system used here can be expanded to other responsive systems with different content of hydrogen bonding moieties. It would be worth investigating how the content of hydrogen bonding interactions affects the weight of the two exponential decay steps.

3.5 References

(1) Yoon, J.; Cai, S.; Suo, Z.; Hayward, R. C. Poroelastic Swelling Kinetics of Thin Hydrogel Layers: Comparison of Theory and Experiment. *Soft Matter* **2010**, *6* (23), 6004. https://doi.org/10.1039/c0sm00434k.

(2) Doi, M. Gel Dynamics. *J. Phys. Soc. Japan* **2009**, *78* (5), 1–19. https://doi.org/10.1143/JPSJ.78.052001.

(3) Hauser, A. W.; Evans, A. A.; Na, J. H.; Hayward, R. C. Photothermally Reprogrammable Buckling of Nanocomposite Gel Sheets. *Angew. Chemie - Int. Ed.* **2015**, *54* (18), 5434–5437. https://doi.org/10.1002/anie.201412160.

(4) Zhou, Y.; Hauser, A. W.; Bende, N. P.; Kuzyk, M. G.; Hayward, R. C. Waveguiding Microactuators Based on a Photothermally Responsive Nanocomposite Hydrogel. *Adv. Funct. Mater.* **2016**. https://doi.org/10.1002/adfm.201601569.

(5) Chiappelli, M. C.; Hayward, R. C. Photonic Multilayer Sensors from Photo-Crosslinkable Polymer Films. *Adv. Mater.* **2012**. https://doi.org/10.1002/adma.201202459.

(6) Yoon, J.; Cai, S.; Suo, Z.; Hayward, R. C. Poroelastic Swelling Kinetics of Thin Hydrogel Layers: Comparison of Theory and Experiment. *Soft Matter* **2010**, *6* (23), 6004–6012. https://doi.org/10.1039/c0sm00434k.

(7) Schmaljohann, D.; Beyerlein, D.; Nitschke, M.; Werner, G. Thermo-Reversible Swelling of Thin Hydrogel Films Immobilized by Low-Pressure Plasma. *Langmuir* **2004**. https://doi.org/10.1021/la034653f.

(8) Li, Y.; Tanaka, T. Kinetics of Swelling and Shrinking of Gels. *J. Chem. Phys.* **1990**, *92* (2), 1365–1371. https://doi.org/10.1063/1.458148.

(9) Wang, X.; Qiu, X.; Wu, C. Comparison of the Coil-to-Globule and the Globule-to-Coil Transitions of a Single Poly(*N* -Isopropylacrylamide) Homopolymer Chain in Water. *Macromolecules* **1998**. https://doi.org/10.1021/ma971873p.

(10) Lu, Y.; Zhou, K.; Ding, Y.; Zhang, G.; Wu, C. Origin of Hysteresis Observed in Association and Dissociation of Polymer Chains in Water. *Phys. Chem. Chem. Phys.* **2010**. https://doi.org/10.1039/b918969f.

(11) Pang, X.; Cui, S. Single-Chain Mechanics of Poly(N, N -Diethylacrylamide) and Poly(N -Isopropylacrylamide): Comparative Study Reveals the Effect of Hydrogen Bond Donors. *Langmuir* **2013**, *29* (39), 12176–12182. https://doi.org/10.1021/la403132e.

(12) Linder, V.; Gates, B. D.; Ryan, D.; Parviz, B. A.; Whitesides, G. M. Water-Soluble Sacrificial Layers for Surface Micromachining. *Small* **2005**, *1* (7), 730–736.

https://doi.org/10.1002/smll.200400159.

(13) Bhowmick, S.; Iodice, M.; Gioffrè, M.; Breglio, G.; Irace, A.; Riccio, M.; Romano, G.; Grilli, S.; Ferraro, P.; Mecozzi, L.; Coppola, S.; Gennari, O.; Rega, R.; Coppola, G. Investigation of Pyroelectric Fields Generated by Lithium Niobate Crystals through Integrated Microheaters. *Sensors Actuators, A Phys.* **2017**. https://doi.org/10.1016/j.sna.2017.05.010.

(14) Velmathi, G.; Ramshanker, N.; Mohan, S. Design , Electro-Thermal Simulation and Geometrical Optimization of Double Spiral Shaped Microheater on a Suspended Membrane for Gas Sensing. *IECON 2010 - 36th Annu. Conf. IEEE Ind. Electron. Soc.* **2010**, 1258–1262. https://doi.org/10.1109/IECON.2010.5675550.

(15) Zhou, Y. SWELLING INDUCED DEFORMATION OF THERMALLY RESPONSIVE HYDROGELS, 2018.

CHAPTER 4

CREASES ON HYDROGEL SURFACES WITH PATTERNED STIFF FILMS

4.1 Introduction

Creases are found to exist in biological systems, for example the sulci in the primate cerebral cortex[1], neurogenic placodes in embryos[2] and certain tumors[3]. There has been growing interest in the biological relevance of such surface instabilities, as well as how these processes might enable the design of sensors and actuators[4]. As hydrogels are widely adopted platforms for mimicking a biological environments *in vitro*, the study of creasing instabilities in hydrogel systems is important not only for fundamental understanding but also for leading us to better understand more complex biological phenomena and finally guiding us in better designs of biomimetic devices[5].

Experimentally, creases are observed in compressed elastomers and gels[6,7]. A hydrogel undergoes extensive volume change upon immersion into a penetrating solvent so that the osmotic pressure induced by mixing with solvent is balanced by the elastic tension of the polymeric network. A free standing hydrogel can expand isotropically in three dimensions, however, a hydrogel that is constrained to a stiff substrate and has a thickness much lower than its lateral dimensions can only expand in the direction normal to the substrate. The constrained swelling can be decomposed into two steps: an isotropic 3-d swelling to the stress-free state followed by a biaxial compression back to the initial lateral dimensions;

whenever this compression locally exceeds a critical strain, creases are formed to relieve stress.

In many applications such as actuators[8–10], microfluidics[11], flexible electronics[12–14] and cell culture[15,16], the spatial patterning of hydrogels is required. Although there have been a number of studies about wrinkling instabilities of patterned surfaces[17–21], there is limited understanding about how surface creases will form and develop with the existence of spatially patterned modulus contrast[22,23]. It should be noted that Ouchi et al conducted research on surface instabilities of elastomers capped with patterned stiff films in response to uniaxial compression[24]. To extend this line of inquiry to surface attached hydrogel systems that are under biaxial compression, this chapter describes the study of the formation and development of creases on spatially patterned hydrogel surface. It should be noted that the content in this chapter is more preliminary than a usual thesis chapter.

4.2 Materials and methods

The hydrogel was prepared on a silicon wafer, cleaned by sonication in water, ethanol and acetone followed by a pre-treatment with [3-(methacryloxy)-propyl]trichlorosilane to provide covalent anchoring. The degassed aqueous pre-gel solution contained 766 mM N-isopropylacrylamide (NIPAM), 136 mM sodium acrylate (NaAc), and 4.5 mM N,N'-methylenebisacrylamide (BisAA). For hydrogels prepared for fluorescent confocal imaging, methacrylate functionalized Rhodamine B was added to the pre-gel solution. To initiate free radical polymerization, 0.3 mL of N,N,N',N'-tetramethylethylenediamine and 1.0 mL of a 10 wt% aqueous ammonium persulfate solution were added to 200 mL of pre-gel solution. The mixture was loaded by capillary action between a substrate and a release

coverslip separated by 125 μm Kapton spacers. The gelation was carried out in a sealed chamber under positive pressure of nitrogen, and was allowed to proceed for 30 min before separating the release coverslip from the gel. The hydrogel composition was chosen so that the critical strain for crease formation is within the swelling ratio range achieved by temperature change of 22 ℃ to 50 ℃, so the onset and disappearance of the creases can be observed by temperature change[25].

Epoxy-based photoresist SU-8 2000.5 was firstly spin-coated onto a substrate previously coated with a thin layer of poly(acrylic acid) (30 kg mol^{-1}, Aldrich) crosslinked with Ca^{2+} as a sacrificial layer. Then the film was transferred to the hydrogel by pressure, and released in phosphate buffered saline (PBS). But the attachment between the epoxy film and the hydrogel was sometimes poor. Also, it required a physical mask for the patterning, so this method was used only in early stage fabrications.

For better attachment, the poly(p-methylstyrene) (PpMS) copolymer film was used for later fabrication. The PpMS copolymer was prepared by radical polymerization, with a feeding ratio of 95% p-methylstyrene (pMS), 4.9% benzophenone acrylamide (AAmBP) as UV-crosslinker and 0.1% fluorescein-o-acrylate as marker dye for confocal fluorescent imaging. AAmBP was synthesized according to a previously reported literature procedure via reaction of acryloyl chloride and 4-aminobenzophenone in dichloromethane and triethylamine[26]. AIBN was obtained from Aldrich and re-crystallized from methanol prior to use. All other monomers were used as received. After three freeze-pump-thaw cycles and a nitrogen purge for 30 min, the polymerization was initiated by AIBN and carried out at 75 ℃ in 1,4-dioxane for 20 h. The product was purified by precipitation into stirring methanol, washed by filtration and dried in vacuum oven overnight. The composition ratio

in the copolymer was confirmed by ^{1}H NMR in d-DMSO (Bruker 400 MHz) to be the same as the feed ratio, and the molecular weight was determined by size exclusion chromatography (SEC) with dimethylformamide (DMF) (0.01 M LiCl) as the eluent to be M_n of 24 kDa with a dispersity of 2.3 against poly(methyl methacrylate) standards for calibration.

The photo-crosslinkable PpMS was dissolved in toluene to yield 100 mg/mL solution, then spin-coated onto a nitrogen-dried PNIPAM gel surface to achieve a stiff layer of 1μm thickness. This film was then irradiated with a pattern of UV light (365 nm, pE-100, CoolLED) via maskless lithography using a Digital Micromirror Devices (DLP Discovery 4100, 0.7 XGA, Texas Instruments) attached to an inverted optical microscope (Nikon ECLIPSE Ti), followed by immersing the sample to a marginal solution of toluene/hexanes mixture (2.75:1, v/v) to dissolve the uncrosslinked regions. The thickness of the stiff patterns was measured by Stylus Profilometer (Dektak 150, Veeco Instruments, Inc.).

The formation and disappearance of creases were monitored by an upright optical microscope (Zeiss, Axiotech Vario). The cross-sectional profile was reconstructed using Nikon's Confocal NIS-Elements software from z-stack figures taken from a laser scanning confocal microscope (Nikon A1 Spectral Confocal).

4.3 Results and discussion

4.3.1 Dimension design

First, we consider the characteristic length scales determined by the modulus and thickness of PNIPAM hydrogel and PpMS stiff layer, namely the theoretical wavelength of wrinkling

(λ_w) and creasing (λ_c). It was revealed that in a uniaxially compressed elastomer system, the surface buckling patterns changed with the dimensions of the stiff patterns, and these regimes were decided by the ratio of the actual dimensions in regards of the characteristic lengths[24]. So with the goal of investigating the conditions for crease formation on the surface of a hydrogel under biaxial compression, it is important to first calculate the wavelength of wrinkling (λ_w) and creasing (λ_c) from equations $\lambda_w = 2\pi h_f \left(\frac{\bar{E}_f}{3\bar{E}_s}\right)^{1/3}$ and $\lambda_w \approx 3H$, where h_f is the thickness of the stiff film, H is the thickness of the hydrogel substrate, $\overline{E_f}$ is the plane strain modulus of the film, $\overline{E_s}$ is the plane strain modulus of the substrate[21,27]. In this system, the dimensions and properties of the materials were chosen so that the wavelength of wrinkling and creasing are almost the same, i.e. $h_f = 0.5\ \mu m$, $H = 125\ \mu m$, $\overline{E_f} = 2\ GPa$ and $\overline{E_s} = 3\ kPa$, giving λ_w of 380 μm and λ_w of 375 μm.

These calculations gave a characteristic length of 380 μm, and the patterns were designed accordingly, as shown in Figure 4-1, l_a and l_b are the pattern lengths perpendicular to and parallel to the gap, respectively.

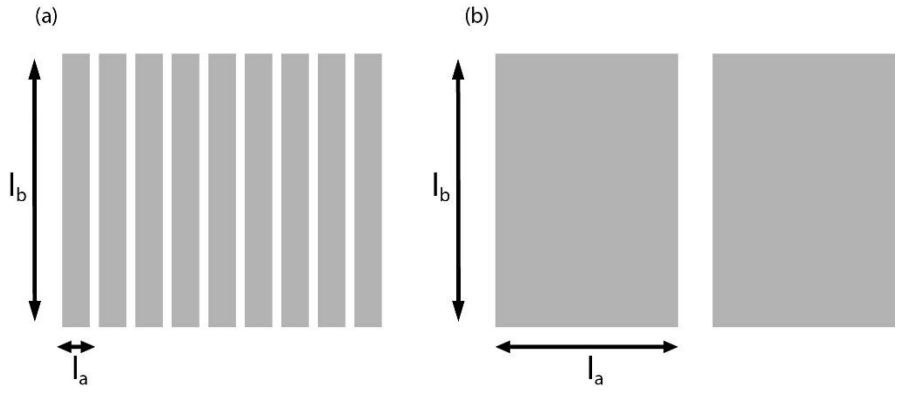

Figure 4- 1 Stiff pattern design on (a) 1-D patches and (b) 2-D islands

4.3.2 Effect of 1-D strips on creasing formation

Firstly, we studied the problem in a 1-D manner, to see how the stiff patches, where l_a was comparable to the characteristic length while l_b was much longer, influence creasing behavior. The SU-8 stripes were 2 cm in length, 2 orders of magnitudes larger than the characteristic length, and several hundred microns wide, comparable to the characteristic length. Figure 4-2 is a cross-sectional view under fluorescent confocal microscope of SU-8 stripes (160 μm wide with 10 μm gap) on a hydrogel. We can change the swelling ratio of the hydrogel substrate by changing temperature and ionic strength of the PBS solution. At 20 ℃ and 68 mM PBS (0.5x PBS), the swelling ratio of a free-standing hydrogel was approximately 1.61 in length, corresponding to a compressive strain of 0.38 for the constrained system. The SU-8 stripes appeared to be flat on the gel surface, and the gap distance was the same as initially patterned, as shown in the top picture where the red features are the SU-8 stripes and dark gaps are of the same width. As we elevated the temperature and reduced the salt concentration, at 50 ℃ and 27 mM PBS (0.2x PBS), the swelling ratio was increased to 1.73 and the system was under 42% strain. Due to the contrast of fluorescent microscopy, the creases could not be observed, but the obvious gap narrowing indicated by arrows implied the presence of creases. Furthermore, when we lowered the temperature back to 20 ℃ and diluted the salt concentration of the environment to 14 mM PBS (0.1x PBS), the swelling ratio was elevated to 1.92 and the system was under 48 % strain. In this condition, every other gap between two stripes disappeared, as shown by the arrows, which confirmed the deepening of the creases were capable of

bringing two neighboring stripes into contact. It is noted that the other gap was widened because the surface area remained the same.

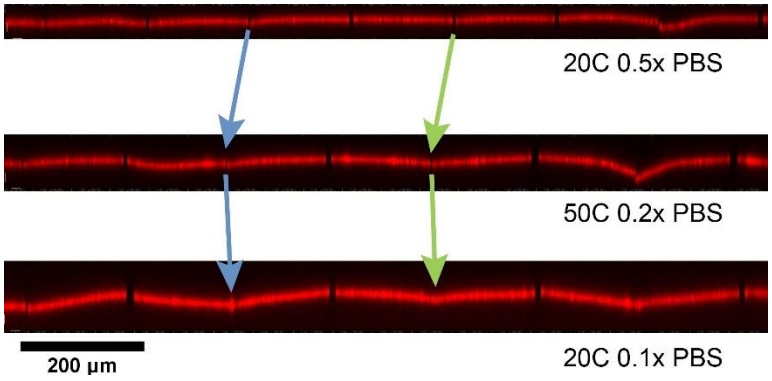

Figure 4- 2 Surface topographical change with temperature and ionic strength: SU-8 stripe on PNIPAM hydrogel.

4.3.3 Effect of 2-D patches on crease formation

With the knowledge that under 1-D conditions, creases tend to form parallel to the stiff pattern's long axis, it is natural to move on to the 2-D case where both dimensions of the stiff film pattern are comparable to the characteristic length.

To start, as shown in Figure 4-3, two 547 µm × 547 µm squares separated by a 34 µm gap were patterned on the hydrogel. When the sample was swelled in 20 ℃ 136 mM PBS (1x PBS), which equates to a strain of 37.5%, the creases formed perpendicularly to the sides of the PpMS pads, which were pushed together due to the compression from the gel. This is shown in the two confocal images that a crease was formed in the center of the gap (Figure 4-3 (c)), and the stiff film was bent in the direction perpendicular to the gap to release stress (Figure 4-3(b)).

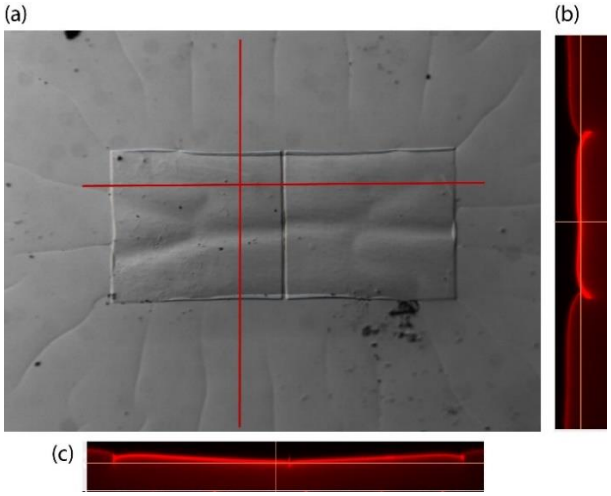

Figure 4- 3 (a) Optical micrograph of creases on hydrogel surface with two 547 μm × 547 μm square PpMS stiff patterns. (b) and (c) are fluorescent confocal images of the cross-sectional view of the stiff pattern on hydrogel along the two indicated lines.

As is demonstrated in Figure 4-4, the formation and disappearance of creases can be modulated by temperature changes because of the thermally-responsive nature of PNIPAM. At 50 ℃, the swelling ratio of the hydrogel was low and the induced compression was below the threshold for creasing, so there were no creases observed. When the temperature was decreased to 20 ℃, the swelling of the hydrogel led to the increase of compressive strain, and a crease formed in the gap, bringing the two pads together. The side along the gap (l_b) was 1 mm.

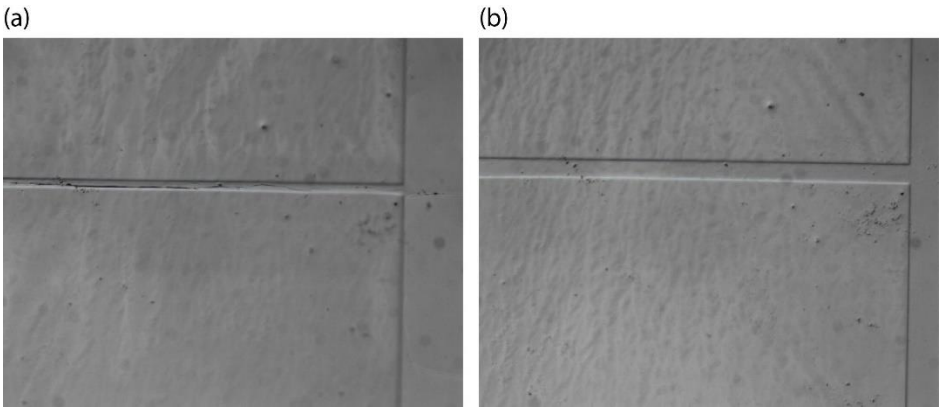

Figure 4- 4 Optical micrographs of hydrogel surface topography in 1x PBS with 547μm × 1mm stiff PpMS patterns with 34 μm gap at (a) 20 ℃ and (b) 50 ℃.

However, when we decreased the stiff pattern side length along the gap, the influence on the crease was changed. As shown in Figure 4-5(a), when l_b was halved from the initial square shape, there was no sign of creases forming in the gap. The stiff film was also bent under the compression from the swelling of neighboring hydrogel. As we further decreased the side length to 137 μm, Figure 4-5(b) shows that the swollen hydrogel invades onto the stiff pattern and forces the film to rotate in width direction into the hydrogel below to release the strain.

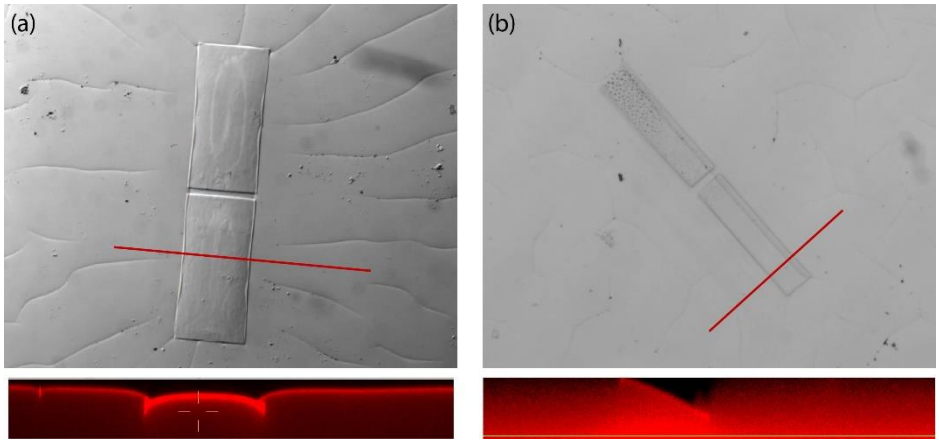

Figure 4- 5 Optical micrograph and confocal images (taken from the cross-section indicated by the red line) of PpMS film of (a) 547 μm × 137 μm and (b) 547 μm × 273 μm on hydrogel.

Other dimensions of the PpMS patterns were tested and the results were summarized in Table 4-1. In the table, ⊥ stands for creasing direction perpendicular to gap, // for creasing direction parallel to gap and × for creasing directions not influenced.

Table 4- 1 Crease direction vs. stiff pattern dimensions

l_a (μm)	Ratio to characteristic length	Aspect ratio (l_a:l_b)				
		4:1	2:1	1:1	1:2	1:4
547	1.44	⊥	⊥	‖	‖	
274	0.72			×	‖	
137	0.36					×

4.4 Conclusion and future work

By fabricating surface attached hydrogel thin films with covalently bonded stiff patterns on top, it is demonstrated that the stiff patterns influence the formation of creases on the hydrogel surface. When the stiff film is slender and has the shorter side length comparable to the characteristic length while the longer side is much longer, the creases tend to orient themselves along the gaps and can bring the two neighboring stripes into contact. When the stiff patterns have both sides comparable to the characteristic length, the direction of the creases is relevant to the pattern dimensions. It is observed that creases tend to form in the gap between two islands until the gap is too short then the creases from perpendicular to the gap to bend or rotate the island. When the crease forms in the gap, the deepening of the crease can close the gap and bring the pads together.

The findings from this project can contribute to both fundamental study of soft matter mechanics and the development of environment sensors. The study of the effect of stiff

patterns on the creases can be enriched by varying the dimension and ratios to construct a phase diagram, as well as be extended to the strain aspect of how the critical strain where creases start to form will be affected. On the application aspect, the phenomenon of creases deepening upon temperature change, thus bringing two neighboring patterns into contact can be applied to design sensors. If the conductivity of the system is controlled by the contact between two patterns, then by triggering the underlying hydrogel to change its swelling ratio and form self-contacting creases, a sensor with a very high on/off ratio can be constructed. This design has been carried out on an elastomer-based sensor for mechanical strain[28], and it is expected that a stimuli-responsive hydrogel system would have broader stimuli choices and a wider application potential.

4.5 References

(1) Welker, W. Why Does Cerebral Cortex Fissure and Fold? A Review of Determinants of Sulci an Gyri. In Cerebral Cortex; 1990. https://doi.org/10.1007/978-1-4615-3824-0.

(2) Dervaux, J.; Ben Amar, M. Localized Growth of Layered Tissues. IMA J. Appl. Math. (Institute Math. Its Appl. 2010. https://doi.org/10.1093/imamat/hxq023.

(3) Dervaux, J.; Couder, Y.; Guedeau-Boudeville, M. A.; Ben Amar, M. Shape Transition in Artificial Tumors: From Smooth Buckles to Singular Creases. Phys. Rev. Lett. 2011. https://doi.org/10.1103/PhysRevLett.107.018103.

(4) Chortos, A.; Liu, J.; Bao, Z. Pursuing Prosthetic Electronic Skin. Nat. Mater. 2016, No. July. https://doi.org/10.1038/nmat4671.

(5) Kim, J.; Yoon, J.; Hayward, R. C. Dynamic Display of Biomolecular Patterns through an Elastic Creasing Instability of Stimuli-Responsive Hydrogels. Nat. Mater. 2010, 9 (2), 159–164. https://doi.org/10.1038/nmat2606.

(6) Tanaka, T.; Sun, S.-T.; Hirokawa, Y.; Katayama, S.; Kucera, J.; Hirose, Y.; Amiya, T. Mechanical Instability of Gels at the Phase Transition. Nature. 1987, pp 796–798. https://doi.org/10.1038/325796a0.

(7) Kang, M. K.; Huang, R. Swell-Induced Surface Instability of Confined Hydrogel Layers on Substrates. J. Mech. Phys. Solids 2010, 58 (10), 1582–1598. https://doi.org/10.1016/j.jmps.2010.07.008.

(8) Bassik, N.; Abebe, B. T.; Laflin, K. E.; Gracias, D. H. Photolithographically Patterned Smart Hydrogel Based Bilayer Actuators. Polymer (Guildf). 2010, 51 (26), 6093–6098. https://doi.org/10.1016/j.polymer.2010.10.035.

(9) Li, G.-Y.; Zheng, Y.; Cao, Y.-P.; Feng, X.-Q.; Zhang, W. Controlling Elastic Wave Propagation in a Soft Bilayer System via Wrinkling-Induced Stress Patterns. Soft Matter 2016, 12, 4204–4213. https://doi.org/10.1039/C6SM00265J.

(10) Thérien-Aubin, H.; Moshe, M.; Sharon, E.; Kumacheva, E. Shape Transformations of Soft Matter Governed by Bi-Axial Stresses. Soft Matter 2015, 11 (23), 4600–4605. https://doi.org/10.1039/C5SM00561B.

(11) Harmon, M. E.; Tang, M.; Frank, C. W. A Microfluidic Actuator Based on Thermoresponsive Hydrogels. Polymer (Guildf). 2003, 44 (16), 4547–4556. https://doi.org/10.1016/S0032-3861(03)00463-4.

(12) Lin, S.; Yuk, H.; Zhang, T.; Parada, G. A.; Koo, H.; Yu, C.; Zhao, X. Stretchable Hydrogel Electronics and Devices. Adv. Mater. 2015, 1–9. https://doi.org/10.1002/adma.201504152.

(13) Sun, Y.; Choi, W. M.; Jiang, H.; Huang, Y. Y.; Rogers, J. a. Controlled Buckling of Semiconductor Nanoribbons for Stretchable Electronics. Nat. Nanotechnol. 2006, 1 (3), 201–207. https://doi.org/10.1038/nnano.2006.131.

(14) Oyewole, O. K.; Yu, D.; Du, J.; Asare, J.; Oyewole, D. O.; Anye, V. C.; Fashina, a.; Zebaze Kana, M. G.; Soboyejo, W. O. Micro-Wrinkling and Delamination-Induced Buckling of Stretchable Electronic Structures. J. Appl. Phys. 2015, 117 (23), 235501. https://doi.org/10.1063/1.4922665.

(15) Tekin, H.; Tsinman, T.; Sanchez, J. G.; Jones, B. J.; Camci-Unal, G.; Nichol, J. W.; Langer, R.; Khademhosseini, A. Responsive Micromolds for Sequential Patterning of Hydrogel Microstructures. J. Am. Chem. Soc. 2011, 133 (33), 12944–12947. https://doi.org/10.1021/ja204266a.

(16) Tekin, H.; Anaya, M.; Brigham, M. D.; Nauman, C.; Langer, R.; Khademhosseini, A. Stimuli-Responsive Microwells for Formation and Retrieval of Cell Aggregates. Lab Chip 2010, 10 (18), 2411. https://doi.org/10.1039/c004732e.

(17) Wang, J.; Li, B.; Cao, Y. P.; Feng, X. Q.; Gao, H. Wrinkling Micropatterns Regulated by a Hard Skin Layer with a Periodic Stiffness Distribution on a Soft Material. Appl. Phys. Lett. 2016, 108 (2). https://doi.org/10.1063/1.4939741.

(18) Nogales, A.; Del Campo, A.; Ezquerra, T. A.; Rodriguez-Hernández, J. Wrinkling and Folding on Patched Elastic Surfaces: Modulation of the Chemistry and Pattern Size of Microwrinkled Surfaces. ACS Appl. Mater. Interfaces 2017, 9 (23), 20188–20195. https://doi.org/10.1021/acsami.7b03161.

(19) Wang, J.-W.; Li, B.; Cao, Y.-P.; Feng, X.-Q. Surface Wrinkling Patterns of Film–Substrate Systems With a Structured Interface. J. Appl. Mech. 2015, 82 (5), 051009. https://doi.org/10.1115/1.4030010.

(20) Bae, H. J.; Bae, S.; Yoon, J.; Park, C.; Kim, K.; Kwon, S.; Park, W. Self-Organization of Maze-like Structures via Guided Wrinkling. Sci. Adv. 2017, 3 (6), e1700071. https://doi.org/10.1126/sciadv.1700071.

(21) Genzer, J.; Groenewold, J. Soft Matter with Hard Skin: From Skin Wrinkles to Templating and Material Characterization. Soft Matter 2006, 2 (4), 310. https://doi.org/10.1039/b516741h.

(22) Shin, H.; Choi, Y.; Cha, J.; Kim, P. Spatially Controlled Folding Instability of Moduli-Patterned and Bilayered Membrane under Compressive Stresses. Adv. Mater. Interfaces 2016, 1600105. https://doi.org/10.1002/admi.201600105.

(23) DuPont Jr., S. J.; Cates, R. S.; Stroot, P. G.; Toomey, R. Swelling-Induced Instabilities in Microscale, Surface-Confined Poly(N-Isopropylacryamide) Hydrogels. Soft Matter 2010, 6 (16), 3876. https://doi.org/10.1039/c0sm00021c.

(24) Ouchi, T.; Yang, J.; Suo, Z.; Hayward, R. C. Effects of Stiff Film Pattern Geometry

on Surface Buckling Instabilities of Elastic Bilayers. ACS Appl. Mater. Interfaces 2018. https://doi.org/10.1021/acsami.8b04916.

(25) Yoon, J.; Kim, J.; Hayward, R. C. Nucleation, Growth, and Hysteresis of Surface Creases on Swelled Polymer Gels. Soft Matter 2010, 6 (22), 5807. https://doi.org/10.1039/c0sm00372g.

(26) Chiappelli, M. C.; Hayward, R. C. Photonic Multilayer Sensors from Photo-Crosslinkable Polymer Films. Adv. Mater. 2012. https://doi.org/10.1002/adma.201202459.

(27) Trujillo, V.; Kim, J.; Hayward, R. C. Creasing Instability of Surface-Attached Hydrogels. Soft Matter 2008, 4 (3), 564. https://doi.org/10.1039/b713263h.

(28) Xu, B.; Chen, D.; Hayward, R. C. Mechanically Gated Electrical Switches by Creasing of Patterned Metal/Elastomer Bilayer Films. Adv. Mater. 2014, 26 (25), 4381–4385. https://doi.org/10.1002/adma.201400992.

CHAPTER 5

PHOTOPATTERNABLE SACRIFACIAL LAYER WITH ORTHOGONAL CROSSLINKING MECHANISMS

5.1 Introduction

Microelectromechanical systems (MEMS) are miniature integrated devices or systems that combine electronical and mechanical components, and they are usually fabricated by manufacturing techniques adapted from the semiconductor industry, including lithography, electrodeposition, etching and molding[1,2]. MEMS have been applied to micro-sensors, micro-actuators, microfluidic devices, biomedical devices, micromachines and microrobotics, among other systems[3,4]. In the fabrication of MEMS devices, sacrificial layers play important roles in extending the complexity of structures that are accessible. A sacrificial layer is a thin layer of material deposited between structural layers for mechanical separation, which is later removed to free the structural layers and allow mechanical devices to move relative to the substrate. The most widely used sacrificial layer materials are silica and other metal oxides, which can be etched by hydrofluoric acid, but they suffer from the limited selectivity in more complex systems and the high risk of the HF etching process[5,6]. Organic polymers are investigated to be release layers for different systems. For example, polyimide later removed by reactive ion etching (RIE) is used in inorganic systems, but this process has little selectivity for organic materials[7,8]; photoresists can be removed by acetone wash or thermal degradation, but these release methods are not compatible with polymeric materials systems[9,10]. Poly(vinyl acid) (PVA) and poly(acrylic acid) (PAA) are also developed as sacrificial layers that can be removed by water or

aqueous solution, and they are used in surface micromachining with different materials systems[11].

Due to the increasing complexity of MEMS structures, there is a growing need for sacrificial layers that can be spatially patterned, so that a higher precision of selective release of actuating components within devices can be achieved, and the downsizing of MEMS device can be furthered. It is reported by Chen and coworkers that by combining a photoresist layer with an oxide layer as a hard mask, followed by RIE, an underlying polyimide sacrificial layer can be patterned, and finally released by oxygen plasma[12]. Also, Harnett developed a heat-depolymerizable polycarbonate sacrificial layer system that can be patterned by electron beam lithography and then released in isopropanol[13]. But both methods have a rather harsh patterning process that can likely only be used for inorganic MEMS systems, and not for organic MEMS systems. A milder method that can be used in organic systems has been developed by Ferrell and coworkers, but process was very complicated: first, a PVA sacrificial layer was coated with PMMA and photoresist, and then patterned by photolithography, then the structural polymer was applied by a PDMS stamp-assisted micromolding process followed by a bonding process under heat and pressure, and finally the PVA sacrificial layer was released by immersion in water[14].

In this chapter, a photo-patternable sacrificial layer with two orthogonal crosslinking mechanisms is developed, as is shown in Figure 5-1. The photo-patternable feature is from the UV crosslinkable benzophenone moieties in the polymer, and the release is achieved by the pH-sensitive imine bonds formed between the diamine crosslinker and the benzaldehyde functional group in the polymer system. The density of crosslinks is controlled such that the absence of either type of crosslinking will place the loosely

crosslinked polymers below the gel point; while the activation of both crosslinking groups will render the material an insoluble network. The content in this chapter is more preliminary than a typical thesis chapter.

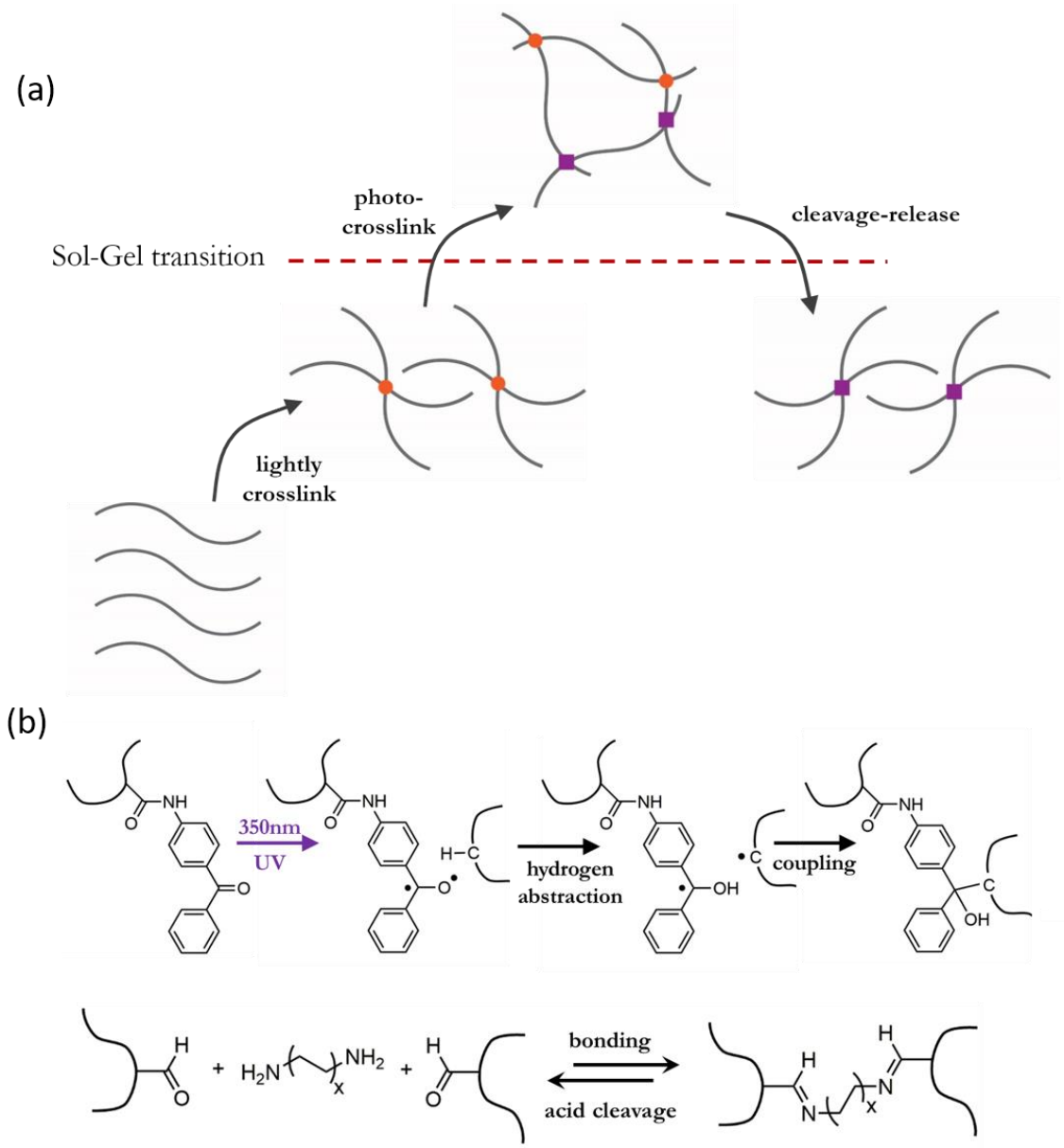

Figure 5- 1 (a) Mechanism of the photo-patternable sacrificial layer using two orthogonal crosslinking methods; (b) the mechanism of the two orthogonal crosslinking methods.

5.2 Materials and methods

Firstly, the monomer 4-formylphenyl methacrylate (BA) was synthesized by a reaction of 4-hydroxybenzaldehyde (2.5 g) and methacryloyl chloride (2.4 mL). The reactants were dissolved in 20 mL of anhydrous dichloromethane (DCM) with 3.13 mL trimethylamine, and allowed to react for 20 h in room temperature, followed by extraction by ethyl acetate. The solution was washed by brine and then dried with sodium sulfate, then finally dried in a vacuum oven overnight. The structure was confirmed by ^{1}H NMR.

The monomers oligo (ethylene glycol) methyl ether methacrylate (OEGMA) (2.375 g), 4-formylphenyl methacrylate (BA) (0.114 g) and 4-acrylamidobenzophenone (BP) (0.050 g) were copolymerized by reversible addition−fragmentation chain-transfer (RAFT) polymerization. The initiator was 2,2'-azobis(2-methylpropionitrile) (AIBN) and the chain transfer agent was butyl 2-cyanopropan-2-yl-carbonotrithioate. The reactants were polymerized in a mixture of 10 mL ethanol and 10 mL 1,4-dioxane at 65 ℃ for 20 h under nitrogen following three freeze-pump-thaw cycles. The resulting polymer was purified by dialysis in water and lyophilization. ^{1}H NMR (Bruker 400 MHz) revealed the copolymer composition as OEGMA:BA:BP = 19:3.6:1. DMF GPC was used to determine a M_n of 5.5 kg/mol with a dispersity of 1.3 against PMMA standards.

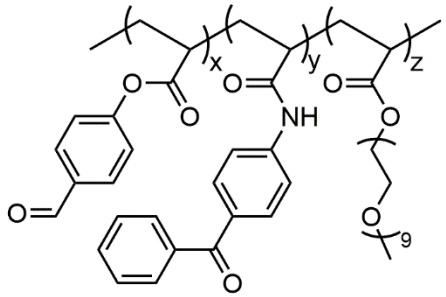

Figure 5- 2 Chemical structure of the P(OEGMA-BA-BP) copolymer.

Then the linear copolymer was crosslinked by imine bonding with a diamine small molecule. The P(OEGMA-BA-BP) copolymer (0.212 g) and hexamethlenediamine (4.4 mg) were dissolved in deionized water and allowed to react for 24 h under room temperature. The resulting polymer was dialyzed against water and lyophilized to purify. Gel permeation chromatography (DMF as eluent) showed an increase in molecular weight, ^{1}H NMR showed a decrease of approximately 30% in the aldehyde proton signal, and infrared spectroscopy showed an increase in the C=N stretching peak, revealing the formation of the imine bond.

The lightly-crosslinked polymer were then dissolved in methanol and spin-casted into a thin film. Parts of the film was exposed to 365 nm UV illumination (Lumen Dynamics, XCite 120Q) through a mask, and then the film was developed in a marginal solution of toluene/hexane mixture (11:3, v/v). Finally, the film was dissolved in a pH=4 hydrochloric acid solution. The optical micrographs are taken with an upright optical microscope (Zeiss, Axiotech Vario).

5.3 Results and discussion

5.3.1 Photo-patterning and acid release

To start with, the feasibility of constructing a photo-patternable sacrificial layer by benzophenone crosslinking and imine bonding was tested. When the copolymer was lightly crosslinked by the diamine linking two aldehyde moieties through imine bonding, it was still soluble in toluene and can be casted into thin films. The benzophenone moieties in the thin film will be activated under 365 nm UV light and form covalent bonds with neighboring chains. The activation of the benzophenone crosslinking will render the film

insoluble in the developer solvent mixture. So when this film is partially exposed and developed, the illuminated area will remain on the substrate, while the unexposed part will be washed away by the developer, as is shown in Figure 5-3 (a).

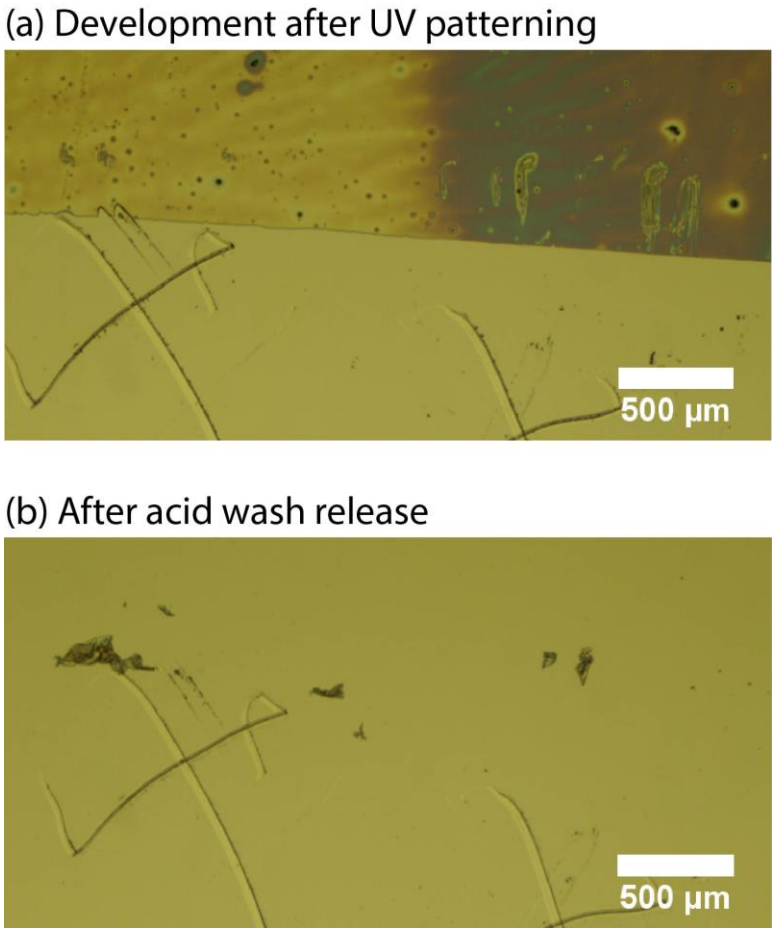

Figure 5- 3 (a) Spin-cast diamine-crosslinked copolymer film after UV patterning and POEGMA developing; (b) the UV crosslinked layer is released after acid wash

After patterning and developing, it is important to fully dissolve the film to release the overlaying structure. The film was immersed into a mildly acidic (pH=3) aqueous solution to break the imine bonds, leaving only benzophenone crosslinking in the film, bringing the system below the gel point and rendering the polymer soluble again in the aqueous solution,

as is shown in Figure 5-3 (b) that the the UV-exposed portion of the film is washed away. The crossed scratches are to show the position is the same in Figure 5-3 (a) and (b).

5.3.2 Suspended cantilever structure

The next step is to demonstrate that this photo-patternable sacrificial layer can be used to construct a suspended cantilever structure. The P(pMS-BP) copolymer from Chapter 4 was used as a stiff structural layer. The sacrificial layer was firstly spin-casted and patterned, then at the stage of some part of the substrate was exposed after development, the P(pMS-BP) copolymer was spin-coated onto the substrate and patterned under 365 nm UV light by digital mirror devices. After developing, a glassy polymeric rectangle shape is deposited onto the edge of the sacrificial layer, part of the structural film on the sacrificial layer and the other part is directly on the bare Si substrate, as in Figure 5-4 (a). Then the sacrificial layer is released in acidic solution, but the PpMS layer is not damaged by the acid, left as a cantilever, as in Figure 5-4 (b). The suspension of the released part of the PpMS film was confirmed by mechanically poking the right part of PpMS film with tweezers. It should be noted that the sacrificial layer was not uniform across the sample, which can possibly be improved by changing to other spin-coating solvents in the future.

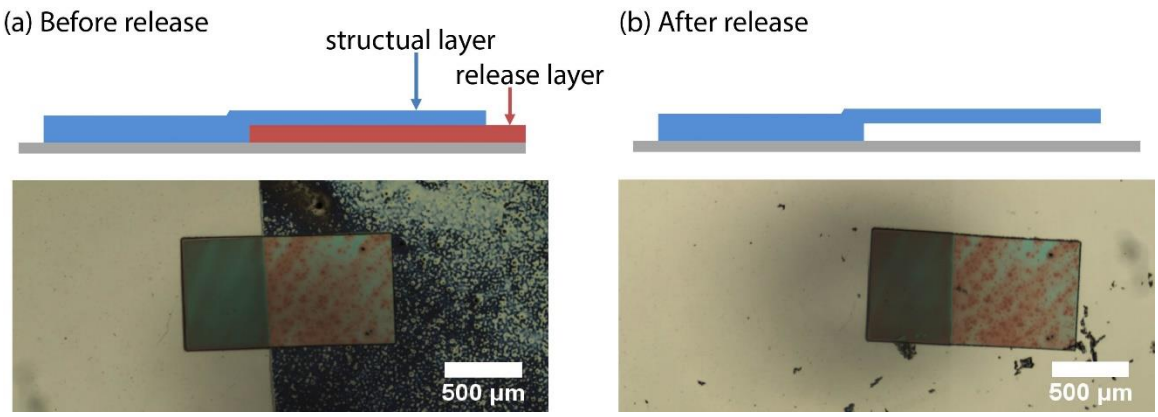

Figure 5- 4 The construction of a PpMS cantilever using the photo-patternable sacrificial layer. (a) Scheme and micrograph of structural layer deposited on the edge of sacrificial layer; (b) Scheme and micrograph of structural layer suspended after the release of the underlying sacrificial layer.

5.4 Conclusion and future work

In this chapter, a photopatternable sacrificial layer was developed by incorporating two orthogonal crosslinking mechanisms, benzophenone crosslinking under UV illumination and acid-cleavable imine bonding between aldehyde and diamine. The patterning was carried out by maskless lithography and the development conditions used were mild. A freely suspended layer of PpMS was constructed by this method.

This photopatternable sacrificial layer has great potential in being applied in the fabrication of complex MEMS devices. Instead of the current mechanical scratching operations, this photopatternablity offers improved precision and complexity. For example, biomedical MEMS devices are usually made from polymeric materials due to their biocompatibility, and their development trend of miniaturizing and more complex hierarchical architectures will benefit from this method.

5.5 References

(1) Maluf, N. An Introduction to Microelectromechanical Systems Engineering. *Meas. Sci. Technol.* **2002**. https://doi.org/10.1088/0957-0233/13/2/701.

(2) University, L. *An Introduction to MEMS (Micro-Electromechanical Systems)*; 2002.

(3) Grayson, A. C. R.; Shawgo, R. S.; Johnson, A. M.; Flynn, N. T.; Li, Y.; Cima, M. J.; Langer, R. A BioMEMS Review: MEMS Technology for Physiologically Integrated Devices. In *Proceedings of the IEEE*; 2004. https://doi.org/10.1109/JPROC.2003.820534.

(4) Gad-el-Hak, M. *MEMS: Applications*; 2005. https://doi.org/10.1006/rwvb.2001.0075.

(5) Madou, M. *Fundamentals of Microfabrication: The Science of Miniaturization*; 2002.

(6) Westberg, D.; Paul, O.; Andersson, G. I.; Baites, H. Surface Micromachining by Sacrificial Aluminium Etching. *J. Micromechanics Microengineering* **1996**. https://doi.org/10.1088/0960-1317/6/4/004.

(7) Bagolini, A.; Pakula, L.; Scholtes, T. L. M.; Pham, H. T. M.; French, P. J.; Sarro, P. M. Polyimide Sacrificial Layer and Novel Materials for Post-Processing Surface Micromachining. *J. Micromechanics Microengineering* **2002**. https://doi.org/10.1088/0960-1317/12/4/306.

(8) Boroumand Azad, J.; Rezadad, I.; Nath, J.; Smith, E.; Peale, R. E. Release of MEMS Devices with Hard-Baked Polyimide Sacrificial Layer. In *Advances in Resist Materials and Processing Technology XXX*; 2013. https://doi.org/10.1117/12.2018628.

(9) Walsh, K.; Norville, J.; Tai, Y. C. Photoresist as a Sacrificial Layer by Dissolution in Acetone. In *Proceedings of the IEEE Micro Electro Mechanical Systems (MEMS)*; 2001. https://doi.org/10.1109/memsys.2001.906492.

(10) Song, I. H.; Ajmera, P. K. Use of a Photoresist Sacrificial Layer with SU-8 Electroplating Mould in MEMS Fabrication. *J. Micromechanics Microengineering* **2003**. https://doi.org/10.1088/0960-1317/13/6/304.

(11) Linder, V.; Gates, B. D.; Ryan, D.; Parviz, B. A.; Whitesides, G. M. Water-Soluble Sacrificial Layers for Surface Micromachining. *Small* **2005**, *1* (7), 730–736. https://doi.org/10.1002/smll.200400159.

(12) Chen, Y.; Mao, H.; Tan, Q.; Xue, C.; Ou, W.; Liu, J.; Chen, D. Fabrication of Polyimide Sacrificial Layers with Inclined Sidewalls Based on Reactive Ion Etching. *AIP Adv.* **2014**. https://doi.org/10.1063/1.4868379.

(13) Harnett, C. K.; Coates, G. W.; Craighead, H. G. Heat-Depolymerizable Polycarbonates as Electron Beam Patternable Sacrificial Layers for Nanofluidics. *J. Vac. Sci. Technol. B Microelectron. Nanom. Struct.* **2001**, *19* (6), 2842. https://doi.org/10.1116/1.1409383.

(14) Ferrell, N.; Woodard, J.; Hansford, D. Fabrication of Polymer Microstructures for MEMS: Sacrificial Layer Micromolding and Patterned Substrate Micromolding. *Biomed. Microdevices* **2007**, *9* (6), 815–821. https://doi.org/10.1007/s10544-007-9094-y.

CHAPTER 6

CONCLUSION AND OUTLOOK

The aim of this thesis was to further the understanding and explore the application of nano- and micro- structured responsive hydrogel systems by interfacing with microelectromechanical systems (MEMS). Upon the change of environmental stimuli, free-standing hydrogels undergo volumetric change, known as swelling and deswelling, and surface-attached hydrogels may buckle into creases when under sufficient compression. MEMS devices and micro-fabrication techniques allow for investigations of the hydrogel system in the aspects of kinetics, mechanics and responsiveness, in local regions and micro-scale features, in contrast to bulk materials that are more often studied.

A major limitation in the application of responsive hydrogel systems is that the swelling kinetics are limited by the diffusion limit of solvent molecules, so miniature features and shorter transport distance are desired. Micro-heaters fabricated through traditional microfabrication procedures were used to achieve fast and regional temperature change by Joule heating, and were used in both the development of an *in vitro* platform for biomedical studies and the fundamental investigation of hydrogel swelling and deswelling kinetics. In Chapter 2, the fast temperature change induced the cyclic swelling and deswelling of the PNIPAM hydrogel, and the deepening and relaxation of parallel creases exerted stretching strain on the human artery smooth muscle cell (HASMC) attached in between. This hydrogel-based system was optimized mechanically and chemically to mimic the *in vivo* environment of a HASMC in the aspects of artery wall stiffness, rate and magnitude of cyclic mechanical stretch, and integrin-binding sites. The resulting platform was well-

controllable and biologically relevant, and was used to study the expression change of differentiation marker proteins in SMCs. In Chapter 3, microheaters were used to investigate the source of a widely-observed but not well-understood phenomenon that PNIPAM hydrogel systems with a high solid content exhibit a two-step pattern in the swelling/deswelling kinetics. Free standing PNIPAM hydrogel sheets and PDEAM hydrogel sheets that lack inter-chain hydrogen bonding were prepared and compared systematically, leading to the conclusion that inter-chain hydrogen bonding was associated with the two-step pattern of PNIPAM gels, while the kinetics of PDEAM gel volumetric change was limited by mass transport in poroelastic networks. These two works showed that introducing MEMS into responsive hydrogel systems can overcome the limitation of bulk hydrogel systems in ambient environment, and many research and applications can be derived from this interface.

These two examples lead us to expect the wide possibilities arise at the interface of responsive hydrogel systems and MEMS technology. MEMS being a mass-producible low-cost technology, responsive hydrogel systems can be fabricated into arrays to amplify their output to small changes in the environmental stimuli. The dramatic volumetric change in hydrogel swelling and deswelling process exhibits high reversibility and reproducibility, making them desirable triggering or actuating components in microfluidic devices. Also, one could imagine the incorporation of polymeric MEMS system into hydrogel-based biomedical sensors and actuators, where the biocompatibility and responsiveness of hydrogels are preserved, while the MEMS devices would provide environmental cues with better precision and remote controllability. Furthermore, incorporating MEMS into soft hydrogel systems would open up new approaches in the fabrication of flexible electronics,

soft sensors and actuators. Surely there are still challenges in this field, for example: the poor affinity between water-containing organic network and the inorganic rigid MEMS materials may result in delamination failure of the device; the dramatic thermal, electrical and mechanical property mismatch of components may render the device only functional under some specific environmental requirements; and the slow kinetics of hydrogel systems will be the rate-limiting step of MEMS sensors and actuators. These challenges may spur the advance of adhesion sciences and processing technologies, but also can be turned into new innovation possibilities, such as the mismatch being exploited to construct instability-based actuators where higher on/off ratio, and the kinetics lag contributing to self-sustaining oscillator designs.

Besides incorporating MEMS devices into hydrogel systems as the trigger, photo-patterning techniques were also applied to hydrogel systems in order to introduce modulus contrast in the study of hydrogel surface instability mechanics. Stiff pads were patterned onto the soft hydrogel substrate by photolithography, and it was demonstrated that stiff pads can influence the formation of creases nearby, and the crease direction .can be altered by changing the dimension of the pads.

Moreover, the knowledge in hydrogel networks and crosslinking mechanisms contributed to a potentially powerful tool in MEMS fabrication. A photo-patternable sacrificial layer was obtained by the careful design of two orthogonal crosslinking mechanisms. The sacrificial layer could be patterned under UV illumination by benzophenone grafting, and was released by the cleavage of imine bonds in mild acidic aqueous solution.

Although this thesis mainly used temperature-responsive hydrogel systems, it should be noted that the integration of MEMS could extend the possibilities offered by hydrogel systems with responsiveness to other stimuli, such as pH, electric fields and magnetic fields. I hope our work presented in this thesis can contribute to the future fundamental studies and application developments regarding responsive hydrogel systems and MEMS techniques in a various fields.

BIBILOGRAPHY

Buwalda, S. J.; Boere, K. W. M.; Dijkstra, P. J.; Feijen, J.; Vermonden, T.; Hennink, W. E. Hydrogels in a Historical Perspective: From Simple Networks to Smart Materials. *Journal of Controlled Release*. 2014.

Tokarev, I.; Minko, S. Stimuli-Responsive Hydrogel Thin Films. *Soft Matter*. 2009.

Ganji, F.; Vasheghani-Farahani, S.; Vasheghani-Farahani, E. Theoretical Description of Hydrogel Swelling: A Review. *Iran. Polym. J. (English Ed.* **2010**.

Roy, D.; Cambre, J. N.; Sumerlin, B. S. Future Perspectives and Recent Advances in Stimuli-Responsive Materials. *Progress in Polymer Science (Oxford)*. 2010.

Gerlach, G.; Arndt, K.-F. Hydrogel Sensors and Actuators. *Springer Ser. Chem. Sensors Biosens.* **2009**, *6*, 1–15.

Jeon, S. J.; Hauser, A. W.; Hayward, R. C. Shape-Morphing Materials from Stimuli-Responsive Hydrogel Hybrids. *Acc. Chem. Res.* **2017**, *50* (2), 161–169.

Stuart, M. A. C.; Huck, W. T. S.; Genzer, J.; Müller, M.; Ober, C.; Stamm, M.; Sukhorukov, G. B.; Szleifer, I.; Tsukruk, V. V.; Urban, M.; et al. Emerging Applications of Stimuli-Responsive Polymer Materials. *Nature Materials*. 2010.

Hoffman, A. S. Hydrogels for Biomedical Applications. *Advanced Drug Delivery Reviews*. 2012.

Hoare, T. R.; Kohane, D. S. Hydrogels in Drug Delivery: Progress and Challenges. *Polymer*. 2008.

Schmidt, S.; Zeiser, M.; Hellweg, T.; Duschl, C.; Fery, A.; Möhwald, H. Adhesion and Mechanical Properties of PNIPAM Microgel Films and Their Potential Use as Switchable Cell Culture Substrates. *Adv. Funct. Mater.* **2010**.

Holtz, J. H.; Asher, S. A. Polymerized Colloidal Crystal Hydrogel Films as Intelligent Chemical Sensing Materials. *Nature* **1997**.

Xue, W.; Huglin, M. B.; Khoshdel, E. Behaviour of Crosslinked and Linear Poly[1-(3-sulphopropyl)-2-vinyl-pyridinium-betaine] in Aqueous Salt Solutions. *Polym. Int.* **1999**.

Katono, H.; Maruyama, A.; Sanui, K.; Ogata, N.; Okano, T.; Sakurai, Y. Thermo-Responsive Swelling and Drug Release Switching of Interpenetrating Polymer Networks Composed of Poly(Acrylamide-Co-Butyl Methacrylate) and Poly (Acrylic Acid). *J. Control. Release* **1991**.

Feil, H.; Bae, Y. H.; Feijen, J.; Kim, S. W. Effect of Comonomer Hydrophilicity and

Ionization on the Lower Critical Solution Temperature of N-Isopropylacrylamide Copolymers. *Macromolecules* **1993**.

Liu, H. Y.; Zhu, X. X. Lower Critical Solution Temperatures of N-Substituted Acrylamide Copolymers in Aqueous Solutions. *Polymer (Guildf).* **1999**.

Furyk, S.; Zhang, Y.; Ortiz-Acosta, D.; Cremer, P. S.; Bergbreiter, D. E. Effects of End Group Polarity and Molecular Weight on the Lower Critical Solution Temperature of Poly(N-Isopropylacrylamide). *J. Polym. Sci. Part A Polym. Chem.* **2006**.

Dalkas, G.; Pagonis, K.; Bokias, G. Control of the Lower Critical Solution Temperature - Type Cononsolvency Properties of Poly(N-Isopropylacrylamide) in Water - Dioxane Mixtures through Copolymerisation with Acrylamide. *Polymer (Guildf).* **2006**.

Costa, R. O. R.; Freitas, R. F. S. Phase Behavior of Poly (N-Isopropylacrylamide) in Binary Aqueous Solutions. *Polymer (Guildf).* **2002**.

Senff, H.; Richtering, W. Influence of Cross-Link Density on Rheological Properties of Temperature-Sensitive Microgel Suspensions. *Colloid Polym. Sci.* **2000**.

Schild, H. G. Poly(N-Isopropylacrylamide): Experiment, Theory and Application. *Progress in Polymer Science*. 1992.

Idziak, I.; Avoce, D.; Lessard, D.; Gravel, D.; Zhu, X. X. Thermosensitivity of Aqueous Solutions of Poly(N,N-Diethylacrylamide). *Macromolecules* **1999**.

Cho, S. H.; Jhon, M. S.; Yuk, S. H. Temperature-Sensitive Swelling Behavior of Polymer Gel Composed of Poly (N,N-Dimethylaminoethyl Methacrylate) and Its Copolymers. *Eur. Polym. J.* **1999**.

Akashi, M.; Nakano, S.; Kishida, A. Synthesis of Poly(N-Vinylisobutyramide) from Poly(N-Vinylacetamide) and Its Thermosensitive Property. *J. Polym. Sci. Part A Polym. Chem.* **1996**.

Winnik, F. M. Effect of Temperature on Aqueous Solutions of Pyrene-Labeled (Hydroxypropyl)Cellulose. *Macromolecules* **1987**.

Cho, E. C.; Lee, J.; Cho, K. Role of Bound Water and Hydrophobic Interaction in Phase Transition of Poly(N-Isopropylacrylamide) Aqueous Solution. *Macromolecules* **2003**.

Ashraf, S.; Park, H. K.; Park, H.; Lee, S. H. Snapshot of Phase Transition in Thermoresponsive Hydrogel PNIPAM: Role in Drug Delivery and Tissue Engineering. *Macromolecular Research*. 2016.

Hirokawa, Y.; Tanaka, T. Volume Phase Transition in a Nonionic Gel. *J. Chem. Phys.* **1984**.

Bae, Y. H.; Okano, T.; Kim, S. W. Temperature Dependence of Swelling of Crosslinked

Poly(N,N′-alkyl Substituted Acrylamides) in Water. *J. Polym. Sci. Part B Polym. Phys.* **1990**.

Koetting, M. C.; Peters, J. T.; Steichen, S. D.; Peppas, N. A. Stimulus-Responsive Hydrogels: Theory, Modern Advances, and Applications. *Materials Science and Engineering R: Reports*. 2015.

Lu, Y.; Zhou, K.; Ding, Y.; Zhang, G.; Wu, C. Origin of Hysteresis Observed in Association and Dissociation of Polymer Chains in Water. *Phys. Chem. Chem. Phys.* **2010**.

Pang, X.; Cui, S. Single-Chain Mechanics of Poly(N, N -Diethylacrylamide) and Poly(N -Isopropylacrylamide): Comparative Study Reveals the Effect of Hydrogen Bond Donors. *Langmuir* **2013**, *29* (39), 12176–12182.

Genzer, J.; Groenewold, J. Soft Matter with Hard Skin: From Skin Wrinkles to Templating and Material Characterization. *Soft Matter* **2006**, *2* (4), 310.

Wang, Q.; Zhao, X. A Three-Dimensional Phase Diagram of Growth-Induced Surface Instabilities. *Sci. Rep.* **2015**, *5* (iv), 8887.

Wang, Q.; Zhao, X. Beyond Wrinkles: Multimodal Surface Instabilities for Multifunctional Patterning. *MRS Bull.* **2016**, *41* (02), 115–122.

Chen, D.; McKinley, G. H.; Cohen, R. E. Spontaneous Wettability Patterning via Creasing Instability. *Proc. Natl. Acad. Sci.* **2016**, *113* (29), 8087–8092.

Görrn, P.; Lehnhardt, M.; Kowalsky, W.; Riedl, T.; Wagner, S. Elastically Tunable Self-Organized Organic Lasers. *Adv. Mater.* **2011**.

Khang, D. Y.; Jiang, H.; Huang, Y.; Rogers, J. A. A Stretchable Form of Single-Crystal Silicon for High-Performance Electronics on Rubber Subtrates. *Science (80-.).* **2006**.

Gau, H.; Herminghaus, S.; Lenz, P.; Lipowsky, R. Liquid Morphologies on Structured Surfaces: From Microchannels to Microchips. *Science (80-.).* **1999**.

Stafford, C. M.; Harrison, C.; Beers, K. L.; Karim, A.; Amis, E. J.; Vanlandingham, M. R.; Kim, H. C.; Volksen, W.; Miller, R. D.; Simonyi, E. E. A Buckling-Based Metrology for Measuring the Elastic Moduli of Polymeric Thin Films. *Nat. Mater.* **2004**.

Biot, M. A. Surface Instability of Rubber in Compression. *Appl. Sci. Res. Sect. A* **1963**.

Chen, D.; Cai, S.; Suo, Z.; Hayward, R. C. Surface Energy as a Barrier to Creasing of Elastomer Films: An Elastic Analogy to Classical Nucleation. *Phys. Rev. Lett.* **2012**.

Mora, S.; Abkarian, M.; Tabuteau, H.; Pomeau, Y. Surface Instability of Soft Solids under Strain. *Soft Matter* **2011**.

Hohlfeld, E.; Mahadevan, L. Scale and Nature of Sulcification Patterns. *Phys. Rev. Lett.*

2012.

Cai, S.; Chen, D.; Suo, Z.; Hayward, R. C. Creasing Instability of Elastomer Films. *Soft Matter* **2012**.

Weiss, F.; Cai, S.; Hu, Y.; Kyoo Kang, M.; Huang, R.; Suo, Z. Creases and Wrinkles on the Surface of a Swollen Gel. *J. Appl. Phys.* **2013**, *114* (7).

Trujillo, V.; Kim, J.; Hayward, R. C. Creasing Instability of Surface-Attached Hydrogels. *Soft Matter* **2008**, *4* (3), 564.

DuPont Jr., S. J.; Cates, R. S.; Stroot, P. G.; Toomey, R. Swelling-Induced Instabilities in Microscale, Surface-Confined Poly(N-Isopropylacryamide) Hydrogels. *Soft Matter* **2010**, *6* (16), 3876.

Kim, J.; Yoon, J.; Hayward, R. C. Dynamic Display of Biomolecular Patterns through an Elastic Creasing Instability of Stimuli-Responsive Hydrogels. *Nat. Mater.* **2010**, *9* (2), 159–164.

Yoon, J.; Bian, P.; Kim, J.; McCarthy, T. J.; Hayward, R. C. Local Switching of Chemical Patterns through Light-Triggered Unfolding of Creased Hydrogel Surfaces. *Angew. Chemie - Int. Ed.* **2012**, *51* (29), 7146–7149.

Xu, B.; Hayward, R. C. Low-Voltage Switching of Crease Patterns on Hydrogel Surfaces. *Adv. Mater.* **2013**.

Chen, D.; Hyldahl, R. D.; Hayward, R. C. Creased Hydrogels as Active Platforms for Mechanical Deformation of Cultured Cells. *Lab Chip* **2015**, *15* (4), 1160–1167.

Arifuzzaman, M.; Wu, Z. L.; Kurokawa, T.; Kakugo, A.; Gong, J. P. Swelling-Induced Long-Range Ordered Structure Formation in Polyelectrolyte Hydrogel. *Soft Matter* **2012**.

Arifuzzaman, M.; Wu, Z. L.; Takahashi, R.; Kurokawa, T.; Nakajima, T.; Gong, J. P. Geometric and Edge Effects on Swelling-Induced Ordered Structure Formation in Polyelectrolyte Hydrogels. *Macromolecules* **2013**.

Chan, E. P.; Karp, J. M.; Langer, R. S. A "Self-Pinning" Adhesive Based on Responsive Surface Wrinkles. *J. Polym. Sci. Part B Polym. Phys.* **2011**, *49* (1), 40–44.

Bouklas, N.; Huang, R. Swelling Kinetics of Polymer Gels: Comparison of Linear and Nonlinear Theories. *Soft Matter* **2012**.

Tanaka, T.; Hocker, L. O.; Benedek, G. B. Spectrum of Light Scattered from a Viscoelastic Gel. *J. Chem. Phys.* **1973**.

Tanaka, T.; Fillmore, D. J. Kinetics of Swelling of Gels. *J. Chem. Phys.* **1979**, *70* (3), 1214–1218.

Biot, M. A. General Theory of Three-Dimensional Consolidation. *J. Appl. Phys.* **1941**.

Scherer, G. W. Drying Gels. VIII. Revision and Review. *J. Non. Cryst. Solids* **1989**.

Doi, M. Gel Dynamics. *J. Phys. Soc. Japan* **2009**, *78* (5), 1–19.

Galli, M.; Comley, K. S. C.; Shean, T. A. V.; Oyen, M. L. Viscoelastic and Poroelastic Mechanical Characterization of Hydrated Gels. *J. Mater. Res.* **2009**.

Hu, Y.; Zhao, X.; Vlassak, J. J.; Suo, Z. Using Indentation to Characterize the Poroelasticity of Gels. *Appl. Phys. Lett.* **2010**.

Durning, C. J.; Morman, K. N. Nonlinear Swelling of Polymer Gels. *J. Chem. Phys.* **1993**, *98* (5), 4275–4293.

Rajagopal, K. R. Diffusion through Polymeric Solids Undergoing Large Deformations. *Materials Science and Technology*. 2003.

Hong, W.; Zhao, X.; Zhou, J.; Suo, Z. A Theory of Coupled Diffusion and Large Deformation in Polymeric Gels. *J. Mech. Phys. Solids* **2008**.

Baek, S.; Srinivasa, A. R. Diffusion of a Fluid through an Elastic Solid Undergoing Large Deformation. *Int. J. Non. Linear. Mech.* **2004**.

Yoon, J.; Cai, S.; Suo, Z.; Hayward, R. C. Poroelastic Swelling Kinetics of Thin Hydrogel Layers: Comparison of Theory and Experiment. *Soft Matter* **2010**, *6* (23), 6004–6012.

Franssila, S. *Introduction to Microfabrication*; 2010.

Dormán, G.; Prestwich, G. D. Benzophenone Photophores in Biochemistry. *Biochemistry* **1994**.

Prucker, O.; Naumann, C. A.; Rühe, J.; Knoll, W.; Frank, C. W. Photochemical Attachment of Polymer Films to Solid Surfaces via Monolayers of Benzophenone Derivatives. *J. Am. Chem. Soc.* **1999**.

Scott, G. Mechanisms of Photophysical Processes and Photochemical Reactions in Polymers: Theory and Applications J. F. Rabek, John Wiley and Sons, Chichester, 1987. Pp. Xix + 756, Price £99.00. ISBN 0-47 1-9 11 80-1. *Br. Polym. J.* **1988**.

Li, G.; He, G.; Zheng, Y.; Wang, X.; Wang, H. Surface Photografting Initiated by Benzophenone in Water and Mixed Solvents Containing Water and Ethanol. *J. Appl. Polym. Sci.* **2012**.

Higuchi, H.; Yamashita, T.; Horie, K.; Mita, I. Photo-Cross-Linking Reaction of Benzophenone-Containing Polyimide and Its Model Compounds. *Chem. Mater.* **1991**.

Christensen, S. K.; Chiappelli, M. C.; Hayward, R. C. Gelation of Copolymers with

Pendent Benzophenone Photo-Cross-Linkers. *Macromolecules* **2012**, *45* (12), 5237–5246.

Lin, A. A.; Sastri, V. R.; Tesoro, G.; Reiser, A.; Eachus, R. On the Crosslinking Mechanism of Benzophenone-Containing Polyimides. *Macromolecules* **1988**.

Kim, J.; Hanna, J. A.; Byun, M.; Santangelo, C. D.; Hayward, R. C. Designing Responsive Buckled Surfaces by Halftone Gel Lithography. *Science (80-.).* **2012**.

Kim, J.; Hanna, J. A.; Hayward, R. C.; Santangelo, C. D. Thermally Responsive Rolling of Thin Gel Strips with Discrete Variations in Swelling. *Soft Matter* **2012**.

Chopra, K. L.; Paulson, P. D.; Dutta, V. Thin-Film Solar Cells: An Overview. *Prog. Photovoltaics Res. Appl.* **2004**.

Mahan, J. E. Physical Vapor Deposition of Thin Films. *Physical Vapor Deposition of Thin Films, by John E. Mahan, pp. 336. ISBN 0-471-33001-9. Wiley-VCH , January 2000.* 2000.

Martin, P. M. *Introduction to Surface Engineering and Functionally Engineered Materials*; 2011.

Holmberg, K.; Mathews, A. Coatings Tribology: A Concept, Critical Aspects and Future Directions. *Thin Solid Films* **1994**.

Li, Y.; Mann, D.; Rolandi, M.; Kim, W.; Ural, A.; Hung, S.; Javey, A.; Cao, J.; Wang, D.; Yenilmez, E.; et al. Preferential Growth of Semiconducting Single-Walled Carbon Nanotubes by a Plasma Enhanced CVD Method. *Nano Lett.* **2004**.

Hozumi, A.; Takai, O. Preparation of Ultra Water-Repellent Films by Microwave Plasma-Enhanced CVD. *Thin Solid Films* **1997**.

Libby, P.; Ridker, P. M.; Hansson, G. K. Progress and Challenges in Translating the Biology of Atherosclerosis. *Nature*. 2011.

Libby, P. Vascular Biology of Atherosclerosis: Overview and State of the Art. In *American Journal of Cardiology*; 2003.

Glass, C. K.; Witztum, J. L. Atherosclerosis: The Road Ahead. *Cell*. 2001.

Ip, J. H.; Fuster, V.; Badimon, L.; Badimon, J.; Taubman, M. B.; Chesebro, J. H. Syndromes of Accelerated Atherosclerosis: Role of Vascular Injury and Smooth Muscle Cell Proliferation. *Journal of the American College of Cardiology*. 1990.

Li, Z.; Cheng, H.; Lederer, W. J.; Froehlich, J.; Lakatta, E. G. Enhanced Proliferation and Migration and Altered Cytoskeletal Proteins in Early Passage Smooth Muscle Cells from Young and Old Rat Aortic Explants. *Exp. Mol. Pathol.* **1997**, *64* (1), 1–11.

Stegemann, J. P. Mechanical, Biochemical, and Extracellular Matrix Effects on Vascular Smooth Muscle Cell Phenotype. *J. Appl. Physiol.* **2005**, *98* (6), 2321–2327.

Gomez, D.; Owens, G. K. Smooth Muscle Cell Phenotypic Switching in Atherosclerosis. *Cardiovasc Res* **2012**, *95* (2), 156–164.

Rensen, S. S. M.; Doevendans, P. A. F. M.; Van Eys, G. J. J. M. Regulation and Characteristics of Vascular Smooth Muscle Cell Phenotypic Diversity. *Netherlands Heart Journal*. 2007.

Milewicz, D. M.; Kwartler, C. S.; Papke, C. L.; Regalado, E. S.; Cao, J.; Reid, A. J. Genetic Variants Promoting Smooth Muscle Cell Proliferation Can Result in Diffuse and Diverse Vascular Diseases: Evidence for a Hyperplastic Vasculomyopathy. *Genetics in Medicine*. 2010.

Blindt, R.; Vogt, F.; Lamby, D.; Zeiffer, U.; Krott, N.; Hilger-Eversheim, K.; Hanrath, P.; Vom Dahl, J.; Bosserhoff, A. K. Characterization of Differential Gene Expression in Quiescent and Invasive Human Arterial Smooth Muscle Cells. *J. Vasc. Res.* **2002**.

Trappmann, B.; Chen, C. S. How Cells Sense Extracellular Matrix Stiffness: A Material's Perspective. *Curr. Opin. Biotechnol.* **2013**, *24* (5), 948–953.

Mann, B. K.; Gobin, A. S.; Tsai, A. T.; Schmedlen, R. H.; West, J. L. Smooth Muscle Cell Growth in Photopolymerized Hydrogels with Cell Adhesive and Proteolytically Degradable Domains: Synthetic ECM Analogs for Tissue Engineering. *Biomaterials* **2001**, *22* (22), 3045–3051.

Leung, D. Y. M.; Glagov, S.; Mathews, M. B.; Url, S.; Brient, L. V. O. Cyclic Stretching Stimulates Synthesis of Matrix Components by Arterial Smooth Muscle Cells in Vitro Cyclic Stretching Stimulates Synthesis of Matrix Components by Arterial Smooth Muscle Cells in Vitro Abstract . Rabbit Aortic Medial Cells Were Grown on P. **2014**, *191* (4226), 475–477.

Peyton, S. R.; Raub, C. B.; Keschrumrus, V. P.; Putnam, A. J. The Use of Poly(Ethylene Glycol) Hydrogels to Investigate the Impact of ECM Chemistry and Mechanics on Smooth Muscle Cells. *Biomaterials* **2006**, *27* (28), 4881–4893.

Matheson, L. A.; Fairbank, N. J.; Maksym, G. N.; Santerre, J. P.; Labow, R. S. Characterization of the Flexcell^{TM} Uniflex^{TM} Cyclic Strain Culture System with U937 Macrophage-like Cells. *Biomaterials* **2006**.

Chandorkar, Y.; Castro Nava, A.; Schweizerhof, S.; Van Dongen, M.; Haraszti, T.; Köhler, J.; Zhang, H.; Windoffer, R.; Mourran, A.; Möller, M.; et al. Cellular Responses to Beating Hydrogels to Investigate Mechanotransduction. *Nat. Commun.* **2019**, *10* (1), 1–13. https://doi.org/10.1038/s41467-019-11475-4.

Mantella, L. E.; Quan, A.; Verma, S. Variability in Vascular Smooth Muscle Cell Stretch-Induced Responses in 2D Culture. *Vasc. Cell* **2015**, *7* (1), 1–9.

Kona, S.; Chellamuthu, P.; Xu, H.; Hills, S. R.; Nguyen, K. T. Effects of Cyclic Strain and Growth Factors on Vascular Smooth Muscle Cell Responses. *Open Biomed. Eng. J.* **2009**, *3* (1), 28–38.

Putnam, A. J.; Cunningham, J. J.; Dennis, R. G.; Linderman, J. J.; Mooney, D. J. Microtubule Assembly Is Regulated by Externally Applied Strain in Cultured Smooth Muscle Cells. *J Cell Sci* **1998**, *111 (Pt 2*, 3379–3387.

Liu, G.; Hitomi, H.; Hosomi, N.; Lei, B.; Nakano, D.; Deguchi, K.; Mori, H.; Masaki, T.; Ma, H.; Griendling, K. K.; et al. Mechanical Stretch Augments Insulin-Induced Vascular Smooth Muscle Cell Proliferation by Insulin-like Growth Factor-1 Receptor. *Exp. Cell Res.* **2011**.

Rowley, J. A.; Madlambayan, G.; Mooney, D. J. Alginate Hydrogels as Synthetic Extracellular Matrix Materials. *Biomaterials* **1999**.

Wozniak, M. A.; Desai, R.; Solski, P. A.; Der, C. J.; Keely, P. J. ROCK-Generated Contractility Regulates Breast Epithelial Cell Differentiation in Response to the Physical Properties of a Three-Dimensional Collagen Matrix. *J. Cell Biol.* **2003**.

Pelham, R. J.; Wang, Y. L. Cell Locomotion and Focal Adhesions Are Regulated by Substrate Flexibility. *Proc. Natl. Acad. Sci. U. S. A.* **1997**.

Fairbanks, B. D.; Schwartz, M. P.; Halevi, A. E.; Nuttelman, C. R.; Bowman, C. N.; Anseth, K. S. A Versatile Synthetic Extracellular Matrix Mimic via Thiol-Norbornene Photopolymerization. *Adv. Mater.* **2009**.

Zaman, M. H.; Trapani, L. M.; Siemeski, A.; MacKellar, D.; Gong, H.; Kamm, R. D.; Wells, A.; Lauffenburger, D. A.; Matsudaira, P. Migration of Tumor Cells in 3D Matrices Is Governed by Matrix Stiffness along with Cell-Matrix Adhesion and Proteolysis. *Proc. Natl. Acad. Sci. U. S. A.* **2006**.

Hern, D. L.; Hubbell, J. A. Incorporation of Adhesion Peptides into Nonadhesive Hydrogels Useful for Tissue Resurfacing. *J. Biomed. Mater. Res.* **1998**.

Bryant, S. J.; Anseth, K. S. Controlling the Spatial Distribution of ECM Components in Degradable PEG Hydrogels for Tissue Engineering Cartilage. *J. Biomed. Mater. Res. - Part A* **2003**.

Peyton, S. R.; Putnam, A. J. Extracellular Matrix Rigidity Governs Smooth Muscle Cell Motility in a Biphasic Fashion. *J. Cell. Physiol.* **2005**, *204* (1), 198–209.

Engler, A.; Bacakova, L.; Newman, C.; Hategan, A.; Griffin, M.; Discher, D. Substrate Compliance versus Ligand Density in Cell on Gel Responses. *Biophys. J.* **2004**.

Herrick, W. G.; Rattan, S.; Nguyen, T. V.; Grunwald, M. S.; Barney, C. W.; Crosby, A. J.; Peyton, S. R. Smooth Muscle Stiffness Sensitivity Is Driven by Soluble and Insoluble

ECM Chemistry. *Cell. Mol. Bioeng.* **2015**, *8* (3), 333–348.

Kim, B. S.; Nikolovski, J.; Bonadio, J.; Mooney, D. J. Cyclic Mechanical Strain Regulates the Development of Engineered Smooth Muscle Tissue. *Nat. Biotechnol.* **1999**.

Yuk, H.; Zhang, T.; Parada, G. A.; Liu, X.; Zhao, X. Skin-Inspired Hydrogel-Elastomer Hybrids with Robust Interfaces and Functional Microstructures. *Nat. Commun.* **2016**.

Herrick, W. G.; Nguyen, T. V.; Sleiman, M.; McRae, S.; Emrick, T. S.; Peyton, S. R. PEG-Phosphorylcholine Hydrogels as Tunable and Versatile Platforms for Mechanobiology. *Biomacromolecules* **2013**.

Jufri, N. F.; Mohamedali, A.; Avolio, A.; Baker, M. S. Mechanical Stretch: Physiological and Pathological Implications for Human Vascular Endothelial Cells. *Vascular Cell*. 2015.

Weintraub, A. S.; Schnapp, L. M.; Lin, X.; Taubman, M. B. Osteopontin Deficiency in Rat Vascular Smooth Muscle Cells Is Associated with an Inability to Adhere to Collagen and Increased Apoptosis. *Lab. Investig.* **2000**.

Clark, J. M.; Glagov, S. Transmural Organization of the Arterial Media. The Lamellar Unit Revisited. *Arterioscler. Thromb. Vasc. Biol.* **1985**.

Voss, B.; Rauterberg, J. Localization of Collagen Types I, III, IV and V, Fibronectin and Laminin in Human Arteries by the Indirect Immunofluorescence Method. *Pathol. Res. Pract.* **1986**.

Guruviah, V. Design of Microheaters with Better Thermal Management for Sensor Applications. *Int. J. Mech. Eng. Technol.* **2017**.

Felder, E.; Siebenbrunner, M.; Busch, T.; Fois, G.; Miklavc, P.; Walther, P.; Dietl, P. Mechanical Strain of Alveolar Type II Cells in Culture: Changes in the Transcellular Cytokeratin Network and Adaptations. *Am. J. Physiol. - Lung Cell. Mol. Physiol.* **2008**.

Haga, J. H.; Li, Y. S. J.; Chien, S. Molecular Basis of the Effects of Mechanical Stretch on Vascular Smooth Muscle Cells. *Journal of Biomechanics*. 2007.

Lacolley, P.; Regnault, V.; Nicoletti, A.; Li, Z.; Michel, J. B. The Vascular Smooth Muscle Cell in Arterial Pathology: A Cell That Can Take on Multiple Roles. *Cardiovascular Research*. 2012.

Rezvani-Sharif, A.; Tafazzoli-Shadpour, M.; Avolio, A. Progressive Changes of Elastic Moduli of Arterial Wall and Atherosclerotic Plaque Components during Plaque Development in Human Coronary Arteries. *Medical and Biological Engineering and Computing*. 2018.

Yoon, J.; Cai, S.; Suo, Z.; Hayward, R. C. Poroelastic Swelling Kinetics of Thin Hydrogel Layers: Comparison of Theory and Experiment. *Soft Matter* **2010**, *6* (23), 6004.

Zhou, Y.; Hauser, A. W.; Bende, N. P.; Kuzyk, M. G.; Hayward, R. C. Waveguiding Microactuators Based on a Photothermally Responsive Nanocomposite Hydrogel. *Adv. Funct. Mater.* **2016**.

Chiappelli, M. C.; Hayward, R. C. Photonic Multilayer Sensors from Photo-Crosslinkable Polymer Films. *Adv. Mater.* **2012**.

Schmaljohann, D.; Beyerlein, D.; Nitschke, M.; Werner, G. Thermo-Reversible Swelling of Thin Hydrogel Films Immobilized by Low-Pressure Plasma. *Langmuir* **2004**.

Li, Y.; Tanaka, T. Kinetics of Swelling and Shrinking of Gels. *J. Chem. Phys.* **1990**, *92* (2), 1365–1371.

Wang, X.; Qiu, X.; Wu, C. Comparison of the Coil-to-Globule and the Globule-to-Coil Transitions of a Single Poly(*N* -Isopropylacrylamide) Homopolymer Chain in Water. *Macromolecules* **1998**.

Wang, X.; Qiu, X.; Wu, C. Comparison of the Coil-to-Globule and the Globule-to-Coil Transitions of a Single Poly(*N* -Isopropylacrylamide) Homopolymer Chain in Water. *Macromolecules* **1998**, *31* (9), 2972–2976.

Linder, V.; Gates, B. D.; Ryan, D.; Parviz, B. A.; Whitesides, G. M. Water-Soluble Sacrificial Layers for Surface Micromachining. *Small* **2005**, *1* (7), 730–736.

Bhowmick, S.; Iodice, M.; Gioffrè, M.; Breglio, G.; Irace, A.; Riccio, M.; Romano, G.; Grilli, S.; Ferraro, P.; Mecozzi, L.; et al. Investigation of Pyroelectric Fields Generated by Lithium Niobate Crystals through Integrated Microheaters. *Sensors Actuators, A Phys.* **2017**.

Velmathi, G.; Ramshanker, N.; Mohan, S. Design , Electro-Thermal Simulation and Geometrical Optimization of Double Spiral Shaped Microheater on a Suspended Membrane for Gas Sensing. *IECON 2010 - 36th Annu. Conf. IEEE Ind. Electron. Soc.* **2010**, 1258–1262.

Zhou, Y. SWELLING INDUCED DEFORMATION OF THERMALLY RESPONSIVE HYDROGELS, 2018.

Welker, W. Why Does Cerebral Cortex Fissure and Fold? A Review of Determinants of Sulci an Gyri. In *Cerebral Cortex*; 1990.

Dervaux, J.; Ben Amar, M. Localized Growth of Layered Tissues. *IMA J. Appl. Math. (Institute Math. Its Appl.* **2010**.

Dervaux, J.; Couder, Y.; Guedeau-Boudeville, M. A.; Ben Amar, M. Shape Transition in Artificial Tumors: From Smooth Buckles to Singular Creases. *Phys. Rev. Lett.*

2011.

Chortos, A.; Liu, J.; Bao, Z. Pursuing Prosthetic Electronic Skin. *Nat. Mater.* **2016**, No. July.

Kim, J.; Yoon, J.; Hayward, R. C. Dynamic Display of Biomolecular Patterns through an Elastic Creasing Instability of Stimuli-Responsive Hydrogels. *Nat. Mater.* **2010**, *9* (2), 159–164.

Tanaka, T.; Sun, S.-T.; Hirokawa, Y.; Katayama, S.; Kucera, J.; Hirose, Y.; Amiya, T. Mechanical Instability of Gels at the Phase Transition. *Nature*. 1987, pp 796–798.

Kang, M. K.; Huang, R. Swell-Induced Surface Instability of Confined Hydrogel Layers on Substrates. *J. Mech. Phys. Solids* **2010**, *58* (10), 1582–1598.

Bassik, N.; Abebe, B. T.; Laflin, K. E.; Gracias, D. H. Photolithographically Patterned Smart Hydrogel Based Bilayer Actuators. *Polymer (Guildf).* **2010**, *51* (26), 6093–6098.

Li, G.-Y.; Zheng, Y.; Cao, Y.-P.; Feng, X.-Q.; Zhang, W. Controlling Elastic Wave Propagation in a Soft Bilayer System via Wrinkling-Induced Stress Patterns. *Soft Matter* **2016**, *12*, 4204–4213.

Thérien-Aubin, H.; Moshe, M.; Sharon, E.; Kumacheva, E. Shape Transformations of Soft Matter Governed by Bi-Axial Stresses. *Soft Matter* **2015**, *11* (23), 4600–4605.

Harmon, M. E.; Tang, M.; Frank, C. W. A Microfluidic Actuator Based on Thermoresponsive Hydrogels. *Polymer (Guildf).* **2003**, *44* (16), 4547–4556.

Lin, S.; Yuk, H.; Zhang, T.; Parada, G. A.; Koo, H.; Yu, C.; Zhao, X. Stretchable Hydrogel Electronics and Devices. *Adv. Mater.* **2015**, 1–9.

Sun, Y.; Choi, W. M.; Jiang, H.; Huang, Y. Y.; Rogers, J. a. Controlled Buckling of Semiconductor Nanoribbons for Stretchable Electronics. *Nat. Nanotechnol.* **2006**, *1* (3), 201–207.

Oyewole, O. K.; Yu, D.; Du, J.; Asare, J.; Oyewole, D. O.; Anye, V. C.; Fashina, a.; Zebaze Kana, M. G.; Soboyejo, W. O. Micro-Wrinkling and Delamination-Induced Buckling of Stretchable Electronic Structures. *J. Appl. Phys.* **2015**, *117* (23), 235501.

Tekin, H.; Tsinman, T.; Sanchez, J. G.; Jones, B. J.; Camci-Unal, G.; Nichol, J. W.; Langer, R.; Khademhosseini, A. Responsive Micromolds for Sequential Patterning of Hydrogel Microstructures. *J. Am. Chem. Soc.* **2011**, *133* (33), 12944–12947.

Tekin, H.; Anaya, M.; Brigham, M. D.; Nauman, C.; Langer, R.; Khademhosseini, A. Stimuli-Responsive Microwells for Formation and Retrieval of Cell Aggregates. *Lab Chip* **2010**, *10* (18), 2411.

Wang, J.; Li, B.; Cao, Y. P.; Feng, X. Q.; Gao, H. Wrinkling Micropatterns Regulated by a Hard Skin Layer with a Periodic Stiffness Distribution on a Soft Material. *Appl. Phys. Lett.* **2016**, *108* (2).

Nogales, A.; Del Campo, A.; Ezquerra, T. A.; Rodriguez-Hernández, J. Wrinkling and Folding on Patched Elastic Surfaces: Modulation of the Chemistry and Pattern Size of Microwrinkled Surfaces. *ACS Appl. Mater. Interfaces* **2017**, *9* (23), 20188–20195.

Wang, J.-W.; Li, B.; Cao, Y.-P.; Feng, X.-Q. Surface Wrinkling Patterns of Film–Substrate Systems With a Structured Interface. *J. Appl. Mech.* **2015**, *82* (5), 051009.

Bae, H. J.; Bae, S.; Yoon, J.; Park, C.; Kim, K.; Kwon, S.; Park, W. Self-Organization of Maze-like Structures via Guided Wrinkling. *Sci. Adv.* **2017**, *3* (6), e1700071.

Shin, H.; Choi, Y.; Cha, J.; Kim, P. Spatially Controlled Folding Instability of Moduli-Patterned and Bilayered Membrane under Compressive Stresses. *Adv. Mater. Interfaces* **2016**, 1600105.

Ouchi, T.; Yang, J.; Suo, Z.; Hayward, R. C. Effects of Stiff Film Pattern Geometry on Surface Buckling Instabilities of Elastic Bilayers. *ACS Appl. Mater. Interfaces* **2018**.

Yoon, J.; Kim, J.; Hayward, R. C. Nucleation, Growth, and Hysteresis of Surface Creases on Swelled Polymer Gels. *Soft Matter* **2010**, *6* (22), 5807.

Xu, B.; Chen, D.; Hayward, R. C. Mechanically Gated Electrical Switches by Creasing of Patterned Metal/Elastomer Bilayer Films. *Adv. Mater.* **2014**, *26* (25), 4381–4385.

Maluf, N. An Introduction to Microelectromechanical Systems Engineering. *Meas. Sci. Technol.* **2002**.

University, L. *An Introduction to MEMS (Micro-Electromechanical Systems)*; 2002.

Grayson, A. C. R.; Shawgo, R. S.; Johnson, A. M.; Flynn, N. T.; Li, Y.; Cima, M. J.; Langer, R. A BioMEMS Review: MEMS Technology for Physiologically Integrated Devices. In *Proceedings of the IEEE*; 2004.

Gad-el-Hak, M. *MEMS: Applications*; 2005.

Madou, M. *Fundamentals of Microfabrication: The Science of Miniaturization*; 2002.

Westberg, D.; Paul, O.; Andersson, G. I.; Baites, H. Surface Micromachining by Sacrificial Aluminium Etching. *J. Micromechanics Microengineering* **1996**.

Bagolini, A.; Pakula, L.; Scholtes, T. L. M.; Pham, H. T. M.; French, P. J.; Sarro, P. M. Polyimide Sacrificial Layer and Novel Materials for Post-Processing Surface Micromachining. *J. Micromechanics Microengineering* **2002**.

Boroumand Azad, J.; Rezadad, I.; Nath, J.; Smith, E.; Peale, R. E. Release of MEMS Devices with Hard-Baked Polyimide Sacrificial Layer. In *Advances in Resist Materials and Processing Technology XXX*; 2013.

Walsh, K.; Norville, J.; Tai, Y. C. Photoresist as a Sacrificial Layer by Dissolution in Acetone. In *Proceedings of the IEEE Micro Electro Mechanical Systems (MEMS)*; 2001.

Song, I. H.; Ajmera, P. K. Use of a Photoresist Sacrificial Layer with SU-8 Electroplating Mould in MEMS Fabrication. *J. Micromechanics Microengineering* **2003**.

Chen, Y.; Mao, H.; Tan, Q.; Xue, C.; Ou, W.; Liu, J.; Chen, D. Fabrication of Polyimide Sacrificial Layers with Inclined Sidewalls Based on Reactive Ion Etching. *AIP Adv.* **2014**.

Harnett, C. K.; Coates, G. W.; Craighead, H. G. Heat-Depolymerizable Polycarbonates as Electron Beam Patternable Sacrificial Layers for Nanofluidics. *J. Vac. Sci. Technol. B Microelectron. Nanom. Struct.* **2001**, *19* (6), 2842.

Ferrell, N.; Woodard, J.; Hansford, D. Fabrication of Polymer Microstructures for MEMS: Sacrificial Layer Micromolding and Patterned Substrate Micromolding. *Biomed. Microdevices* **2007**, *9* (6), 815–821.